TECHNISCHE UNIVERSITÄT WIEN

DIPLOMARBEIT

Potential of hydrogen and power generation from natural gas with quantitative carbon capture using chemical looping technology

ausgeführt zum Zwecke der Erlangung des akademischen Grades eines Diplom-Ingenieurs
unter der Leitung von

Univ. Prof. DI. Dr. Techn. Hermann Hofbauer
DI. Dr. Techn. Tobias Pröll
DI. Johannes Bolhàr-Nordenkampf

Institut für Verfahrenstechnik, Umwelttechnik und Technische Biowissenschaften

eingereicht an der Technischen Universität Wien

Fakultät für Maschinenwesen und Betriebswissenschaften

von

Klemens Marx

0426116

Tuschlgasse 3/34, 1230-Wien

Wien, im März 2009

Klemens Marx

Danksagungen

Ich möchte mich an dieser Stelle dafür bedanken, dass mir die Möglichkeit geboten wurde an einem Thema mit großem Zukunftspotential mitzuarbeiten.

Deshalb gilt hier mein Dank Uni. Prof. DI. Dr. Techn. Hermann Hofbauer für die Möglichkeit der Mitarbeit in der Arbeitsgruppe für Zukunftsfähige Energietechnik um meine Diplomarbeit zu verfassen.

Ganz besonders muss ich mich aber an dieser Stelle bei DI. Johannes Bolhàr-Nordenkampf, Mag. DI. Dr. techn. Phillip Kolbitsch und DI. Dr. techn. Tobias Pröll bedanken für die mir gebotene Unterstützung bei meiner Diplomarbeit.

Bedanken möchte ich mich auch bei meinen Eltern Ludmilla und Eduard Marx, denen ich es zu verdanken habe, dass ich überhaupt die Möglichkeit hatte meinen Geist frei zu entfalten und die mir eine weitestgehend sorgenfreies Studieren ermöglicht haben.

Besonders möchte ich mich noch bei Herrn Dr. Dr. techn. Günter Hackmüller bedanken der mir in einer für mich sehr prägenden Phase meines Lebens mir ein hervorragendes Beispiel, Lehrer und vor allem Inspiration war. Mein Dank gilt auch Herrn Mag. Herbert Nier† dafür, dass er mir die Möglichkeit geboten hat, mich an seinem faszinierenden und beispiellosem Lebensmotto teilhaben zu lassen.

Danke auch an Gottfriede Ebner für die Mühen die ihr diese Arbeit bereitet haben.

Danke auch Kathrin für *du-weist-schon-was* ;)

„Auf das die Saat auf fruchtbaren Boden gefallen, dort sprieße und saftige Früchte hervorbringe.“

Abstract

Carbon capture and storage (CCS) from carbon fueled processes seems to be the key mid-term strategy to limit the carbon dioxide concentration in the atmosphere. Chemical looping is proposed as a combustion technology (CLC) with inherent CO_2 separation and as a hydrogen production process using reforming (CLR). The potential of chemical looping technology is the low energy penalty for CO_2 capture.

This study focuses on the implementation of chemical looping into a power-, and a hydrogen production process in the scale of 10 MW fuel power. The aim is to show achievable efficiencies and optimization potentials of such systems in order to allow the evaluation of the competitiveness of chemical looping. Therefore the processes are simulated by use of the flow sheet simulation software IPSEpro. The modeled reactions are assumed to be in equilibrium.

Different process options for chemical looping combustion (CLC) have been simulated. The simulation shows that a fluidized bed cooler is a key element to increase the power cycle efficiency and that a thermal efficiency of approximately 34% is achievable.

Also, a chemical looping steam reforming (CLR(s)) process has been modeled. In this process a CLC system is used to heat a fluidized bed steam reformer. It has been found out that under certain circumstances it is favorable to keep the process simple in order to achieve high process performance. The simulation shows that an exergetic efficiency of approximately 75% is possible.

A number of different chemical looping autothermal reforming (CLR(a)) process options have been simulated. The results show that the sequence of the process components is very important in the discussed design. The calculation shows that the process is capable to produce practically pure hydrogen, carbon dioxide and nitrogen with an exergetic efficiency of approximately 59%.

The simulation shows rather poor efficiency in case of CLC power generation which is common for small scale applications. Nevertheless, this process may have a great future in large scale carbon dioxide storage ready power generation applications.

Because of its simple structure and the efficiency advantage compared to CLC a CLR(a) process is the best option for the next evolution step.

Hence, it is proposed to use chemical looping autothermal reforming for fuel upgrading or hydrogen production to show the potential of chemical looping in industrial scale.

Kurzfassung

Kohlenstoffabscheidung und Speicherung (CCS-Carbon Capture and Storage) scheint die mittelfristige Lösung um die Kohlendioxidkonzentration in der Atmosphäre zu limitieren. Chemical looping wird zur Verbrennungstechnology (CLC) mit inherenter CO_2 Abtrennung und als Prozess zur Wasserstoffproduktion mittels Reforming (CLR) vorgeschlagen. Das Potential von chemical looping combustion Prozessen besteht darin, dass sie zur CO_2 Abtrennung nur sehr geringe Energiemengen benötigen.

Diese Studie befasst sich mit der Integration von chemical looping in einen Energie-, und einen Wasserstoffproduktionsprozess mit 10 MW Brennstoffleistung. Das Ziel ist erreichbare Wirkungsgrade zu berechnen und eventuelle Optimierungspotentiale aufzuzeigen. Dadurch soll eine Grundlage geschaffen werden, auf deren Basis die Konkurrenzfähigkeit dieser (der hier besprochenen) Systeme besser beurteilt werden kann. Zu diesem Zweck werden verschiedene Prozessoptionen für chemical looping mit Hilfe des Programmes IPSEpro simuliert, wobei die modellierten Reaktionen dabei im Gleichgewicht angenommen werden.

Die Analyse der verschiedenen Simulationen ergab, dass ein Fließbettkühler eines der Schlüsselelemente ist, um den energetischen Wirkungsgrad zu erhöhen und dass thermische Wirkungsgrade von 34% erreichbar sind.

Desweiteren wurde ein chemical looping stem reforming (CLR(s)) Prozess modelliert. In diesem Prozess wird die, im Reaktorsystem produzierte, Wärme verwendet um einen steam reformer, ausgeführt als Fließbettkühler, zu beheizen. Es wurde herausgefunden, dass der Gesamtwirklungsgrad unter gewissen Umständen verbessert werden kann, indem der Prozess möglichst vereinfacht wird. Die Simulation zeigt, dass exergetische Wirkungsgrade von ungefähr 75% möglich sind.

Desweiteren wurde eine Vielzahl von chemical looping autothermal reforming (CLR(a)) Prozessvarianten simultiert. Die Ergebnisse zeigen, dass die Verschaltungsreihenfolge der Prozesskomponenten in dem hier diskutierten Design sehr wichtig ist. Die Berechnungen zeigen witers, dass der Prozess in der Lage ist praktisch reinen Wasserstoff, Kohlendioxid und Stickstoff herzustellen und ein exergetischer Wirkungsgrad von in etwa 59% errreicht werden kann.

Die Simultion zeigt relativ geringe Wirkungsgrade im Falle von CLC power generation was bei Anlagen dieser geringen Größe gewöhnlich ist. Nichtsdestotrotz hat dieser Prozess großes Potential für die kohlendioxidfreie Stromproduktion in großem Massstab.

Der CLR(a)- Prozess ist nicht nur wegen seines simplen Aufbaus, sondern auch aufgrund des höheren Wirkungsgrades, im Vergleich mit CLC- Prozessen, die beste Option für Weiterentwicklung der Technologie.

Daher wird vorgeschlagen, einen chemical looping autothermal reforming- Prozess für Brennstoff „upgrading“ oder Wasserstoffproduktion zu errichten, um das Potential von chemical looping in industriellem Massstab zu zeigen.

Table of Contents

1 Introduction

1.1 The carbon dioxide complexity

In 1827 the mathematician Joseph Fourier wrote an essay about the interaction of greenhouse gases on the world climate which contributed to the better understanding of the topic. (cf. [44])

Actually the greenhouse effect is the basement for formation of any organism populating the earth. It is assumed that the former essential effect of greenhouse is changing to a penalty for human evolution. Rising global temperature accompanied by melting arctic ice reservoirs has influenced the climate of the earth disadvantageously for the being of almost every creature.

There are several gases known which contribute to the greenhouse effect. In order to compare their effect on the greenhouse effect two practical measurements have been established. Most often the Carbon dioxide equivalent (CDE) is used. It describes how much global warming a given type and amount of greenhouse gas may cause, using the functionally equivalent amount as the reference.

Table 1 Carbon dioxide equivalent of different gases [W 5]

Gas		Carbon Dioxide equivalent (CDE)
Carbon dioxide	CO_2	1
Methane	CH_4	21
Nitrous oxide	N_2O	310
Hydrofluorocarbon gases	HFC-23	11,7
	HFC-32	650
	HFC-125	2,8
	HFC-134a	1,3
	HFC-143a	3,8
	HFC-152	140
	HFC-236fa	6,3
Perfluorocarbon gases	CF_4	6,5
	C_2F_6	9,2
	C_4F_{10}	7
	C_6F_{14}	7,4
Sulfur hexafluoride	SF_6	23,9

Not all discharges of greenhouse gases are caused by human activities. For example human activities are not believed to influence the concentration of water vapor (which has got a great influence on the greenhouse effect cf. [12] and [13]) in the atmosphere directly. This is not the case for carbon dioxide. It is well established that our way of living is increasing the concentration of CO_2 in the atmosphere rapidly. But not only carbon dioxide exhaustion is a problem. There are a lot of other gases emitted by human activities accounting to the greenhouse effect, listed in Table 1. Nevertheless, carbon dioxide is the most relevant greenhouse gas caused by anthropogenic activities (cf. [32]) due to the large amounts emitted. According to the IPCC special report on “Carbon Capture and Storage” [32] the power and industrial sectors combined dominate the current global CO_2 emissions.

Since 1958, direct measurements of CO_2 in the atmosphere are done on regular basis. Additionally the historic carbon dioxide concentration of approximately the past 700000 years has been reconstructed by measuring the CO_2 concentration in air trapped in ice cores of glaciers.

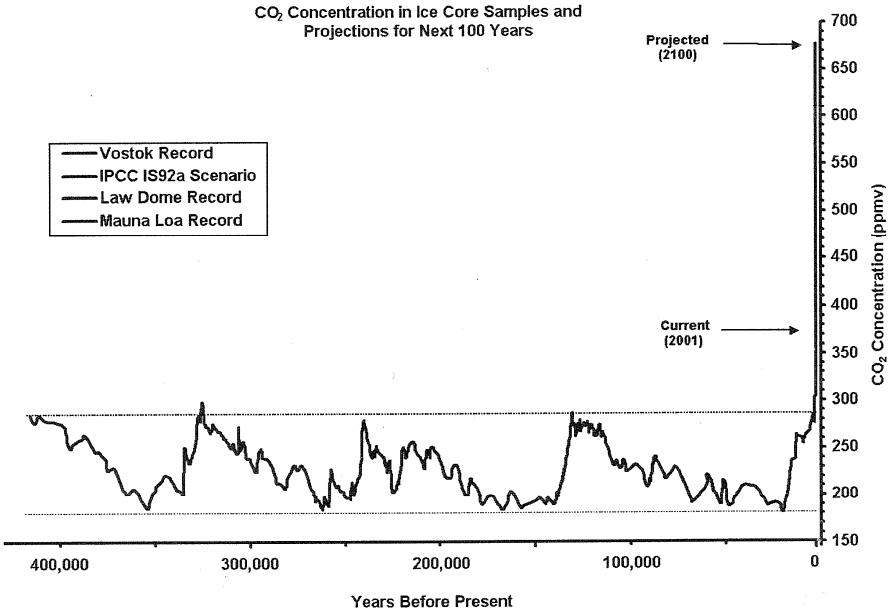

Figure 1 Estimated atmospheric CO_2 concentration for the past 420 000 years [44]

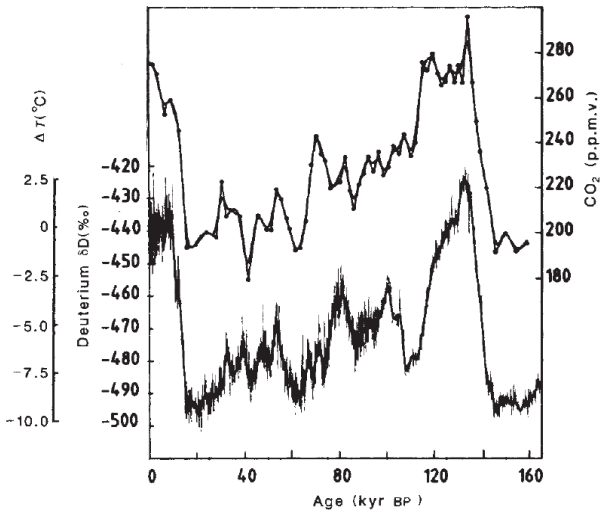

Figure 2 Atmospheric concentration of CO_2 (upper curve) and the temperature dependent isotope deuterium (lower curve) plotted against the age [5]

Although the coherence from Figure 1 and Figure 2 seems to be quite simple the truth is not finally known yet. Anyway it cannot be denied that there is some kind of connection between human behavior and the earth's climate. Apart, there are other factors than combustion of fossil fuels that contribute to the amount of greenhouse gases present in the atmosphere and there are also other factors than the atmospheric concentration of greenhouse gases that affect the climate on the Earth ([12] and [13]). The complexity of the earth's climate system is a considerable scientific challenge since it is also practically impossible to perform controlled experiments on the planet as a whole for validation of theoretical theses.

Nonetheless, nowadays scientists generally agree that endeavors to decrease anthropologic emission of greenhouse gases have to be promoted.

1.2 Possibilities to decrease anthropogenic emissions of greenhouse gases

There are a lot of possibilities to decrease global CO_2 emission. In order to point out the opportunities the identity developed by Kaya, found in [32], is quite helpful.

$$CO_2 emission = Population \times \left(\frac{GDP}{Population}\right) \times \left(\frac{Energy}{GDP}\right) \times \left(\frac{Emissons}{Energy}\right) \quad \text{(eqn 1-1)}$$

Looking on the prediction of the world population and the global per-capita gross domestic product $\left(\frac{GDP}{Population}\right)$ it seems to be quite challenging to decrease die CO_2 emission. Therefore the identity of Kaya says that the only way to solve the problem requires either major reduction of global energy intensity $\left(\frac{Energy}{GDP}\right)$ or steep reduction of carbon emissions from energy technology $\left(\frac{Emissons}{Energy}\right)$.

So, there are several options available to achieve these goals. A comprehensive review can be found in the IPCC report 2001 and 2007 ([12] and [13]). The most discussed and feasible options are summarized below.

Improve energy efficiency

Improving the efficiency of energy conversion, transport and end-use will result in less fossil fuel consumption. By the invention of new technologies in power generation as for example improved turbines, the energy conversion efficiency has already been increased. However improved energy efficiency on its own is unlikely to be sufficient to achieve deep reductions in emission of greenhouse gases.

Reduction of global energy intensity

This could be achieved either by more efficient energy use in production and consumption of goods and services, or by a change in consumption patterns away from particularly energy-demanding products. Reducing global energy intensity sounds rational to start limiting global CO_2 emissions, but it is unlikely that it would be enough to mitigate global warming.

Increasing use of renewable energy sources

Switching to non carbon energy sources is an outraging possibility because they do not affect the CO_2 balance. But, using a renewable energy like the sun or biomass is not always an option. Often an energy carrier with a high energy density is needed, which is the fact especially for transportation. Renewable energy sources have large potential in power generation confirmed by the multitude of recent projects. Renewable energy in large scale is still under development and the investment costs are very high. Therefore, it seems to be an option for long term carbon dioxide reduction.

Increase the use of nuclear power

Due to no emission of CO_2 nuclear power seems to be an option. Problems of nuclear waste and fugacious uranium are limiting the state of the art technology for nuclear power generation as a medium term supplier option.

Switch to less carbon intense fuels

Since coal contains more carbon per unit of energy than oil or natural gas does replacing coal would result in less carbon dioxide emission (see Table 2). The IPCC Report names the possibility on 420kg CO_2 less per MW/h. Nevertheless known deposits of oil and natural gas are limited and strained, while there are still immense amounts of coal available at relative low cost. Therefore, fuel switch from coal to fossil fuels with less carbon intensity does not seem like a viable long term strategy.

Table 2 Direct CO_2 emission factor for some examples for carbonaceous fuels from [32] Annex I

Carbonaceous Fuel	Heat Content (HHV) $^{MJ}/_{kg}$	Emission Factor $^{gCO2}/_{MJ}$
Coal		
Anthracite	26,2	96,8
Bituminous	27,8	87,3
Sub-bituminous	19,9	90,3
Lignite	14,9	91,6
Biofuel		
Wood (dry)	20,0	78,4
Natural Gas	$^{MJ}/_{m^3}$	
	37,3	50
Petroleum Fuel	$^{MJ}/_{m^3}$	
Distillate Fuel Oil (#1, 2 &4)	38,650	68,6
Residual Fuel Oil (#5 &6)	41,716	73,9
Kerosene	37,622	67,8
LPG (average fuel use)	25,220	59,1
Motor Gasoline	-	69,3

Enhance carbon dioxide uptake in biomass

Carbon dioxide is a major player in the process of photosynthesis which is needed for plant growing. The carbon dioxide is converted into various fixed carbons building up the biomass. Because of that an increase on earth's biomass will result in a drain of CO_2 of the atmosphere by accumulation in the biomass. Nowadays even the opposite happens since great forest areas have had to give way to the expansionist tendencies of human being.

Decrease non-carbon dioxide greenhouse-gas emissions

As mentioned before not only CO_2 contributes to climate change. Especially a lot of refrigerants, methane as well as various nitrogen oxides have to be mentioned.

CCS-Carbon Capture and Storage

Carbon capture and storage is the key midterm strategy to decrease the CO_2 content in the atmosphere. CCS is much cheaper than the use of renewable energy and the potential is huge compared to all other options.

Costs of mitigation

Costs of mitigation of carbon dioxide emission underlie a great variety depending on the avoiding mechanism. The IPCC Fourth Assessment Report / Working Group III Report "Mitigation of Climate Change" chapter 4: Energy Supply gives a great overview on that topic.

The combination of all options is the most viable strategy for steep reduction of anthropogenic greenhouse gas emission.

1.3 CCS - Carbon capture an storage

The goal of carbon dioxide capture is to get sufficiently pure CO_2 ready for storage. This means that the purity of the carbon dioxide is sufficient enough that less energy and space is needed for compression, transport and storage. Impurities, for example water or sulfur, may impact the process of compression negatively or even make it technically unfeasible. They also will affect the transportability of the compressed CO_2 by causing corrosion. Furthermore, some impurities may underlie international treaties, like sulfur, in the future.

1.3.1 Carbon Dioxide and its physical properties

Carbon dioxide is a chemical compound of two elements, carbon and oxygen. Its molecular formula is CO_2. At standard pressure and temperature, carbon dioxide is a gas. Its physical state varies with pressure and temperature (Figure 3). Carbon dioxide has its triple point at -56,5°C and 5,1 bar by increasing temperature and pressure it reaches its critical point at 31,1°C and 73,9 bar.

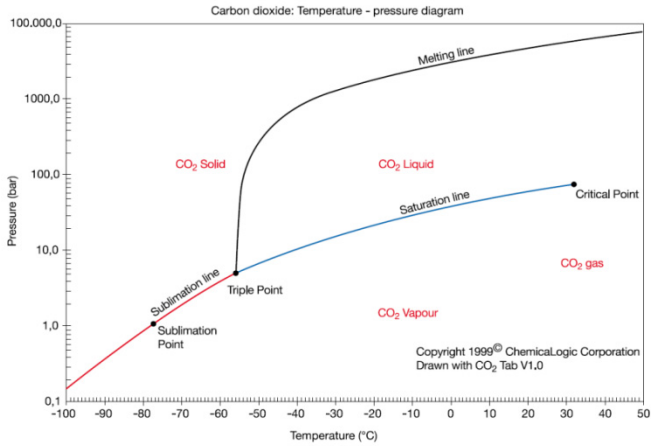

Figure 3 Phase diagram for CO_2 [32] Annex I

Above the critical point CO_2 is in the supercritical state where it behaves as a gas. However under high pressure the density of the gas can be very large, approaching or even exceeding the density of liquid water (Figure 4). This behavior is particularly important for CO_2 storage.

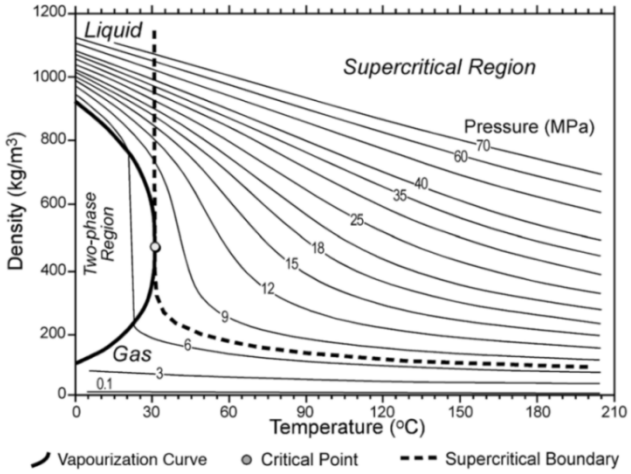

Figure 4 Variation of CO_2 density as a function of temperature and pressure [32] Annex I

1.3.2 Possible ways of carbon dioxide capture

Capture of CO_2 on industrial scale is a well known topic since it has been practiced for more than 80 years. It was used by the cleaning of the so called “town gas” or by enhancing the purity of natural gas. Carbon dioxide sequestration for power generation has changed the requirements because new technologies have to be developed.

Post combustion capture

The Post combustion technology is the most developed process and is more or less state of the art. The process is a conventional technical combustion with an additional attached carbon dioxide sequestration by chemical absorption from the flue gas.

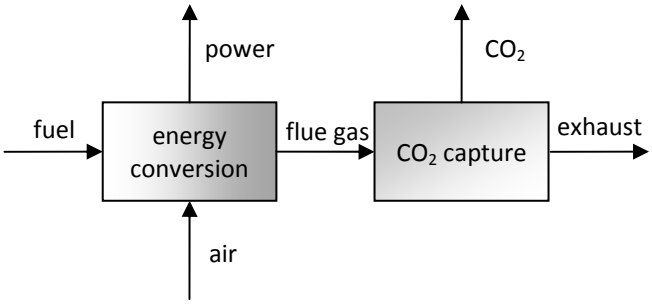

Figure 5 Scheme of post-combustion process

Because of these characteristics the method is also called “end-of-pipe” solution.

The biggest advantage of the post combustion method is that the process of flue gas scrubbing is well known and has been used since many years i.e. in hydrogen purification and in enhanced oil or gas recovery (although in smaller scale and higher pressure than required for power generation). It is also a feasible technology for retrofitting of aged power plants for clean energy generation. The high costs of flue gas scrubbing, the poor carbon dioxide sequestration-ratio of only approximately 80-90% and the slip of solvent result that this method is not very competitive compared to the other CCS options.

Pre combustion capture

In this technology the fuel-fixed carbon is sequestrated from the fossil fuel prior the real firing.

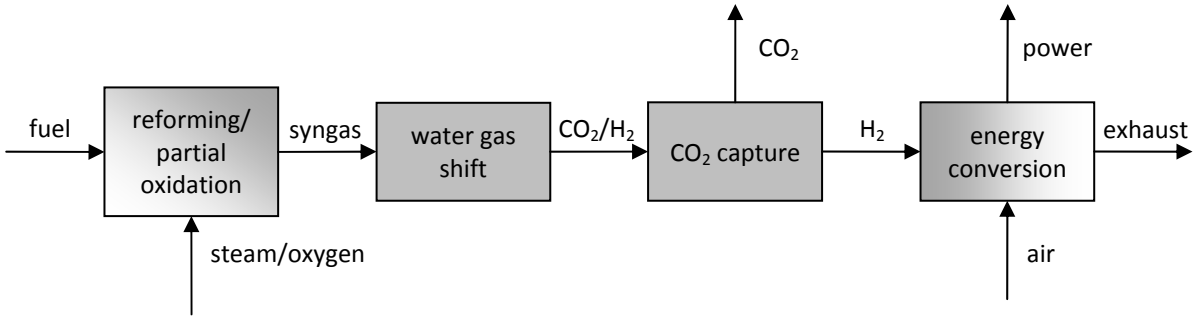

Figure 6 Scheme of pre-combustion process

This is achieved by producing a synthesis gas. In case of solid fuels the synthesis gas is produced by gasification and in case of gaseous fuels by steam reforming.

Afterwards the synthesis gas is conducted into a reactor where it is converted into CO_2 and H_2 by means of water gas shift reaction utilizing steam.

$$CO + H_2O \rightarrow CO_2 + H_2$$

Subsequently the carbon dioxide is separated from the gas stream in an adsorption or absorption process, for example in a pressure swing absorption column. Only the hydrogen is burned for power generation.

Since almost all of the components are well known and used in chemical industry (for example in refineries and ammonia production) there is a lot of experience in utilizing these methods. This process is also less expensive than post combustion CO_2 capture because the carbon dioxide can be physically or chemically adsorbed which requires less energy than absorption. Like in the post combustion method the CO_2-sequestration-ratio is only approximately 80-90% since the complete separation of carbon dioxide is technically impossible. Furthermore, there is a lack of experience in large scale firing of hydrogen.

Oxyfuel combustion

This process has been developed for, so called, "green" firing of coal. But it is also a possible process for burning gaseous or liquid fuels. As the name says in the oxyfuel combustion process pure oxygen is used for burning. Due to absence of nitrogen from the air the flue gas mass flow is reduced and consists mainly of carbon dioxide and steam. After separation of the water, for example by condensation or adsorption, a CO_2 rich stream, ready for compression and sequestration is produced.

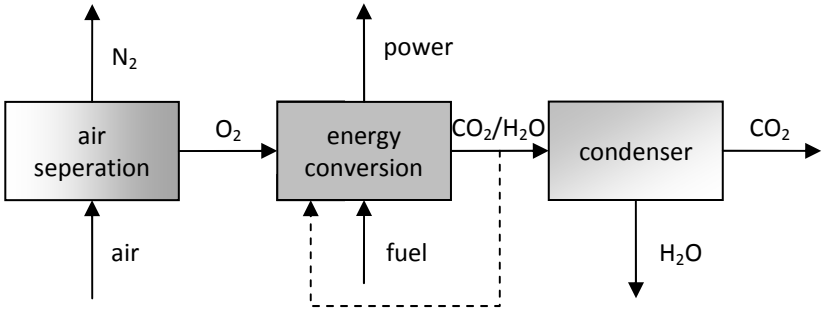

Figure 7 Scheme of Oxyfuel-process

Due to firing with almost pure oxygen the adiabatic flame temperature would rise approximately about 1000-1500 degree Kelvin. This requires the recirculation of parts of the exhaust stream for cooling of the flame and the combustion chamber.

The greatest advantage of the Oxyfuel combustion is that almost all CO_2 can be sequestrated and due to absence of air-nitrogen the production of NO_x is inhibited (see [9]). Since the process requires pure oxygen an air separation unit is needed. The air separation unit needs a lot of energy resulting in costs similar to that of the pre-combustion technology (see [59]). Because of that, scientists spend great hope in the low energy supply of pure oxygen by membrane separation processes.

Chemical looping

The aim of chemical looping is to reduce the costs of CO_2 sequestration by reducing the costs of the oxygen separation from the air.

Chemical looping combustion

In the chemical looping combustion process the air separation is driven by a metallic oxygen carrier. The oxygen carrier is circulated between two reactors. In the so called air-reactor the metallic oxygen carrier is oxidized. Afterwards it is transported to the fuel reactor where it is reduced again by a gas-solid reaction with the fuel.

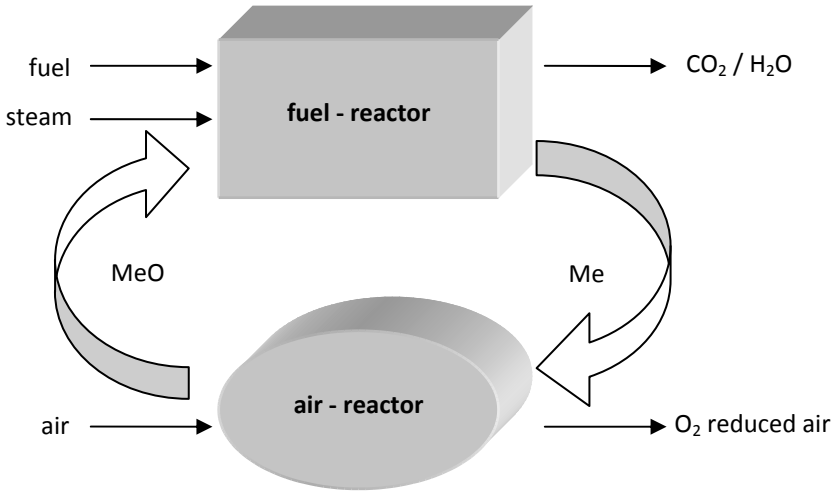

Figure 8 Scheme of chemical looping-process

Therewith the complex and expensive air separation can be skipped. Also the amount of not condensable inert gases in the exhaust stream is reduced which results in lower costs of compression and liquefaction. The CLC process is under development till now and shows great potential in reducing the energy penalty for carbon capture.

Chemical looping reforming

The chemical looping technology is also proposed for production of hydrogen with inherent carbon-dioxide capture. It is intended to use the hydrogen either for power generation or in chemical processes. There are basically two different ways of production of hydrogen by chemical looping. The first one is the so called chemical looping steam reforming where a conventional steam reformer uses the heat of chemical looping. The second possibility is the so called chemical looping autothermal reforming where the hydrogen is produced inherently inside the fuel reactor at below stoichiometric conditions and by directly injected steam.

Comparison of costs for CCS-technologies

To get a better understanding about the costs of the different sequestration processes the following table is introduced. According to Scheffknecht et al. [59] chemical looping combustion has a great potential to reduce carbon capture and storage costs.

Table 3 Carbon capture and storage penalties [59]

	Δ-degree of efficiency [%-points]	Δ-cost of production [€/MWh]	CO_2-avoidance costs [€/t]
Post-Combustion	14-17	17-20	25-30
Pre-Combustion	9	12-16	18-24
Oxyfuel	7-9	11-16	16-21
CLC	~3	~8	~10

1.3.3 Carbon dioxide storage

The IPCC Special Report on Carbon Dioxide Capture and Storage [32] shows that there are three possible storage sites for sequestration of carbon dioxide: geological or ocean storage or by mineral carbonation.

Geological storage

For geological storage CO_2 must first be compressed till it becomes a dense fluid also known as supercritical state. Depending on the rate that temperature increases with depth (geothermal gradient), the density of CO_2 will increase with depth. At a depth of 800 m or greater, the injected CO_2 will become a dense supercritical fluid.

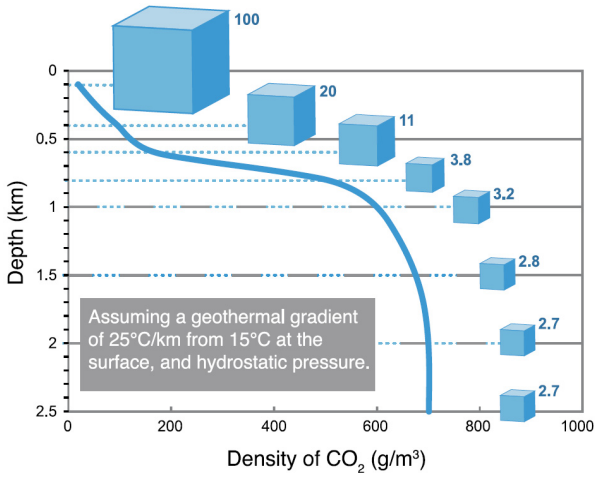

Figure 9 Density of CO_2 depending on depth [32]

For technical reinjection of CO_2 the crust of the earth offers a lot of possibilities like oil- or gas-fields, deep coal seams and saline formations. The selection of the storage site has to be done carefully with respect to long term storage and low leaking. The captured CO_2 can be used as a cushion gas in order to increase the productivity of oil or gas fields. This technology is also known as Enhanced Oil Recovery EOR or Enhanced Gas Recovery EGR. Both technologies are used, for example EOR at the Weyburn project [W 10] and EGR at the In Salah, Algeria, CO_2 Storage Project, nowadays, and since years, very successfully.

Ocean storage

Another approach is the injection of carbon dioxide into the ocean. The sequestrated CO_2 is therefore transported by ship or pipeline to the injection site. Because of its physical properties CO_2 has got a higher density than water if it is injected deeper than 3000 m. Therefore, injecting the carbon dioxide depths lower than 3000 m will result in so called "rising CO_2 plume" or by injecting it deeper than 3000m will result in "sinking CO_2 plume" or in "CO_2 lakes". The environmental impact of such lakes is unpredictable. It is confirmed that anthropologic CO_2 has already influenced the pH-units of the ocean ([31]).

Numerical analysis has shown that placing of CO_2 into the ocean in deeper sea is going to isolate anthropogenic CO_2 for several centuries, but over long times the ocean and the atmosphere would equilibrate.

Mineral storage

Mineral carbonation is based on the reaction of CO_2 and metal oxide bearing materials to form carbonates. Calcium and magnesium are the most attractive metals. The process in the nature is called silicate weathering. Suitable materials may be abundant silicate rocks, serpentine and olivine materials. However, today mineral carbonation is still an immature technology.

Effects of impurities an CCS and enhanced hydrocarbon recovery

Core flood cell experiments [50] figured out that impurities, like oxygen (O_2), sulfur dioxide (SO_2), nitrogen oxide (N_2O) or carbon monoxide (CO), seem to have no great impact on the volume of the gas mixture as long as the sum of impurities is less than 1 mole%. Therefore, the effect on storage capacity of a reservoir is negligible. That's quite important since polluted gases, conditioned like mentioned before, have the advantage of a cheaper separation process.

It was also discovered that a small amount of impurities might have positive effects on the amount of natural gas recovery by advantageously influencing the gas properties like the viscosity.

2 Theory

2.1 The chemical looping combustion process

In chemical looping combustion the direct contact of fuel and combustion air is impeded by the separation of the two combustion steps, the oxidation of the metal oxide and oxidation of the fuel, in two separated reactors. That's why this kind of combustion is also called "unmixed combustion".

The basic idea of CLC is quite old and was introduced by Knoche and Richter (1968) [35] and Ishida et. al (1987) [33]. The reason was to increase the thermal efficiency of combustion by increasing the reversibility of the combustion process by avoidance of the inherent disorder of normal combustion. Hence higher thermal efficiencies should be obtained.

Basically a CLC-System consists of two parts; an air-reactor and a fuel-reactor. The required oxygen for oxidation of the fuel is transported from the air- to the fuel-reactor by means of a metallic oxygen carrier.

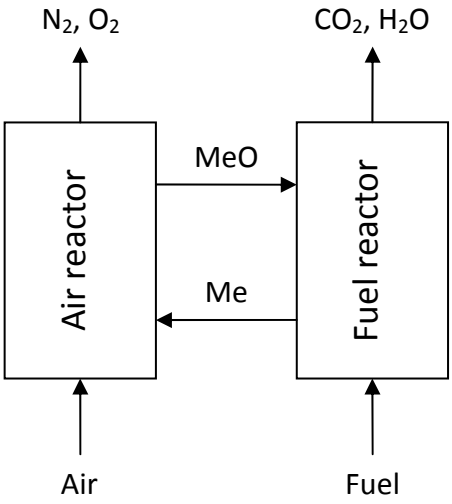

Figure 10 CLC process scheme

As seen in Figure 10 the exhaust stream from the fuel-reactor consists of carbon dioxide and water vapor. Therefore, the CLC process attaches great attention for the Carbon-Capture-And-Storage-Technology. The advantage of CLC is that it gets along without an additional oxygen separation unit and therefore the process is very competitive compared to other CCS-processes.

Although recent works focus on gaseous fuels CLC seems to be a process which can also be used for solid fuels.

The general reaction of fossil fuels in the fuel reactor is as following:

$$C_xH_y + \left(2x + \frac{y}{2}\right) MeO_\alpha \rightarrow xCO_2 + \frac{y}{2}H_2O + \left(2x + \frac{y}{2}\right) MeO_{\alpha-1} \qquad \text{(reac 2-1)}$$

$$CO + MeO_\alpha \rightarrow CO_2 + MeO_{\alpha-1} \qquad \text{(reac 2-2)}$$

$$H_2 + MeO_\alpha \rightarrow H_2O + MeO_{\alpha-1}$$

The reactions show that if the oxygen carrier is selected adequately and the residence time is sufficient the exhaust stream consists only of carbon dioxide and water.

After transportation of the reduced metal oxide from the fuel to the air reactor the metal oxide is re-oxidized following the reaction:

$$MeO_{\alpha-1} + \frac{1}{2}O_2 \rightarrow MeO_{\alpha} \qquad \text{(reac 2-3)}$$

Theoretically the entire oxygen can be detracted from the air if enough reduced metal oxide is present and sufficient residence time is granted.

While the reaction inside the air reactor is always strongly exothermic the reaction inside the fuel reactor can be slightly endothermic or exothermic (Abad et al. (2006a) [2]). The thermodynamic state of the fuel reactor reactions depends on the choice of oxygen carrier and fuel.

As example, if pure methane is used as fuel and a nickel based oxygen carrier the following reactions occur:

air-reactor $$4Ni + 2O_2 \rightarrow 4NiO \qquad \Delta H_{1200} = -938{,}2\frac{kJ}{mol} \qquad \text{(reac 2-4)}$$

fuel-reactor $$CH_4 + 4NiO \rightarrow CO_2 + 2H_2O + 4Ni \qquad \Delta H_{1200} = 136{,}5\frac{kJ}{mol} \qquad \text{(reac 2-5)}$$

While the whole amount of released energy is the same as in case of a conventional firing which can be derived from (reac 2-4) and (reac 2-5) leading to the global reaction:

Total reaction $$CH_4 + 2O_2 \rightarrow CO_2 + 2H_2O \qquad \Delta H_{1200} = -802{,}7\frac{kJ}{mol} \qquad \text{(reac 2-6)}$$

CLC compared to conventional firing offers a lot of advantages. The flue gas exiting the air reactor is harmlessly consisting of mainly nitrogen and some excess oxygen. If the chemical looping system is designed deftly the formation of thermal nitrogen oxides (NO_x) will be inhibited due to the absence of hot spots, evolving for example from flames, and because of low global temperatures inside the reactor. As mentioned before the fuel reactor exhaust gases consist mainly of carbon dioxide and water vapor. After condensation of the water the resulting stream consists mainly of CO_2. Ideally the CO_2 is ready for compression and storage. This represents the major advantage of CLC as almost all other discussed CO_2 capture methods require three fourths of the energy demand for carbon capture and storage ([59]).

2.1.1 Reactor design concepts

Practically a chemical looping reactor can be designed in many different ways. Fluidized beds seem to fit perfectly the requirement of a good gas-solid contact. From this, a lot of concepts have been developed. Two of them are going to be introduced in the following.

CLC Concept at Chalmers University of Technology

The chemical looping combustion reactor concept of the Chalmers University of Technology is built up of a high velocity riser and a low velocity bubbling bed and can perform 10 kW_{th}.

The air reactor (1) is fluidized by air and transports the oxygen carrier, after separation from the air via a cyclone separator (2) to the bubbling bed fuel reactor (3). The exhaust gases of the fuel reactor are cooled down and the water content is released. The residual gas consists mainly of CO_2 and is compressed for further storage. The non condensable gases are conducted back to the fuel reactor. Additionally this design has got a bleed in order to get rid of inert fuel contents.

This design suffers from the risk of fuel bypass via the bubble phase of the fluidized bed (cf. [28]).

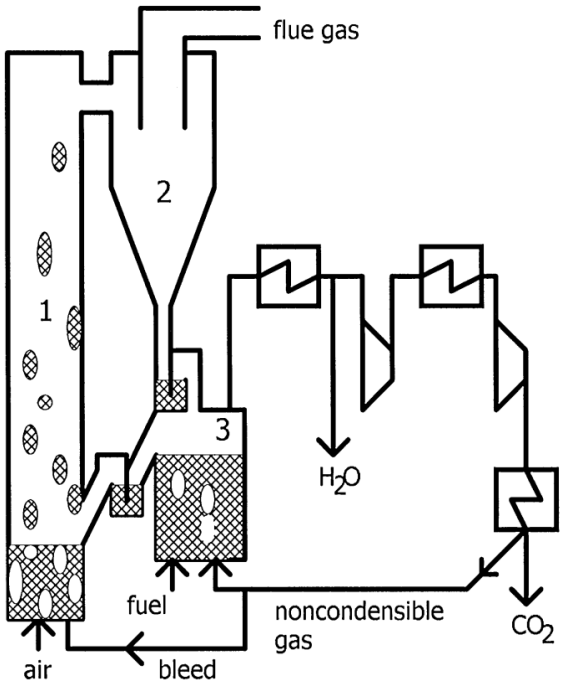

Figure 11 Layout of the chemical looping combustion process used at Chalmers University [41]

CLC Concept of the Vienna University of Technology

After intensive research on the CLC technology at the Institute for Chemical Engineering at the Vienna University of Technology a 120 kW_{th} pilot rig has been erected. Similar to the Chalmers technology two entangled fluidized beds are operated. Therefore, the air-reactor is fluidized with cold or preheated air and operates as a fast fluidized bed. After the oxygen enriched solids are entrained from the air reactor they are separated in a cyclone and transported via a loop seal to the fuel reactor. The fuel reactor is fluidized with a gaseous fuel and operates, in contrast to the Chalmers reactor, close to turbulent regime. The entrained particles are transported back into the fuel reactor after separation from the exhaust gases via a cyclone. The oxygen depleted oxygen carrier is then transported via a loop seal back to the air reactor where it is again oxidized. The exhaust gases leave the reactors and are cooled down and analyzed in order to evaluate the fuel

conversion rate and the leakage of the loop seals. In this design the air reactor is the limiter of the global solid circulation rate which is accomplished by staged air injection into the air reactor.

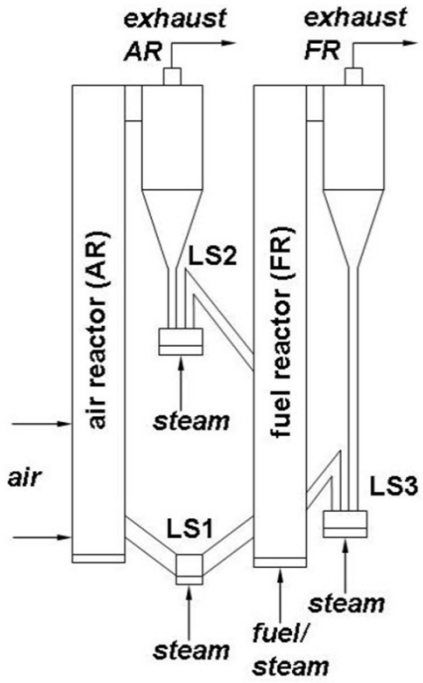

Figure 12 Layout of the chemical looping process used at Vienna University of Technology

Design criteria

In order to optimize a dual-fluidized-bed chemical-looping system two major considerations have to be pointed out:

- The global solid circulation rate between the air and the fuel reactor should be high and
- the gas solid contact in both reactors must be maximized.

Bubbling-Fluidized-Bed (BFB) fuel reactors suffer from the risk of gas bypass through the bubble phase resulting in a significant slip of unconverted fuel. That would result in decreased fuel conversion rates hardly tolerable for an optimized process. To decrease the fuel slip two different approaches are possible, according to Kolbitsch et al. [37].

- Decreased gas velocities, limited by the operation parameters of bubbling bed regime, in order to decrease the residence time of the fuel in the reactive zones of the reactor. This would result in large fuel reactor bed cross section areas and mass of solid inventory.
- Or increase the gas velocity to operate the fuel reactor in a turbulent or fast fluidization regime. These regimes would offer the opportunity that the gas solid contact along the overall height of the reactor and lower solid inventories are required for operation.

Because of this the pilot rig at the Vienna University of Technology is performed as a DCFB-System. A further advantage of the DCFB-Design approach is the inherent stabilization of solid hold-up obtained by the direct hydraulic link between the reactors. Hence the state of the air reactor is the only controller of the global circulation ratio the fuel reactor can be operated independently and its operation state can be optimized with respect to maximum fuel conversion.

Design parameters of the reactor system

Table 4 Design parameters and constants for the CLC reactor system

Parameter	Symbol	Value	Unit
Fuel power (natural gas)	P_{fuel}	120	kW
Lower heating value of fuel	LHV	48,8	MJ/kg
O_2 demand for oxidation	O_{min}	3,88	kg/kg
Air demand for oxidation	l_{min}	16,8	kg/kg
Design air/fuel ratio	λ	1,20	-
Temperature air reactor	T_{AR}	1223	K
Temperature fuel reactor	T_{FR}	1123	K
Oxygen carrier		Ni/NiO	
Active Ni content		40	%
Oxygen ratio	R_0	0,084	%
Particle size	D_m	0,120	mm
Apparent density	ρ_a	3200	kg/m³

2.1.2 Oxygen carrier

The oxygen carrier has to be chosen with respect towards:

- high reactivity towards the fuel gas and air,
- high endurance,
- high resistance to attrition and breakage,
- no agglomeration,
- no carbon deposition
- and environmental and economical aspects.

A great variety of possible oxygen carrier materials have been proposed in the literature. A comprehensive overview can be found in Marcus Johansson et al. [34]. One of the most important factors for the selection of oxygen-carrier material is their oxygen transport capacity, also called oxygen ratio. It was introduced by Mattison et al. 2003 [46] and is defined as

$$R_0 = \frac{m_{ox} - m_{red}}{m_{ox}} \qquad \text{(eqn 2-1)}$$

where m_{ox} and m_{red} are the masses of the oxidized and reduced form of the metal oxide. An oxygen carrier with a great oxygen transport capacity is beneficial as the required amount of oxygen carrier circulation is reduced. The oxygen transport capacities of some oxygen carriers can be found in the table below.

Table 5 Oxygen carrier transport capcities from [46]

Redox System M_yO_x/M_yO_{x-1}	Oxygen-Carrier Transport Capacity R_0
Fe_2O_3/Fe_3O_4	0,03
Mn_3O_4/MnO	0,07
CuO/Cu	0,20
NiO/Ni	0,21
CoO/Co	0,21

Usually the oxygen carrier consists of a metal oxide combined with an inert material which acts as a porous support. That provides a higher surface area for reaction and the inert increases the mechanical strength and attrition resistance. Usually alumina Al_2O_3 is used as inert core of the OC particle. Therefore, the real oxygen transport capacity of the oxygen carrier is lower depending on the amount of inert used. From that follows

$$R_{0,OC} = R_0 \cdot x_{MeO} \qquad \text{(eqn 2-2)}$$

where x_{MeO} represents the mass fraction of metal oxide in the fully oxidized state.

Due to deactivation of parts of the reactive material during the patch process the oxygen-carrier batch transport capacity has to be evaluated by measurement of the mass-change after seasoning the particle at sufficient temperature under an oxidizing and reducing ambient. Nevertheless, the theoretically calculated oxygen carrier transport capacity R_0 is an important value to decide which kind of material to use.

Apart from the theoretical transport capacity it was found that material like copper requires a great amount of inert support to avoid agglomeration when used in fluidized beds (de Diego et al. 2005 [18]). Hence, if CuO is used as RedOx-System the patch requires approximately 90wt% of substrate.

In order to evaluate the state of a partially oxidized oxygen carrier the so called degree of oxidation was introduced.

$$X = \frac{m - m_{red}}{m_{ox} - m_{red}} \qquad \text{(eqn 2-3)}$$

Here m expresses the actual weight of the partial oxidized particle. Since usually the oxygen carrier consists also of inert material another measurement was derived. The new value is the mass conversion based on the mass of the oxygen carrier.

$$\omega = \frac{m}{m_{ox}} = 1 + R_0 \cdot (X - 1) \qquad \text{(eqn 2-4)}$$

This new value is another important value for the selection of the OC-material. Because the time deviation of ω correlates to the reactivity of the material batch. Mattisson et al. [46] have carried out experiments on the reactivity of different oxygen carrier batches.

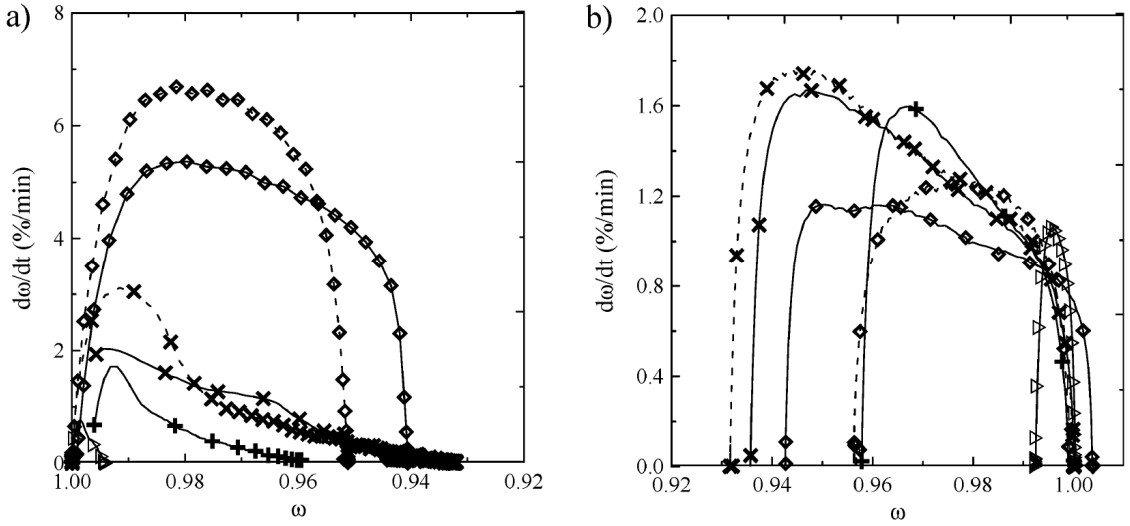

Figure 13 The mass-based rate *dω/dx* as a function of ω for (a) the reduction and (b) oxidation at 850 °C (solid) and 950°C (dashed): CuO ◊, CoO +, Mn_3O_4 ∇, NiO x [46]

From these set of definitions the required amount of bed material can be calculated.

$$m_{bed} = \frac{\omega \cdot \dot{m}_0}{d\omega/dt} \quad \text{(eqn 2-5)}$$

Here $\dot{m}_0$ represents the stoichiometric mass flow of oxygen needed for complete conversion of the fuel.

Additionally the rate of circulation of oxygen carrier between the air and fuel reactor can be calculated

$$\dot{m}_{sol} = \frac{\omega_{AR} \cdot \dot{m}_0}{\Delta\omega} \quad \text{(eqn 2-6)}$$

where ω_{AR} is the conversion in the air reactor and $\Delta\omega$ is the conversion difference between the air and the fuel reactor.

2.1.3 Thermodynamic limits

If two materials or substances react the products try to reach the thermodynamic equilibrium. Therefore, the concentrations of the substances after the reaction can be calculated by calculation of the thermodynamic equilibrium.

Calculation of the thermodynamic equilibrium

In order to calculate a change of state the first and second laws of thermodynamics are quite important.

1st law of thermodynamics

$$du = dq + dw$$
$$h = u + p \cdot v \quad \text{(eqn 2-7)}$$

2nd law of thermodynamics

$$ds = ds_q + ds_{irr}$$
$$ds_q = \frac{dq}{T} \quad \text{(eqn 2-8)}$$

For calculation of a state in thermodynamic equilibrium the variable of state specific Gibbs-function was introduced:

$$g = g(T,p) = h - T \cdot s \quad \text{(eqn 2-9)}$$

Here h stands for the specific enthapy, T for the temperature and s for the entropy. According to the second law of thermodynamics (eqn 2-8) follows that in a state of equilibrium the entropy reaches a maximum. By use of the so called Legendre-Transformation this statement can be transformed to a statement about the connection between equilibrium and the Gibbs function. It follows that a system is in thermodynamic equilibrium if the Gibbs function reaches a minimum.

$$G(p,T) \rightarrow min$$
$$dG(p,T) = 0 \quad \text{(eqn 2-10)}$$

Hence the Gibbs-function depends on the pressure and the temperature the concentrations of the reactants and products also vary with these factors.

Limits of the oxygen carrier

Because of the thermodynamic equilibrium there will be still some "unburned" in the fuel reactor exhaust. The thermodynamic equilibrium concentration depends on the oxygen carrier material used. If the fuel reactor operates at 850°C, 1 bar and methane (CH_4) is used as fuel the resulting equilibrium fuel reactor exhaust composition is shown in Figure 14.

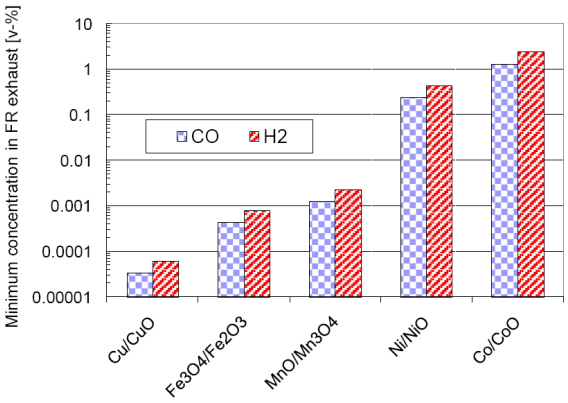

Figure 14 Thermodynamic equilibrium exhaust compositions with pure methane as fuel at 850°C and 1 bar [54]

This comparison shows that especially if nickel or cobalt is used as oxygen carrier the amount of unconverted fuel is rather high which may require a polishing step of the exhaust.

2.2 Chemical looping reforming

Hydrogen is used in many sectors of industry for example for NH_3 synthesis, for refining, in metallurgy and for manufacturing of electronic components. In addition to this, hydrogen is a carbon free energy carrier offering the opportunity to propel systems without hazardous exhaust gases. Even though, there is a great variety of possible hydrogen production processes. Nowadays hydrogen is mainly produced by the conversion of fossil fuel due to economical aspects.

Chemical looping reforming is a process for the production of hydrogen from fossil fuels. Chemical looping reforming utilizes the same basic principles as chemical looping combustion. In difference CLR(a) produces hydrogen and carbon monoxide instead of heat.

The production of hydrogen from carbon based fuels has to be carried out via the intermediate step of synthesis gas production. There are the following possibilities to produce synthesis gas:

- by so called *"steam reforming"* mainly utilized for natural gas reforming,

$$C_nH_m + nH_2O \longrightarrow nCO + \left(n + \frac{1}{2}m\right)H_2 \qquad \text{(reac 2-7)}$$

- via *"partial oxidation"* of the combustibles mainly utilized for heavier fuels such as oil or coal,

$$C_nH_m + \left(\frac{1}{2}n\right)O_2 \longrightarrow nCO + \left(\frac{1}{2}m\right)H_2 \qquad \text{(reac 2-8)}$$

- or by "CO_2 reforming" if a high CO content is required.

$$C_nH_m + nCO_2 \longrightarrow (2n)CO + \left(\frac{1}{2}m\right)H_2 \qquad \text{(reac 2-9)}$$

After synthesis gas production the product gas is upgraded in a water-gas shift reactor where it is refined by means of the water-gas shift reaction:

$$CO + H_2O \longrightarrow CO_2 + H_2 \qquad \Delta H_0 = -41{,}2\,\frac{\mathrm{kJ}}{\mathrm{mol}} \qquad \text{(reac 2-10)}$$

The remaining carbon dioxide has to be separated from the gas in order to receive a stream consisting mainly of hydrogen. The most common separation processes are pressure swing adsorption or physical or chemical absorption by amine solvents. An alternative is membrane separation which shows promising results in laboratory scale.

For hydrogen production with chemical looping two different options are discussed. They are going to be introduced in following.

2.2.1 Autothermal chemical looping reforming CLR(a)

Chemical looping autothermal reforming was originally proposed by Mattissen et al. [45]. Similar ideas have also been explored by Stobbe et al. [60] and Fathi et al. [26].

The layout of a chemical looping autothermal reforming apparatus is mainly the same as that for chemical looping combustion.

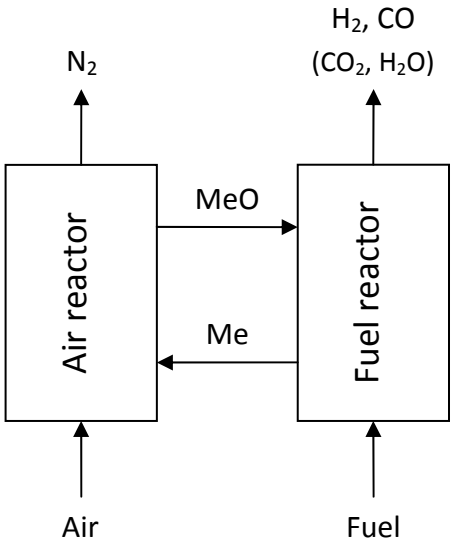

Figure 15 Layout of a chemical looping autothermal reformer

The major difference is that the reactors are operated substoichiometric. Therefore, parts of the fuel undergoes a partial oxidation (reac 2-13), but also complete oxidation (reac 2-12), steam reforming (reac 2-7) and CO_2 reforming (reac 2-9) can occur. Steam could be added to the fuel in order to enhance steam reforming (reac 2-7).

Oxygen carrier re-oxidation:

$$MeO_{\alpha-1} + \frac{1}{2}O_2 \rightleftharpoons MeO_\alpha \qquad \text{(reac 2-11)}$$

Complete oxidation:

$$C_nH_m + \left(2n + \frac{1}{2}m\right) MeO \longrightarrow nCO_2 + \left(\frac{1}{2}m\right) H_2O + \left(2n + \frac{1}{2}m\right) Me \qquad \text{(reac 2-12)}$$

Partial oxidation:

$$C_nH_m + nMeO \longrightarrow nCO + \left(\frac{1}{2}m\right) H_2 + nMe \qquad \text{(reac 2-13)}$$

The amount of heat released or consumed inside the reactors depends on the fuel and the behavior of the oxygen carrier. The re-oxidation of the oxygen carrier (reac 2-11) inside the air reactor is always strongly exothermic. Steam reforming (reac 2-7) and CO_2 reforming (reac 2-9) are always strongly endothermic. The reaction of complete or partial oxidation (reac 2-12) is usually slightly endothermic but also can be exothermic for some fuel oxygen carrier combinations.

Since the fuel reactor has to be in equilibrium according to the first law of thermodynamics usually sensible heat has to be transported from the exothermic air-, to the fuel-reactor via the oxygen carrier.

If methane is used as fuel, nickel oxide (NiO) as oxygen carrier and the reactor temperature is $1200\ K$ the following reactions occur in the system.

OC regeneration:
$$Ni + \frac{1}{2}O_2 \rightarrow NiO \qquad \Delta H_{1200} = -234\ \frac{\text{kJ}}{\text{mol}} \quad \text{(reac 2-14)}$$

Complete oxidation:
$$CH_4 + 4NiO \longrightarrow CO_2 + 2H_2O + 4Ni \qquad \Delta H_{1200} = 136\ \frac{\text{kJ}}{\text{mol}} \quad \text{(reac 2-15)}$$

Partial oxidation:
$$CH_4 + NiO \longrightarrow CO + 2H_2 + Ni \qquad \Delta H_{1200} = 211\ \frac{\text{kJ}}{\text{mol}} \quad \text{(reac 2-16)}$$

Steam reforming:
$$CH_4 + H_2O \longrightarrow CO + 3H_2 \qquad \Delta H_{1200} = 226\ \frac{\text{kJ}}{\text{mol}} \quad \text{(reac 2-17)}$$

CO_2 reforming:
$$CH_4 + CO_2 \longrightarrow 2CO + 2H_2 \qquad \Delta H_{1200} = 259\ \frac{\text{kJ}}{\text{mol}} \quad \text{(reac 2-18)}$$

The offgas of a CLR(a) fuel reactor consists mainly of H_2, CO, CO_2 and H_2O but also small amounts of unconverted fuel. The amount of unconverted fuel depends on the reactor temperature and pressure and is limited thermodynamically. For example, at atmospheric pressure and a fuel reactor temperature of approximately 800°C 99% conversion of methane is obtained. A pressure of 15 bar would require a temperature of more than 1000°C for the same conversion.

Special demands note on oxygen carrier for autothermal chemical looping reforming

Generally every oxygen carrier feasible for chemical looping combustion can also be used for CLR(a). Anyway, a few of them have shown a special suitability regarding hydrogen production. Especially nickel as oxygen carrier attracts great attention because of its strong catalytic properties towards methane conversion. Additionally nickel forms sulfur components. Usually this will result in catalyst poisoning. In case of CLR(a) it is assumed that the nickel-sulfur components will be transported with the reduced metal-oxide stream to the air-reactor where the sulfur is released from the oxygen carrier. Therefore, CLR(a) offers the opportunity of inherent sulfur separation.

2.2.2 Chemical looping steam reforming

Chemical looping steam reforming CLR(s) was introduced by Rydén et al. [43]. CLR(s) uses commonly known steam reformer principles.

Generally CLR(s) is a CLC process in which the produced heat is used to operate a conventional steam reformer. Therefore, the steam reformer is placed in the oxygen carrier loop. After separation of the hydrogen from the steam reformer product-gas the residual gas is conducted to the fuel reactor where it is used to heat the CLC system.

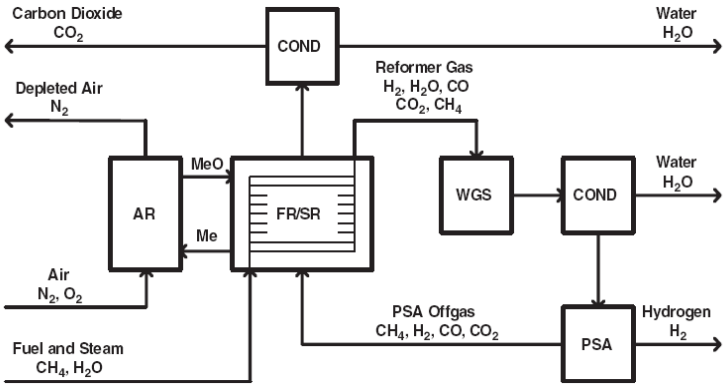

Figure 16 Possible layout for chemical looping steam reforming [43]

In common steam reformers methane reformation takes place inside tubes filled with a catalyst. The required heat for endothermic steam reforming is provided by direct firing of a fuel inside a furnace utilizing the required high heat fluxes by mainly radiation. Because of that, the reformer tubes suffer from high thermal stress and the reactor design is therefore rather complex.

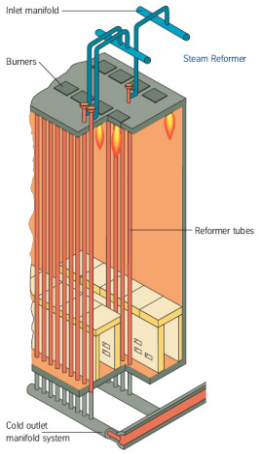

Figure 17 Figure of a conventional steam reformer furnace

For CLR(s) the reformer tubes are not directly heated by flame but placed into a bubbling bed. Due to the optimal contact of the bed material and the reformer tubes and because of the extensive inner bed-material circulation rates driven from the bubble-phase movements the heat transfer is excellent (see [30]). Caused by the extensive heat exchange it is practically possible to assume that the wall temperature of the heat exchanger is almost equal to bed temperature. Hence, the design limiting parameter for reformer tubes placed inside a fluidized bed is the heat transfer coefficient of the tube to the catalyst and the gas.

The reformer tubes are filled with a nickel based catalyst which is required to initialize steam reforming. As nickel tends to react with sulfur its catalytic behavior will be inhibited at the

presence of sulfur compounds. Therefore it is essential that the sulfur is removed from the fuel prior steam reforming. After steam reformation the gas stream is purified via the water-gas-shift reaction (reac 2-10). In the next process step most of the water is removed by condensation and afterwards the hydrogen is separated by the use of for example a pressure-swing-adsorption apparatus. The remaining tail-gas mixture consisting mainly of CH_4, H_2, CO and CO_2 is conducted back to the fuel reactor where it is oxidized to empower the cycle.

In chemical looping steam reforming the reformation takes place at pressures of approximately 15-40 bar (see [22]) and with steam added. The amount of steam added is determined by the so called steam-to-carbon ratio which is defined as the coefficient of the molar amount of steam added and the molar amount of organic carbon and carbon monoxide in the reformer feed gas.

$$S/C = \frac{mole\ H_2O}{mole\ C} \qquad \text{(eqn 2-11)}$$

According to Dybkjaer [22] inside a steam reforming reactor the steam reforming (reac 2-7), the water-gas shift (reac 2-10) and the CO_2 reforming reaction (reac 2-9) occur in parallel if it is assumed that no free oxygen is present. For full conversion of hydrocarbons to hydrogen in an endothermal steam reformer at least a steam-to-carbon ratio of 2 is required. Regarding to the principle of le Chatelier [4] an excess of steam in the reformer feed gas will increase the hydrogen yield. Therefore, the S/C-ratio typically ranges from 2,7 to 4,5 (see [25]).

The advantage of CLR(s) is that the produced hydrogen is directly provided at high pressure and therefore is directly usable i.e. in chemical processes. In difference the CLR(a) product gas is at atmospheric pressure which requires compression before it can be used.

2.3 Power generation aspects

Chemical looping combustion and reforming show great potential for greenhouse gas emission free power or hydrogen production. While a chemical looping combustion system can be used for direct power generation a chemical looping reforming system requires an additional power generation cycle, for example a combined cycle power plant. Therefore, CLC is a cycle for direct- and CLR on for indirect-power production. Additionally, chemical looping reforming offers the opportunity of delivering hydrogen for use in different applications, for example in chemical industry.

Chemical looping combustion and chemical looping autothermal reforming in laboratory scale have been demonstrated and shown great potential. The next step is to demonstrate this technology in the next scale. Therefore, this study focuses on CLC and CLR systems at a scale of 10MW fuel power.

2.3.1 Efficiency definitions

In order to compare the discussed cycles some efficiencies have to be defined.

The so called energetic or thermal efficiency η_{th} is defined as the coefficient of the power delivered to the fuel-injected energy. This value is used to compare the power-generation cycles.

$$\eta_{th} = \frac{P_{produced}}{P_{applied}} = \frac{P_{gen} - P_{compressor} - P_{pump}}{\dot{m}_{fuel} \cdot LHV_{fuel}} \quad \text{(eqn 2-12)}$$

The exergetic efficiency ζ is defined as the coefficient of the exergy produced to the applied exergy. The exergetic efficiency is the more representative efficiency value because it compares only the "true" energies to each other.

$$\zeta = \frac{E_{produced}}{E_{applied}} = \frac{P_{gen} - P_{compressor} - P_{pump}}{E_{fuel}} \quad \text{(eqn 2-13)}$$

Reviewers criticized that chemical looping combustion has got a poor fuel energy conversion compared to conventional firing. Therefore, the loss of unburned fuel is defined according to EN 12952 representing the amount of unburned fuel in the reactor exhaust in percent to the fuel input. For the CLC-process the definition of the unburned fuel of the EN standard has to be extended since in a CLC-process the unburned fuel consists not only of carbon monoxide but also of hydrogen. Therefore, the loss due to unburned fuel was defined as following.

$$l_u = \frac{\dot{m}_f \cdot LHV_f - \left(\dot{m}_f \cdot LHV_f - \dot{m}_{off\_gas} \cdot LHV_{off\_gas}\right)}{\dot{m}_f \cdot LHV_f}$$
$$l_u = \frac{\dot{m}_{off\_gas} \cdot LHV_{off\_gas}}{\dot{m}_f \cdot LHV_f} \quad \text{(eqn 2-14)}$$

2.3.2 Chemical looping combustion combined with a steam cycle

A steam-power process is a closed clockwise-turning thermodynamic working cycle which converts heat into technical work. Often a steam cycle is additionally used for heat extraction of industrial steam or for district heating. Steam-to-power cycle is the dominating thermodynamic working cycle for production of electrical power. A steam cycle is a cycle in which heat is supplied and removed at a lower temperature level. Therefore, it is limited by the Carnot factor.

The Carnot factor describes the maximal possible efficiency of a working cycle with heat supply and removal. The Carnot efficiency is defined as the coefficient of the temperature difference of heat supply to heat removal and the temperature of heat supply.

$$\eta_C = \frac{T_{heat-supply} - T_{heat-removal}}{T_{heat-supply}} = 1 - \frac{T_{heat-removal}}{T_{heat-supply}} \quad \text{(eqn 2-15)}$$

The thermodynamic referred steam cycle is the Clausius-Rankine-Cycle discussed below.

The Clasius-Rankine-Cycle

The Clausius-Rankine-Cycle is the simplest steam to power cycle configuration. The cycle consists mainly of a feed water pump; a steam generator; a turbine and a condenser (see Figure 18).

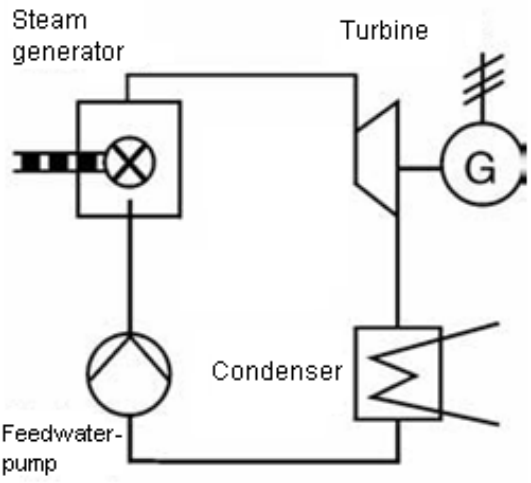

Figure 18 Flow sheet of a Clausius-Rakine-Cycle. Adopted from [21]

After compression in the liquid phase by the feed pump (1→2) the process fluid is heated up inside the steam generator (2→3). Afterwards the highly energetic fluid is expanded to condenser pressure by use of a steam turbine (3→4). Inside the condenser the steam is condensed (4→1) and the cycle starts again. Because of erosion turbines can't work with fluids in two-phase state. Hence, if a regular fluid is used superheating is requires. For water as a working fluid the referring T-s-diagram is schematically shown below.

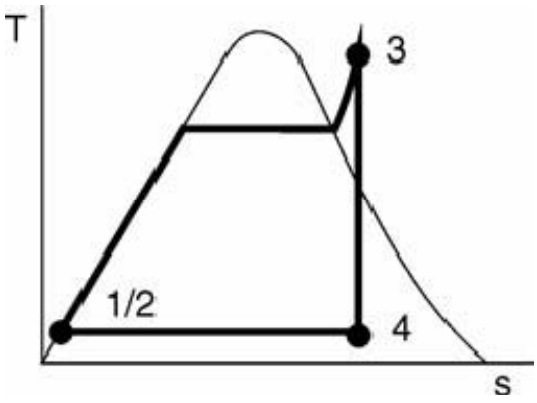

Figure 19 T-s-diagramm of the Clausius-Rankine-Cycle [21]

As mentioned before the efficiency of a steam cycle is limited by the Carnot factor. In order to increase the efficiency of a steam cycle the cycle has to be designed with maximal possible similarity to the Carnot process. Hence, there are two practical possibilities for increasing the thermal efficiency of the steam cycle.

The steam cycle with intermediate superheating

Intermediate superheating means that the working fluid is reheated after expansion in a first turbine stage. Intermediate superheating increases the so called thermodynamic-mean-temperature. The thermodynamic mean temperature is the mean temperature of heat supply. The thermodynamic mean temperature is equivalent with the temperature of heat supply if a Carnot process. Hence, by increasing the thermodynamic mean temperature the thermal efficiency is increased.

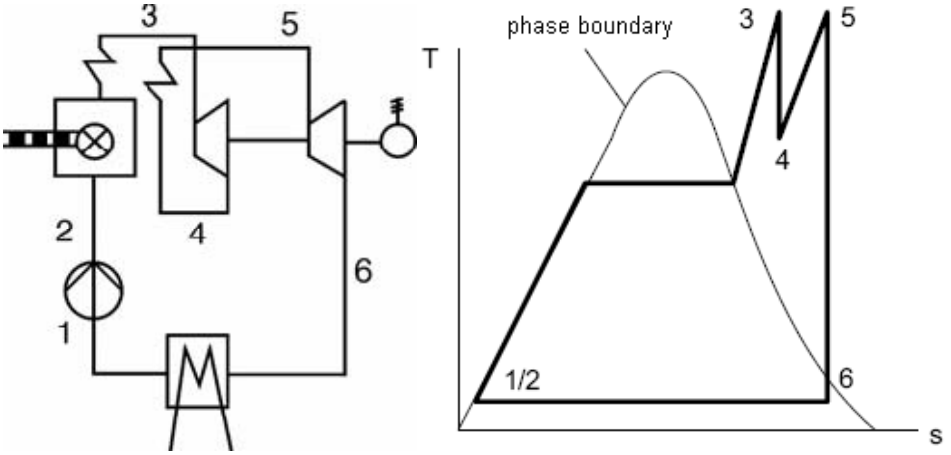

Figure 20 Flow sheet and T-s-diagram of steam cycle with intermediate superheating. Adopted from [21]

Intermediate superheating (Figure 20) is only a viable strategy to increase the steam cycle efficiency at large scale applications.

The steam cycle with regenerative feeding water preheating

According to the second law of thermodynamic every heat exchanges generate a loss of exergy. The exergy loss depends on the temperature difference of the heat exchange and increases with increasing temperature difference. As a consequence heating cold feeding water with high temperatures is thermodynamically inefficient. The steam cycle efficiency can be increased by inner cycle movement of heat. This is usually achieved by heating the feeding water with low caloric steam. If the feeding water enters the steam generator at higher temperature levels the thermodynamic mean temperature of heat input rises. Hence, the efficiency of the cycle increases. The flow sheet of such a configuration and the temperature-entropy diagram is shown below.

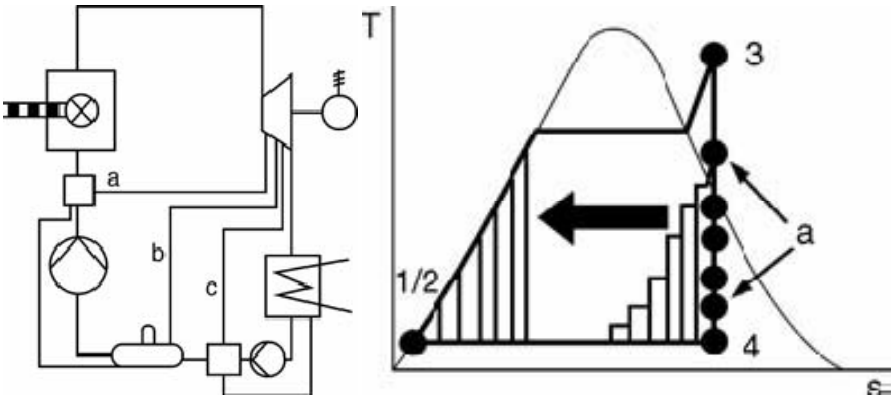

Figure 21 Flow sheet and T-s-diagram of steam cycle with regenerative feeding water preheating [21]

Feed water preheating increases the exergetic efficiency of the steam generator by increasing the thermodynamic mean temperature of heat supply but decreases the exergetic efficiency of the steam turbine process by consuming steam for preheating. Therefore, there is an optimal preheating temperature. The optimal preheating temperature can be calculated by increasing the exergetic efficiency to a maximum.

The exergetic efficiency of the steam generator is calculated as follows:

$$\zeta_{SG} = \eta_{SG} \cdot \frac{LHV}{e_f} \cdot \frac{e_{LS} - e_{ph}}{h_{LS} - h_{ph}} = \eta_{SG} \cdot \frac{LHV}{e_f} \cdot \left(1 - \frac{T_{amb}}{T_m^*}\right) \qquad \text{(eqn 2-16)}$$

with the rectified thermodynamic mean temperature:

$$T_m^* = \frac{h_{LS} - h_{ph}}{s_{LS} - s_{ph}} \quad \text{(eqn 2-17)}$$

The exergetic efficiency of the process is calculated as following:

$$\zeta_P = \frac{-w_t}{e_{LS} - e_{ph}} \quad \text{(eqn 2-18)}$$

$$-w_t = \left(-w_{t,ST}\right) - w_{t,FWP} \quad \text{(eqn 2-19)}$$

The total exergetic efficiency can be calculated as following:

$$\zeta = \zeta_{SG}^{\uparrow} \cdot \zeta_P^{\downarrow} \quad \text{(eqn 2-20)}$$

Table of symbols

Exergetic efficiency of the steam generator	ζ_{SG}
Exergetic efficiency of the process	ζ_P
Thermal efficiency of the steam generator	η_S
Lower heating value and Exergy of the fuel	$LHV \ / \ e_f$
Enthalpy and Exergy of the live steam	$h_{LS} \ / \ e_{LS}$
Enthalpy and Exergy of the feeding water after preheating	$h_{ph} \ / \ e_{ph}$
Temperature of the ambient	T_{amb}
Increased thermodynamic mean temperature	T_m^*
Technical work	w_t
Technical work of the steam turbine	$w_{t,ST}$
Technical work of the feed water pump	$w_{t,FWP}$

Typical qualitative curves for the enhancement of the thermal efficiency depending on the stages of preheating (n) and the preheater temperature is shown below.

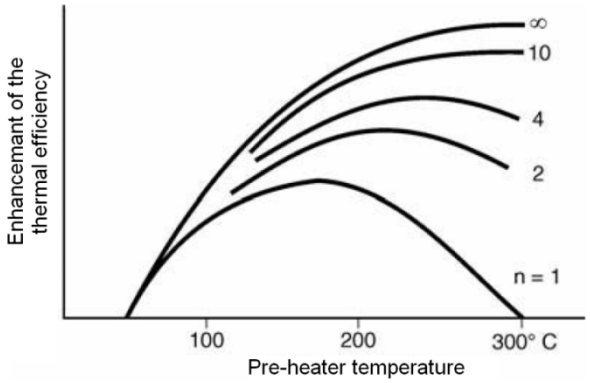

Figure 22 Increase of thermal efficiency depending on the temperature of preheating and on the number of preheating stages n adopted from [55]

Possible process design concepts

As summarized before, there are different possibilities to increase the thermal efficiency of a steam cycle. The type of improvements depends on economic reasons. Intermediate superheating is quite expensive but, if certain live steam parameters are required, indispensable. At lower steam qualities intermediate superheating it is a techno-economic question and hard to generally decide without investigation of the whole plant concept.

At the scale discussed in this study (P_{fuel}=10 MW) intermediate superheating is typically not applied. On the other hand feed water preheating is feasible because water to water heat exchangers are compact, inexpensive and very effective due to the high heat transfer. Therefore, the proposed concept is a simple steam cycle with a two stage feed water preheater without intermediate superheating.

In a chemical looping system the reactor exhaust gas temperatures are limited by the physical properties of the oxygen carrier. Hence, the amount of heat released with the gas streams is limited.

According to thermodynamics it is impossible to withdraw sufficient heat from the air reactor by the air if the CLC reactor system is operated close to stoichiometric conditions and no additional reactor cooling is applied. The excess of heat must be directly withdrawn from the reactor system. To extract the heat a fluidized bed cooler can be used (with fluidized bed cooler design) or the air reactor can be cooled with excess air (λ-cooled design). The process schemes of both process designs are shown below.

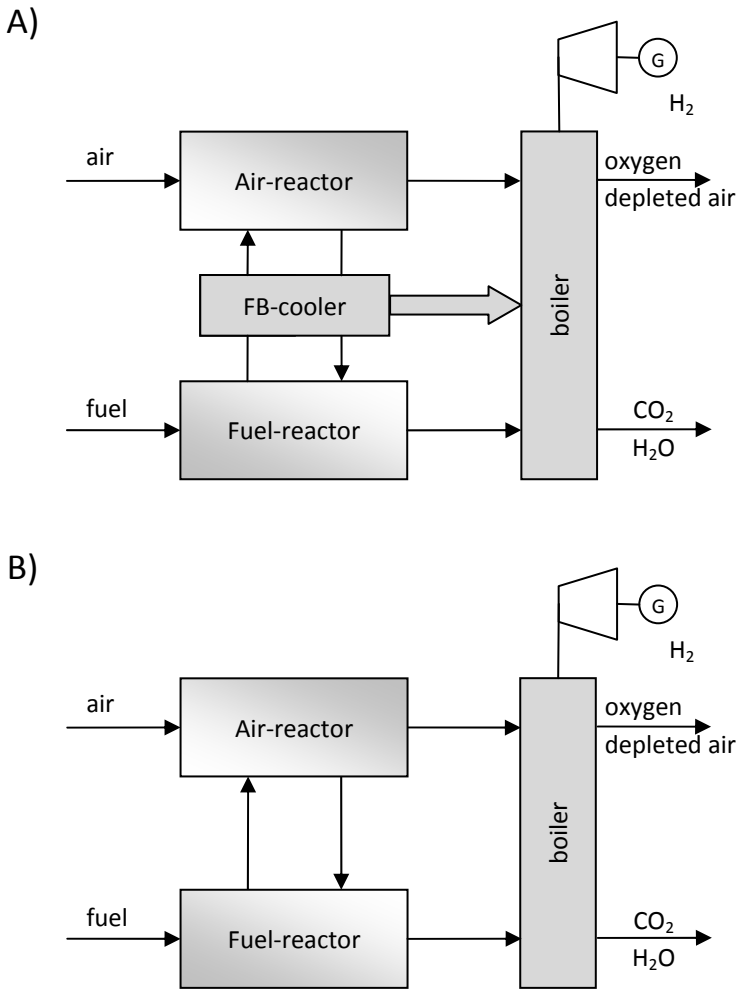

Figure 23 Possible process schemes for an CLC-Power-Cycle
A) with fluidized bed cooler-,
B) λ-cooled-design

Theoretical comparison of the concepts

The use of a fluidized bed cooler is quite a smart design variant. The advantage of a fluidized bed cooler is that the temperature of the heat deliverer (the bed material) in general is quite high. Therefore, the design of the cycle will be easier. Additionally, the heat transfer coefficient from the bed to the heat exchanger is much higher than of a gas-gas heat exchanger. As a result fluidized bed coolers are quite compact and often used in fluidized bed boiler design.

On the other hand the reactor design of the λ-cooled design concept is much simpler. This is an advantage especially in small scale applications due to lower investment costs.

The disadvantage of the λ-cooled design concept is that the stream exiting the air reactor leaves the boiler at higher states of total exergy. That is easy to explain if the two systems are compared directly. If both exiting streams had the same temperature (and therefore the same relative exergy) the one from the λ-cooled design would have a greater mass flow and therefore a higher absolute exergy. Furthermore, the increased mass-flow inside the air reactor requires greater cross section areas since the fluidization velocity should normally remain the same. That would result in higher bed inventories and the design of the nozzle plate would be more complex and as a consequence the system would become more expensive.

A general proposition about the optimum is hard to find since the coherences are rather complex. Therefore, the two designs are compared in detail in chapter 4.1.

2.4 Hydrogen production aspects

Power generation through the intermediate step of hydrogen production seems to have great potential when the hydrogen is used as fuel of a combined cycle. This is the case because modern combined cycles have got very high efficiencies. In addition, the hydrogen can also be used for other purposes. Therefore, it is the aim to increase the hydrogen yield.

2.4.1 Efficiency definitions

Additionally to the exergetic efficiency (see chapter 2.3.1) chemical looping reforming requires extra efficiency definitions.

In case of steam reforming the reactions have got an optimal point regarding hydrogen yield. Therefore, the hydrogen-production-efficiency ξ is introduced which is defined as the coefficient of the hydrogen produced and the in maximal producible amount at the occurring steam to carbon ratio, temperature and pressure.

$$\xi = \frac{\dot{m}_{H_2 prod}}{\dot{m}_{H_2 max}} \qquad \text{(eqn 2-21)}$$

Similar to the loss of carbon due to unburned fuel the carbon loss is introduced. It is defined as the coefficient of the lost amount of carbon to the amount of carbon in the feed and it expresses the relative amount of carbon lost for capture.

$$l_C = \frac{\dot{m}_{C\_lost}}{\dot{m}_{C\_feed}} \qquad \text{(eqn 2-22)}$$

The definition of the loss of carbon is needed since some of the processes require a bleed to ensure that inert gases cannot accumulate inside the circuit.

2.4.2 Chemical looping steam reforming

The main target of CLR(s) is to increase the amount of hydrogen produced. Therefore, a CO-Shift reactor is used in conventional steam reforming plants. In case of CLR(s) the efforts are different and it might be also a possible process design to simplify the process design omitting the CO-Shift. Figure 24 shows the process scheme of a CLR(s) process.

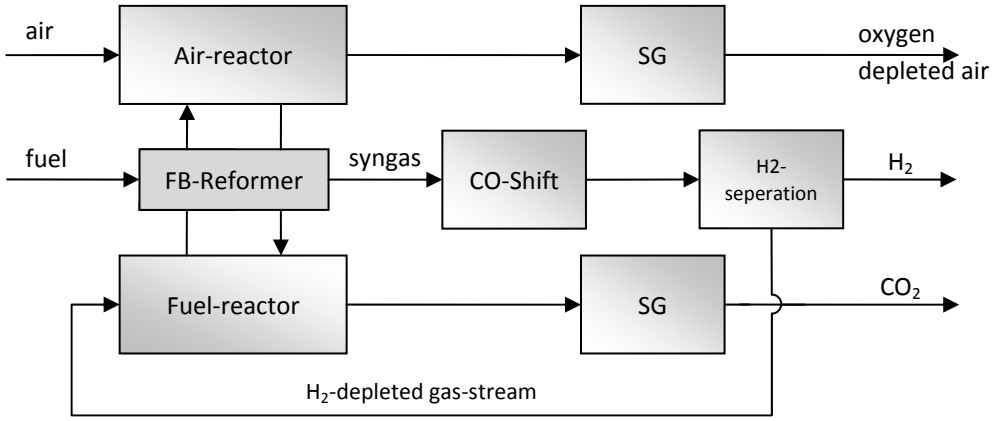

Figure 24 CLR(s) process scheme (SG – steam generator)

2.4.3 Chemical looping autothermal reforming

CLR(a) generally offers a great variety of possible process layouts. With respect to carbon-capture and storage it has to be the aim to reduce the amount of released carbon. This is achieved by recycling the unconverted carbons in the cycle until they are finally converted to carbon dioxide. The recycling loop can be designed in many ways depending on the plant scale and requirements. In order to reduce the amount of required recycling gas the use of a shifting stage is proposed (see Figure 25 Process A, B, C and D).

Additionally the design approach to place the CO-shift after the CO_2 separation unit is discussed. This option seems to be favorable since the required steam at the CO-shift inlet can be reduced since certain CO_2 separation methods enriches the CO_2 depleted gas with steam (see Figure 25 Process E).

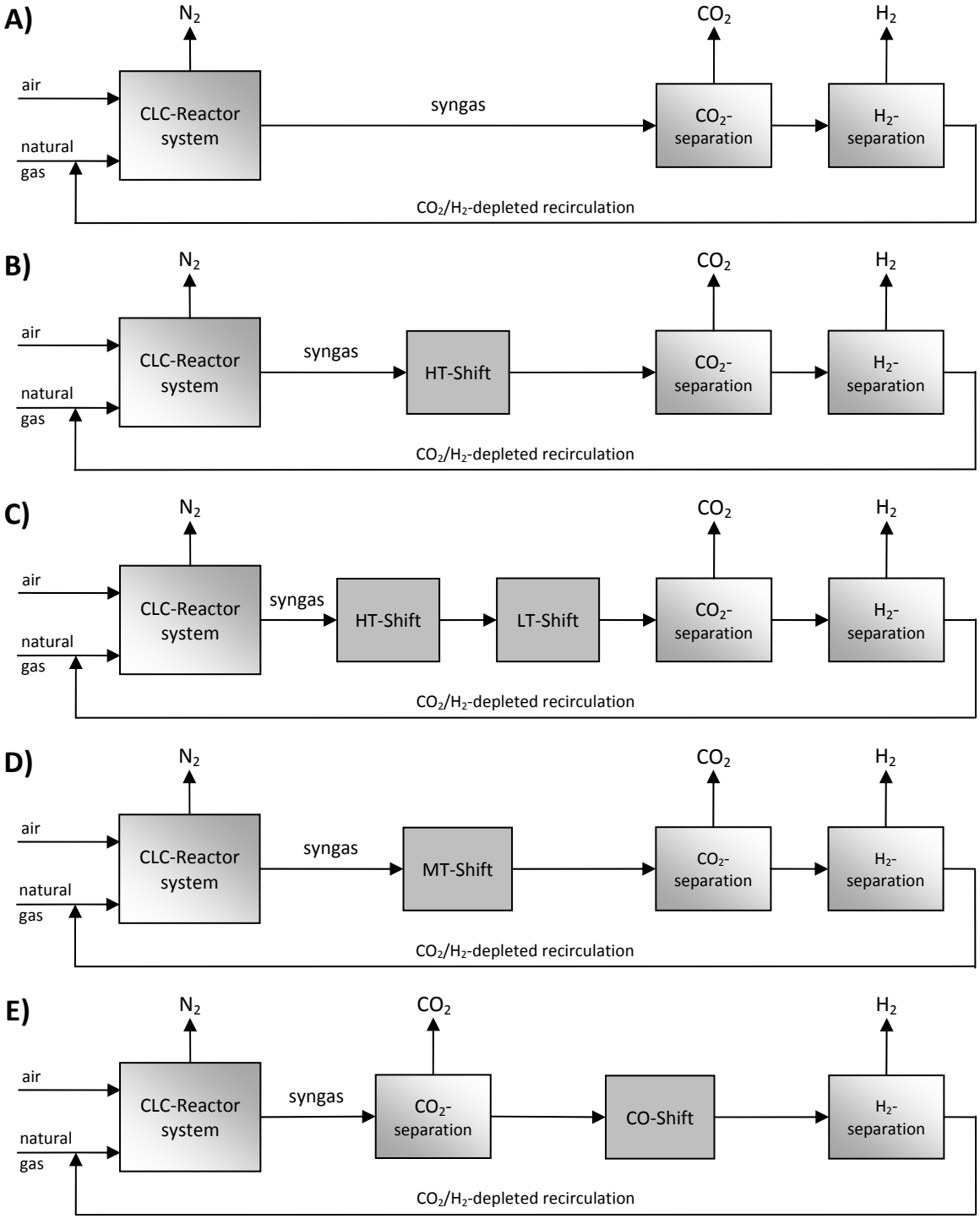

Figure 25 Possible CLR(a) process schemes

A) no CO shift-,
B) HT-CO shift-,
C) HT- and LT-CO shift-,
D) MT-CO shift-,
E) after CO_2 separation CO shift-design

3 Modeling

3.1 SimTech Simulation Technology IPSEpro

SimTech Simulation Technology IPSEpro is a flow sheet simulation tool for use in simulation of power generation cycles and chemical processes. IPSEpro modules can be used for

- calculation of heat balances, prediction of design and part design performance.
- verification and validation of measurements during acceptance tests.
- monitoring and optimization of plant performance on-line.
- estimation of design costs.

IPSEpro was built up with respect to transparency and easy user interaction. Therefore, IPSEpro offers the model development kit (MDK) introducing a unique level of flexibility. Own created new component models or even completely new model libraries can be integrated easily.

In order to solve the more dimensional non linear problems IPSEpro uses a Newton-Raphson method described in 3.1.3.

3.1.1 Modeling concept

The IPSEpro modeling concept bases on standardized components in order to build up the model of a complete process. Each model is mathematically described by a set of equations and variables. The mathematical model of the complete process is built up by joining all equations of the component models into a single system of equations. The resulting non linear system is solved by the use of Newton-Raphson's method.

3.1.2 Major IPSEpro modules

PSE – Process Simulation Environment

PSE is the software surface for development of process flow sheets. The flow sheets are built up by drag-and-drop of the required components from the library menu. All data required the determination of the process are entered directly into the flow-sheet.

MDK – Model Development Kit

MDK offers all possibilities that are required to define new models for use in PSE. MDK consists of a model editor and a model compiler. The model editor allows to describe the model behavior mathematically and to design the icons representing the components in the model library. The model compiler translates the model description into a binary code ready for implementation into the solver algorithm.

MDK's model description language (MDL) is intuitively based on standard mathematical notations and standard programming syntaxes. A sample is represented below.

Sample of a model description syntax [W 11]

```
f1: feed.mass = drain.mass;
f2: time_s/3600 = time_h;
f3: if abs(dt_in/dt_out) >=1.2 || abs(dt_out/dt_in) >=1.2 then
    q_trans*ln(dt_in/dt_out)/(dt_in-dt_out) = htc_area;
    else
    q_trans*2.0/(dt_in+dt_out) = htc_area;

t1: test (mass >=0.0) warning "mass flow negative";
```

A model description consists mainly of two parts, the equation- and the testing-section. The equation-section, notated by `f*:`, where `*` is a continuous number, represents the mathematical description of the model. Essentially these equations are the heat- and mass-balance sustaining the conservation of energy. The testing-section, notated by `t*:`, where `*` is a continuous number, describes the testing conditions to ensure if mathematically correct values are thoughtful or physically plausible.

PSExcel – Process Simulation to Excel

PSExcel is a data exchange module allowing integrating PSE projects into MS-Excel worksheets. The data exchange can be done in both directions. Hence, calculations done in Excel can be integrated in PSE as well as values from PSE can be used in Excel spreadsheets for post processing. PSExcel offers pre-defined macros supporting automatic parameter variations to determine the effects of parameters on the simulation.

PSValidate – Process Simulation for Validation

In many technical cases measurements are carried out. The true value differs from the measurement because every measurement has got a measurement error. If the measurements are carried out on a network of components these measurements usually are connected in a certain way to each other. Such a network could be for example a power plant or a network of heat exchangers. PSValidate offers the opportunity to handle measurement values with errors and redundant systems in order to increase the reliability of the measurements. Therefore, PSValidate uses statistical methods to eliminate redundancies and obtain more accurate data. PSValidate allows to

- identify the most probable and consistent state of a process,
- identify sensor failures
- and to increase the accuracy of a model.

3.1.3 IPSEpro solving mechanism – The Newton-Raphson method

In general there are two possibilities for treating nonlinear equations.

- It is possible to construct the zero point search associated to the solution of the problem in that way that the solution is found by a minimization. Then the solution could be found by finding the way of the deepest descent of the associated function.
- Or to implement a Newton or Newton-Raphson-Method named after Sir Isaac Newton 1669 and Joseph Raphson 1690.

By using the steepest descent method it is nearly always possible to find a minimum. The high stability in finding the solution includes an expense of velocity. This leads to a nearby always convergent but slow (often very slow) procedure. In contrast to the steepest descent method the Newton-Raphson-Method converges very expeditiously. That is why this method has evolved as the mathematical standard procedure for solving non linear equations. The disadvantage of the Newton-Raphson method is that the convergence radius in general is small. Therefore, very good start estimates are required for the convergence of the solution.

One-dimensional case

In case of a one dimensional problem the zero point of a function $x^* \in \mathbb{R}$ of a twice continuously differentiable function $R(x)\colon \mathbb{R} \to \mathbb{R}$ should be approximated without knowing anything about the point $x_0 \in \mathbb{R}$ applies to:

$$x_0 \neq x^* \qquad \text{(eqn 3-1)}$$

Approximating the function $R(x)$ using a Taylor-development of first order

$$R(x) = R(x_0) + \frac{dR(x)}{dx}(x_0) \cdot (x - x_0) + \sigma[(x - x_0)^2] \qquad \text{(eqn 3-2)}$$

and replacing x by x_1 yields to

$$R(x_1) = R(x_0) + \frac{d}{dx}R(x_0) \cdot (x_1 - x_0) + \sigma[(x_1 - x_0)^2]. \qquad \text{(eqn 3-3)}$$

By setting $R(x_1)$ to zero and by manipulating the equation accordingly the outcome of this is:

$$x_1 = x_0 - \frac{R(x_0)}{\acute{R}(x_0)} \qquad \text{(eqn 3-4)}$$

From this follows the procedure of Newton-Raphson

$$x^{(n+1)} = x^{(n)} - \frac{R\left(x^{(n)}\right)}{\acute{R}(x^{(n)})} \qquad \text{(eqn 3-5)}$$

which could be geometrically interpreted evident in the figure below.

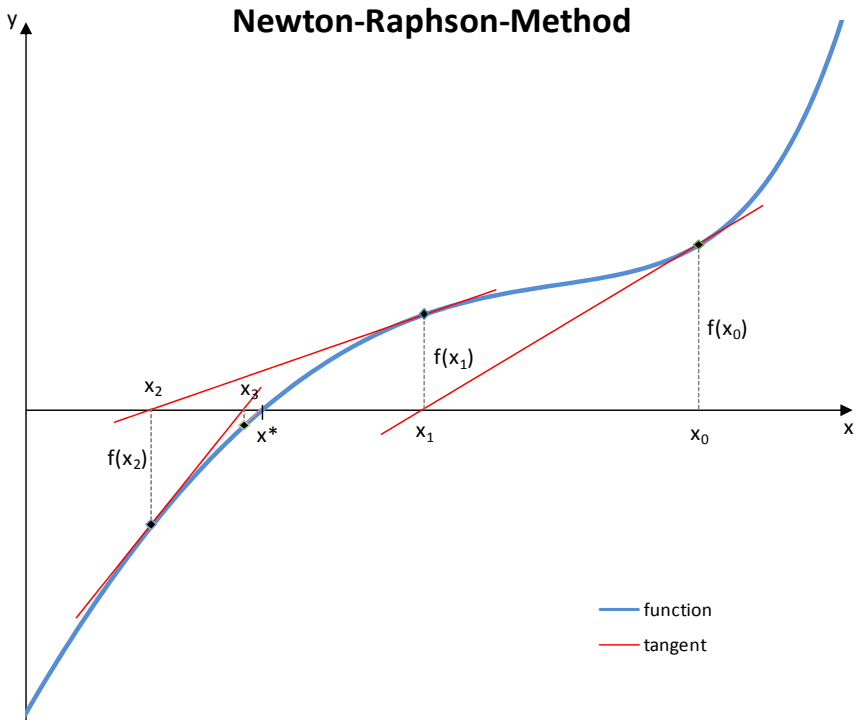

Figure 26 Geometrical interpretation of the Newton-Raphson-Method

N-dimensional case

For an n-dimensional system the problem solution approach is similar to the one-dimensional case. First the problem has to be transformed to a zero-search-problem to obtain the residual $R^{(n)} = R\left(x^{(n)}\right)\colon \mathbb{R}^n \to \mathbb{R}^n$. From this follows for the Newton-Raphson procedure

$$\boldsymbol{x}^{(n+1)} = \boldsymbol{x}^{(n)} - \boldsymbol{R}\left(\boldsymbol{x}^{(n)}\right)[\mathrm{J}^{(n)}]^{-1} \qquad \text{(eqn 3-6)}$$

with the Jacobian matrices $J^{(n)}$ which is defined as follows:

$$J_{ij}^{(n)} = \frac{\partial R_j^{(n)}}{\partial x_{ij}} \qquad \text{(eqn 3-7)}$$

Convergence

Since the Newton-Raphson-Method is a procedure with a fixed point its convergence, following the fixed point theorem of Banach (see [53], [31], [15], [3]), is locally at least with linear convergence. According to [58] it is imperative that the procedure of Newton-Raphson converges in case of local convergence around a zero-point $\boldsymbol{x}^*$ at least with quadratic order.

Constraints and Drawbacks

This method requires well selected starting conditions to make use of local, least, quadratic convergence. A poor choice of starting set could lead to almost everything. It is possible that alternating or even over all growing iteration parameters occur which make the solution of the problem impossible. Hence, when building up a new flow sheet with IPSEpro it is particularly important to remember these facts. Therefore, when simulating a non linear system the starting value has to be near the end point of the iteration. The differences in start and final conditions have to be minimized by means of user interaction. This can be achieved if a reactor is modeled by iteratively increasing the amount of reaction taking place inside the reactor. Therefore, at the very beginning a reactor with no reaction has to be simulated in order to obtain good starting conditions for further calculations.

Another disadvantage of this method is that for every iteration step the Jacobian matrix has to be recalculated. Especially for matrices with high bandwidth this is an “expensive” way.

3.2 The Advanced Energy Technology Library (AET-Lib)

For the simulation of a process the description of the mass and energy balance is always the first step. This requires the knowledge of the thermodynamic properties of the substances involved. IPSEpro has an embedded substance property calculation algorithm to calculate the properties of gas mixtures, water-steam, refrigerants and salt-water mixtures.

As in a chemical looping process there also occur solid streams and gas-solid reactions the advanced energy technology library (AET-Lib) has been developed by T. Pröll et al. at the Institute of Chemical Engineering at the Vienna University of Technology [54]. The properties of 40 solid substances have been collected from databases and implemented into the IPSEpro structure.

Reaction modeled

According to Pröll et al. [54] the global reaction of fuel oxidation (reac 2-5) is divided into more elementary steps. Therefore, the methane conversion rate, the CO-shift reaction (reac 2-10) and the CO oxidation with metal oxide (reac 3-1) are modeled.

The methane conversion rate is defined as the coefficient of the amount of CO and CO_2 in the FR exhaust and the CO, CO_2 and CH_4 in the fuel reactor exhaust.

$$X_{CH_4} = \frac{\left(y_{CO} + y_{CO_2}\right)_{exhaust}}{\left(y_{CO} + y_{CO_2} + y_{CH_4}\right)_{exhaust}} \qquad \text{(eqn 3-8)}$$

The modeled CO oxidation with the metal oxide reaction is shown below.

$$CO + MeO_{\alpha} \longrightarrow CO_2 + MeO_{\alpha-1} \quad \text{(reac 3-1)}$$

Thermodynamic equilibrium formation

The actual state of a substance with respect with respect to the equilibrium of a specific chemical reaction

$$\sum_i v_i \cdot A_i = 0 \quad \text{(eqn 3-9)}$$

is expressed by the logarithmic deviation from equilibrium:

$$p\delta_{eq} = \log_{10} \frac{\prod_i (p_i)^{v_i}}{\prod_i (p_i^*)^{v_i}} = \log_{10} \frac{\prod_i (p_i)^{v_i}}{K_P(T)} \quad \text{(eqn 3-10)}$$

The equilibrium can be calculated by knowledge of the thermodynamic properties via minimization of the Gibbs free enthalpy:

$$\ln K_P(T) = \frac{-G_R^0(T)}{R \cdot T} \quad \text{(eqn 3-11)}$$

3.3 General modeling parameter constraints

3.3.1 Ambient conditions

According to ISO 2314 and ISO 3977-2 the ambient conditions are chosen to be:

Temperature	$\vartheta_{amb} = 25°C$
Pressure	$p_{amb} = 1{,}01325\ bar$
Relative Humidity	$\varphi = 60\%$

With the following dry air composition:

$$20{,}942 vol\%\ O_2, 0{,}934 vol\%\ Ar, 388 ppm CO_2, rest N_2$$

3.3.2 Natural gas and gas quality

Natural gas is a non-toxic, colorless and odorless gas mixture. The ignition temperature of natural gas is approximately 600 degree Celsius and its boiling point is -161°C. The density of natural gas is lower than air and varies depending on the gas composition. Depending on the discovery locality the composition of the natural gas differs. The lion's share of natural gas is methane (CH_4). Often particular amounts of ethane, propane, butane and pentane are included. If this is the case the natural gas is also called "wet" natural gas. The water fraction is not taken into account since wet means only the parts of condensable gases of the gas volume. If there is sulfur (typically as H_2S) in the raw gas it is usually separated in advance.

To classify the type of natural gas classes of quality have been introduced. It is distinguished between natural gases of quality class "L" (low) and "H" (high) from the North Sea region and class "H" from the Commonwealth of Independent States (CIS).

Table 6 Average volumetric composition of different gas qualities [W 14]

Region of finding	Quality class	Portion of: Methane [Vol-%]	Sum of Ethan, Propane, Butane and Pentane [Vol-%]	Inert gases [Vol-%]
North Sea region	"L"	85	4	11
	"H"	89	8	3
Commonwealth of Independent States	"H"	98	1	1

Since natural gas does not smell, small amounts of odorants are added for safety reasons. Usually thioethers like tetrahydrothiophene or thioles (like ethylmercaptan and tertiary butylmercaptan) are used.

Detailed information about the gas composition used in Vienna can be found in appendix A-1 Gas analysis of Vienna in German language.

In order to increase the comparability of the discussed process options it is generally assumed that the fuel consists only of methane.

3.3.3 Reactor system

As mentioned in chapter 2.1 and 2.2 many reactions occur simultaneously. The actual achievable reactor conditions depend mainly on the reactor design, the reactor temperature, the air to fuel ratio and used type of oxygen carrier. Therefore, modeling simplifications have to be adopted.

At the pilot rig at the Vienna University of Technology chemical looping tests with a nickel based oxygen carrier have been carried out. Hence, a nickel based oxygen carrier is chosen with the following properties:

Oxygen transport capacity	$R_0 = 0{,}08568\ kg/kg$
Molar mass of the oxidized oxygen carrier	$M_{ox} = 114{,}26\,kg/kmol$
Molar mass of the reduced oxygen carrier	$M_{red} = 104{,}47\,kg/kmol$
Oxidation state of the oxidized oxygen carrier	$X_{s\_ox} = 27{,}19\%$
Oxidation state of the reduced oxygen carrier	$X_{s\_red} = 14{,}85\%$

Ideally, complete methane conversion is assumed in the fuel reactor.

$$X_{CH_4} = 100\%$$

Furthermore, it is assumed that the CO-shift reaction (reac 2-10) and the CO oxidation with metal oxide reaction (reac 3-1) are in equilibrium. Therefore, the logarithmic deviations from the equilibrium have to be zero.

$$p\delta_{eq\_CO-shift} = 0$$

$$p\delta_{eq\_CO-CO_2} = 0$$

3.3.4 Fluidization

The reactors are fluidized by air and fuel. The reactors have to be gas-tight so that gases from the air reactor cannot enter the fuel reactor or vice versa. Therefore, loop-seals are required. They are fluidized with an inert gas. The cheapest possibility is to use steam for fluidization. The required mass flows are estimated regarding the required loop-seal fluidization mass flows of the Vienna University of Technology test rig. Therefore, the required fluidization mass flow is referred to the gas mass flow entering the reactor. It is assumed the required relative fluidization mass flow is:

$$\dot{m}_{LS\_fluid\_rel} = \frac{\dot{m}_{fluid-steam}}{\dot{m}_{reac-inlet}} = 0{,}2\%$$

3.4 Modeling parameter constraints for CLC-Power-Generation

3.4.1 The condenser

First of all a condenser has to be chosen which represents the basis of the thermodynamic cycle by limiting the condenser temperature and as a consequence the steam turbine back pressure. The condenser temperature depends mainly on the type of cooling available at the plant surrounding environment. Apart of some special applications for power generation the surrounding air or if available cold water reservoirs, like rivers, usually are used for cooling the condenser. An overview of the conventional cooling circuits is shown below.

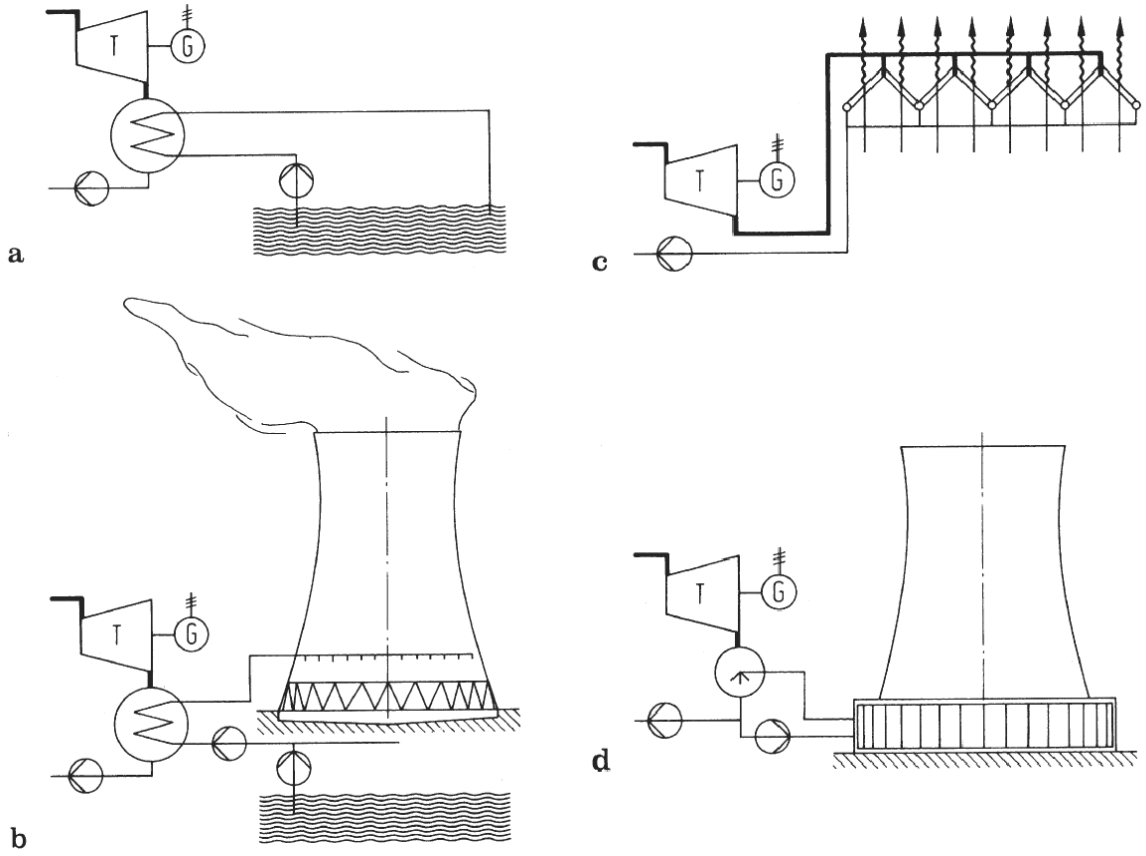

Figure 27 Cooling methods in steam cycles [21].
a) fresh water cooling, b) wet tower, c)direct air-cooling, d) indirect air-cooling

Depending on the type of cooling method the condenser pressure is determined.

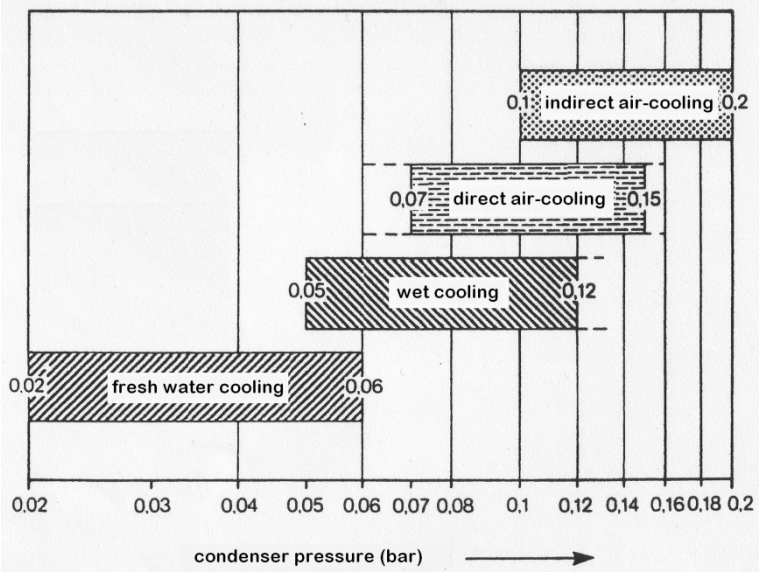

Figure 28 Achievable condenser pressures depending on the type of cooling system. Adopted from [64]

Figure 28 shows that if there is the possibility to use the water of a river this cooling method will be the most favorable choice. Evaporation or direct dry-cooling seems to be more feasible at most scenarios. Therefore, the condenser pressure is chosen to be

$$p_{co} = 0{,}1\ bar$$

According to VDI [62] the according condenser temperature can be calculated to:

$$t_{co} = 45{,}73\ °C$$

3.4.2 Turbine efficiency

In the scale of a 10 MW boiler with an assumed thermal efficiency of approximately 40% the resulting steam turbine power will be approximately 4 MW. This scale represents the class of industrial steam turbines which are usually customer designed. They are offering the advantage of custom steam supply ports and are available as condensing or backpressure types. Table 7 gives an overview of industrial steam turbine producers.

Table 7 Overview of small scale steam turbine producers

Company Name	Available Scales
Siemens Powergeneration [W 9]	$45\ kW \div 700\ MW$
MAN Turbo [W 7]	$1{,}5 \div 150\ MW$
Dresser-Rand [W 3]	$5\ kW \div 20\ MW$
Elliot-Company [W 4]	$\leq 75\ MW$
Prime Steam Turbines [W 1]	$\leq 2{,}2\ MW$
Shin Nippon Machinery [W 12]	$300\ kW \div 50\ MW$
Triveni Eng. & Ind. Ltd [W 13]	$\leq 22\ MW$

Values of industrial steam turbine efficiencies are rare and usually kept as a secret. In order to get an idea of a possible range of the isentropic turbine coefficient the values in Table 8 were found in literature.

Table 8 Typical steam turbine efficiencies found in the literature

Author	Scale	Isentropic turbine efficiency
R. Beebe [6]	$350MW$	$\eta_s = 85 \div 90\%$
Energy Nexus Group [24]	$15MW$	$\eta_s = 80\%$
CHP Quality Assurance Guidance [11]	$5 \div 10MW$	$\eta_s = 75\%$

Since these data are not satisfying and of poor validity technical data of installed industrial steam turbines are taken for the calculation of estimated turbine efficiencies.

Table 9 Installed industrial steam turbine data

Installation Fechenheim Frankfurt / Germany	
Turbo-Generator	MARC4-C12
Customer	MCE Group
Technical Data	
Inlet Pressure	$p_{st} = 65\ bar(a)$
Inlet Temperature	$t_{st} = 450°C$
Inlet Flow	$m_{st} = 52\ t/h$
Exhaust Pressure	$p_{co} = 0{,}1\ bar(a)$
Power Output	$P_{el} = 13060\ kW_{el}$
Assumptions	
Generator Efficiency	$\eta_{ge} = 95\%$
Calculation	
Estimated isentropic Efficiency	$\eta_s \approx 84\%$
Installation BEC Hengelo / The Netherlands	
Turbo-Generator	MARC6-C03
Customer	Standartkessel Lentjes
Technical Data	
Inlet Pressure	$p_{st} = 66\ bar(a)$
Inlet Temperature	$t_{st} = 460°C$
Inlet Flow	$m_{st} = 79\ t/h$
Exhaust Pressure	$p_{co} = 0{,}09\ bar(a)$
Power Output	$P_{el} = 21000\ kW_{el}$
Assumptions	
Generator Efficiency	$\eta_{ge} = 95\%$
Calculation	
Estimated isentropic Efficiency	$\eta_s \approx 83{,}5\%$

Installation Example Neubrücke / Germany	
Turbo-Generator	SST-200
Customer	Reference from Knauf
Technical Data	
Inlet Pressure	$p_{st} = 80\ bar(a)$
Inlet Temperature	$t_{st} = 480°C$
Inlet Flow	$m_{st} = 68{,}4\ t/h$
Backpressure	$p_{bp} = 10\ bar(a)$
Maximal Power Output	$P_{el,max} = 9000\ kW_{el}$
Assumptions	
Generator Efficiency	$\eta_{ge} = 95\%$
Calculation	
Estimated isentropic Efficiency	$\eta_s \approx 89\%$
Installation Example from Knauf Dampfturbinen	
Turbo-Generator	SST-300
Customer	Reference from Knauf
Technical Data	
Inlet Pressure	$p_{st} = 120\ bar(a)$
Inlet Temperature	$t_{st} = 510°C$
Inlet Flow	$m_{st} = 316{,}8\ t/h$
Backpressure	$p_{bp} = 10\ bar(a)$
Maximal Power Output	$P_{el,max} = 40000\ kW_{el}$
Assumptions	
Generator Efficiency	$\eta_{ge} = 95\%$
Calculation	
Estimated isentropic Efficiency	$\eta_s \approx 86\%$

The Enthalpy–Entropy diagram of a steam turbine

The typical h-s-diagram of a steam turbine is shown below

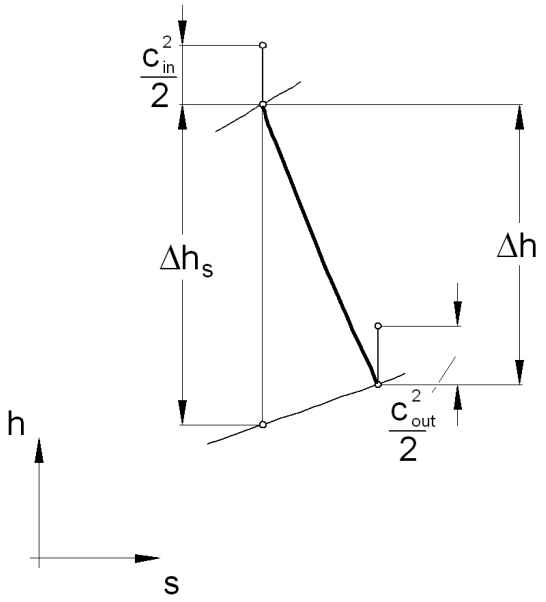

Figure 29 Typical h-s-diagram of a steam turbine

Steam turbine efficiency definitions

Inner efficiency

The inner efficiency of a steam turbine is also called the total to total efficiency. This efficiency definition takes into account any loss of energy.

$$\eta_i = \frac{\Delta h + \frac{c_{in}^2 - c_{out}^2}{2}}{\Delta h_s + \frac{c_{in}^2 - c_{out}^2}{2}} \quad \text{(eqn 3-12)}$$

Isentropic efficiency

The isentropic efficiency is the more practical efficiency definition since it doesn't take the velocities into account which in design-case are usually unknown and the kinetic energy can be usually neglected compared to the enthalpy difference.

$$\eta_s = \frac{\Delta h}{\Delta h_s} \quad \text{(eqn 3-13)}$$

Mechanical efficiency

The mechanical efficiency considers any loss occurring between the turbine and the clutch.

$$\eta_m = \frac{P_c}{P_t} \quad \text{(eqn 3-14)}$$

Clutch efficiency

The clutch efficiency is the combination of the inner and the mechanical efficiency.

$$\eta_c = \eta_i \cdot \eta_m \quad \text{(eqn 3-15)}$$

The clutch efficiency diagram

The most practical information about actual turbine efficiencies can be found in the book of Dubbel [20]. It reports the clutch efficiency depending on the mean volume flow and the rotations per minute (Figure 30).

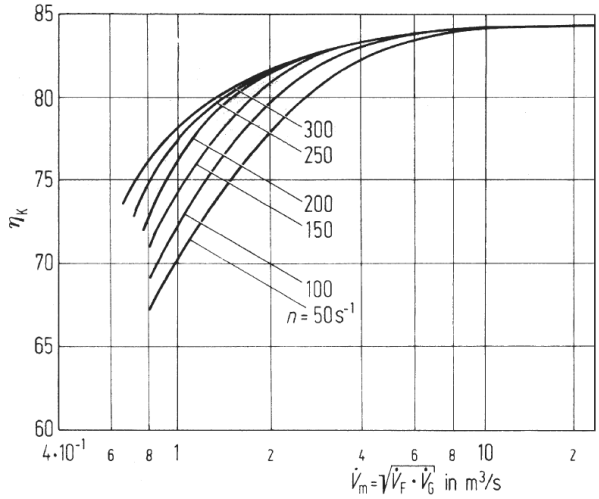

Figure 30 Clutch-Efficiency of a steam turbine depending on the mean volume flow [20]

3.4.3 Choice of live steam parameters

High live steam parameters are, as mentioned in chapter 2.3.2, extremely important for a high thermal efficiency. Highest live steam parameters are limited by the toughness of the heat exchanger material and the steam turbine. Especially for small scale plants, as discussed in this work, it is even more important to take into account economic considerations. At a scale of 10 MW_{th} the steam turbine allowing only a certain steam pressure and temperature limits the live steam parameters.

Siemens Powergeneration and MAN Turbo are some of the leading manufacturers of industrial scale steam turbines. Their steam turbine programs were chosen to get knowledge about techno-economically feasible live steam parameters. Their product range is summarized below.

Table 10 Typical industrial steam turbine data

MAN Turbo [W 7]		
MARC 1	$P \leq 3\ MW$	$30\ bar(a)$ / $480°C$
MARC 2	$P \leq 12\ MW$	$90\ bar(a)$ / $520°C$
Siemens Steam Turbines [W 9]		
SST-060	$P \leq 6\ MW$	$131\ bar(a)$ / $530°C$
SST-110	$P \leq 7\ MW$	$131\ bar(a)$ / $530°C$
SST-100	$P \leq 8{,}5\ MW$	$65\ bar(a)$ / $480°C$
SST-120	$P \leq 10\ MW$	$131\ bar(a)$ / $530°C$

Therefore, a live steam temperature of

$$\vartheta_{LS} = 500°C$$

is chosen for simulation.

According to Willinger et al. ([49] & [64]), Müller et al. [49] or Dubbel [20] the water content (definition see Willinger et al. [49]) after a steam turbine must be lower than 15%. For further investigations the steam mass fraction is assumed to be:

$$x = 90\ \%$$

According to chapter 3.4.2 it can be estimated that an average isentropic turbine coefficient of

$$\eta_{s,t} = 80 \div 85\%$$

is practically possible.

According to the definition of the isentropic turbine efficiency and by taking the previous assumptions into account the following diagram can be drawn (Figure 31).

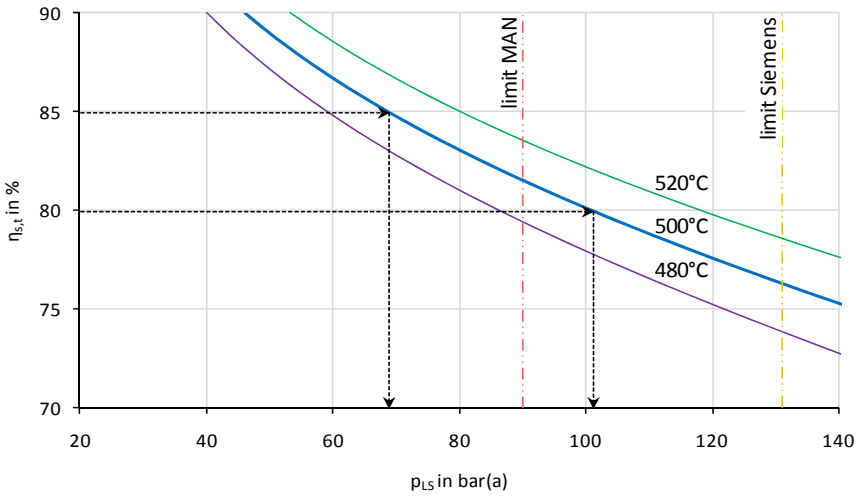

Figure 31 Live steam pressure depending on the isentropic efficiency of the turbine at a live steam temperature of 500°C and a steam mass content at the turbine exit of x=90%

The diagram shows that for a fixed steam mass content of the steam turbine exhaust of x=90% and by assuming that the isentropic efficiency of the turbine is in the range of $\eta_{s,t}$=80-85% the resulting live steam pressure range is

$$p_{LS} \simeq 69 \div 101\ bar.$$

Therefore a live steam pressure of

$$p_{LS} = 80\ bar$$

is chosen.

3.4.4 Relative radiation loss

The radiation loss of a steam generator is caused by the temperature difference of the hot surface of the boiler and the surrounding air. It mainly depends on the quality of the insulation and decreases relatively with increasing heating capacity of the boiler. Apart of its name the radiation loss does not only include the loss caused by radiation but also the convective loss. Since there are no data available for a chemical looping system it is assumed that the radiation and convection loss of the system are similar to that of a conventional steam generator.

Following the European standard EN12952-15 the relative radiation loss of a steam generator is calculated as follows:

$$l_{RC} = \frac{\dot{Q}_{RC}}{\dot{m}_{fuel} \cdot LHV} = \frac{\dot{Q}_{RC}}{P_{fuel}} \quad \text{(eqn 3-16)}$$

The absolute radiation and convection loss is an empirical value and can be approximated by the following formula.

$$\dot{Q}_{RC} \approx C \cdot \dot{Q}_u^{0,7} \quad \text{(eqn 3-17)}$$

$\dot{Q}_u$ is representing the usable heat release (heat of the produced steam) and is calculated as follows:

$$\dot{Q}_u = \eta_{th} \cdot \dot{m}_{fuel} \cdot LHV = \eta_{th} \cdot P_{fuel} \quad \text{(eqn 3-18)}$$

The empirical constant C is provided by the European steam generation standards and depends mainly on the type of fuel used. Common values of C are summarized below.

Table 11 Empirical Values for C from [61]

Type of Fuel	C
Fuel oil or natural gas	$0{,}009 \div 0{,}011$
Semi anthracite coal	$0{,}018 \div 0{,}022$
Lignite	$0{,}025 \div 0{,}030$

Estimating a thermal efficiency of η_{th}=40% for the absolute radiative and convective heat loss of the steam generator of the size discussed in that study is as follows.

$$\dot{Q}_{RC} \approx C \cdot \left(\eta_{SG} \cdot P_{fuel}\right)^{0,7} = 0{,}01 \cdot (0{,}4 \cdot 10)^{0,7} = 0{,}02639\ MW$$

Or relatively:

$$l_{RC} = \frac{\dot{Q}_{RC}}{P_{fuel}} = \frac{0{,}02639}{10} \cong 0{,}265\%$$

3.4.5 Type of circulation system

There are three different types of circulation systems

- natural circulation,
- forced circulation and
- once-through systems.

Natural circulation system

Natural circulation systems are the oldest operation systems of steam generators. The driving force of the water circulation in a natural circulation system is the density difference of the fluid inside the rising-pipes and the downcomer tubes. It is caused by the partial change of state of the working fluid to vapor inside the heated rising-pipes while the fluid inside the usually unheated downcomer-tubes remains at almost constant density. Inside the drum the produced steam is separated from the water. The steam is transported to the superheater while the subtracted water remains inside the circulation system. To identify the state of the circulation system the so-called circulation ratio U is defined. The circulation ratio is the coefficient of the mass flow of the circulating water inside the circulation system and the mass flow of the produced steam.

$$U = \frac{\dot{m}_{circulation}}{\dot{m}_{LS}} \quad \text{(eqn 3-19)}$$

Typical circulation ratios depending on the live steam pressure are summarized below.

Table 12 Typical circulation ratios for coal fired natural-circulating-steam generators [61]

Steam pressure [bar]	80	100	120	140	160	180
Circulation ratio *U*	11,1	10,0	9,0	7,9	6,8	6,0
Steam to water ratio *x*	0,09	0,1	0,11	0,13	0,14	0,16

Natural circulation systems are feasible up to steam pressures of approximately 175 bar. The density difference between the liquid and vapor phase decreases with increasing pressure. Therefore, high pressure steam cycles need a forced circulation or a once-through system can be used.

Forced circulation system

In a forced circulation system a pump assists the natural circulation in the evaporator system. By using an additional pump the steam pressure can be increased up to 200 bar.

Once-Through systems

In a once-through system the working fluid is directly pressed by the use of a feeding pump through the heat exchangers. There is no need of a natural driving force and the steam pressure is physically unlimited regarding the circulation system.

Thus, the steam pressure in this study is p_{LS}=80 bar and a natural circulation system is favorable.

3.4.6 Electric efficiency of the generator

The electric efficiency of the generator is defined as the coefficient of the electrical power output of the generator and the power input at the clutch of the generator.

$$\eta_{el} = \frac{P_{el}}{P_c} \qquad \text{(eqn 3-20)}$$

The electric efficiency depends on the rotations per minute and on the type of cooling applied which is shown below.

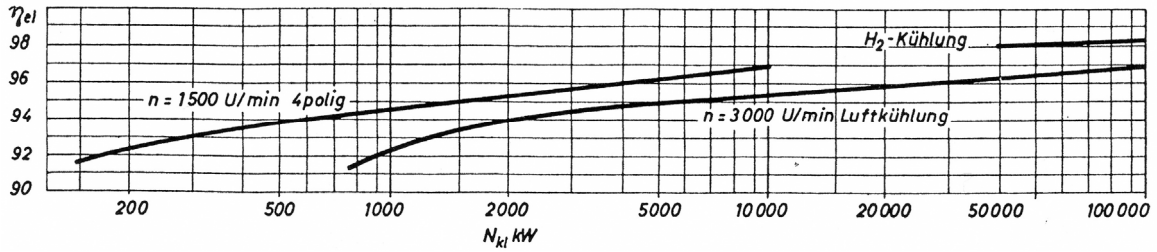

Figure 32 Electrical efficiency of the generator depending on the generator power output [19]

Figure 32 also shows that the generator efficiency changes with changing generator power output. The generator power output varies with changing process efficiency. Hence, the electric efficiency is in every simulation case different. Therefore, it is assumed that the generator efficiency is:

$$\eta_{el} = 96\%$$

3.4.7 Pinch-Point temperature

The pinch-point temperature represents the temperature difference between the gas leaving the evaporator and the saturation temperature of the steam inside the evaporator. A typical exhaust gas temperature profile is presented below showing the pinch-point temperature.

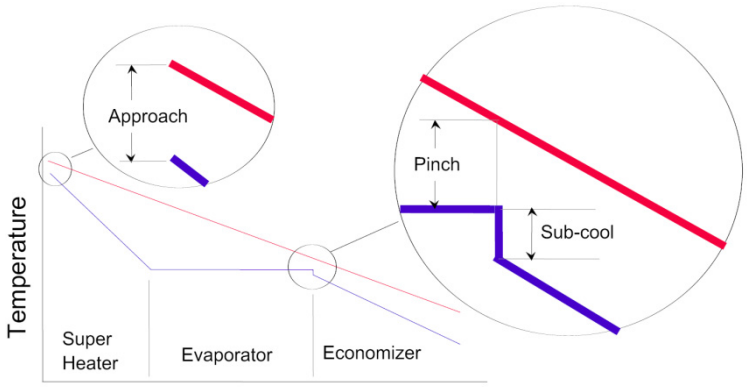

Figure 33 Typical exhaust gas temperature profile – one pressure system [29]

The pinch-point is one of the most important parameters for the design of a steam generator since it symbolizes the hinge of the heat exchanger system. For increasing efficiency it is essential to minimize the pinch-point in order to decrease the exergy loss of the heat exchange. This can be achieved by increasing the evaporator surface which counteracts economical reasons. Thus a optimum has to be found taking economical and technical factors into account. The dependencies are multi dimensional and often influenced by knowledge and production peculiarity of the company. In a case study such detailed pinch-point evaluations are not useful if even possible.

Possible pinch-point temperatures are shown in the following table.

Table 13 Typical pinch-point temperatures

Author / Book	Cross-reference	Pinch-Point temperature
C. Casarosa et al.	[10]	$t_{pinch} = 10 \div 20\ K$
D Blood et al.	[7]	$t_{pinch} = 11 \div 28\ K$
Haider	[29]	$t_{pinch} = 5 \div 15\ K$
Willinger	[64]	$t_{pinch} = 25 \div 50\ K$

A pinch-point temperature of

$$t_{pinch} = 20\ K$$

is chosen because economical reasons are the more important factors at small scale applications. Therefore, a minimal temperature difference for gas-water heat exchangers of

$$\Delta\vartheta_{min,gas-water,htx} = 20°C$$

is chosen.

3.4.8 Air preheater

The air preheater is an important element which increases the thermal efficiency of a power cycle by decreasing the exhaust temperature and by increasing the temperature of the combustion air. In that way the adiabatic exhaust temperature of the combustion chamber is increased or vice versa the required fuel-power is decreased.

The lowest possible exhaust temperature is limited by the sulfur dew point temperature which causes corrosion of the heat exchanger surface. It is distinguished between two different types of air preheaters, recuperative and regenerative (also called Ljungstrom) ones.

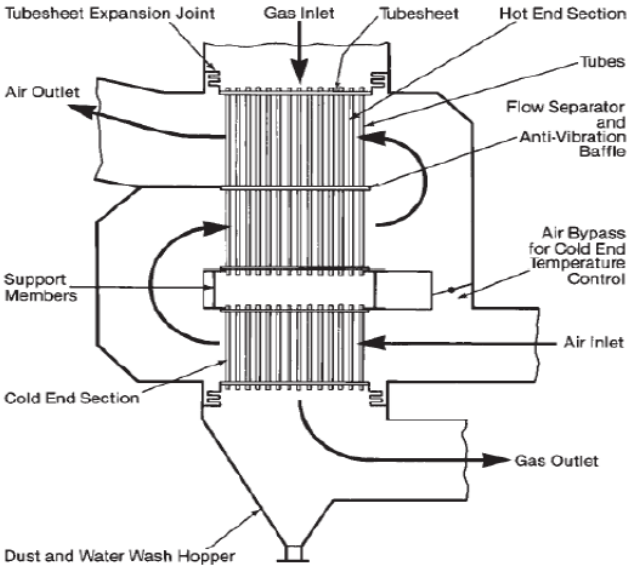

Figure 34 Recuperative air preheater [29]

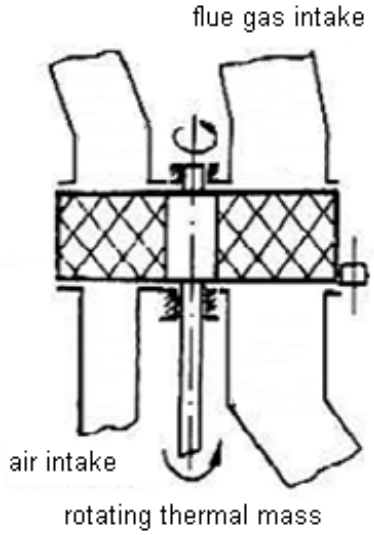

Figure 35 Regenerative air preheater [29]

Recuperative air preheaters are built up of tubes where gas is flowing through. So the gases are strictly separated from each other.

Regenerative air preheaters consist of a rotating thermal mass usually built up of thin steel sheets. During the rotation the steel sheets are heated by the hot exhaust gases and afterwards cooled down by the air. Regenerative air preheaters suffer from leaking and therefore the air is diluted with oxygen depleted off-gas. According to the Alstom Air Preheater Company [W 2] the leakage mass flow is typically approximately 1,5% of the air mass flow. On the other hand regenerative ones are more compact and corrosion is not so important since the heat exchanger surfaces are easier to replace. Due to economical reasons the lowest heat exchange temperature difference is limited.

Table 14 Lowest economical temperature differences for air preheaters [23]

Type of air preheater	Lowest temperature difference
Recuperative	$\Delta\vartheta_{\min} = 50 \div 60\ °C$
Regenerative	$\Delta\vartheta_{\min} = 25\ °C$

Thus a minimal terminal temperature difference for gas-gas heat-exchange of

$$\Delta\vartheta_{\min,\mathrm{gas-gas,htx}} = 50\ °C$$

is assumed.

3.4.9 Pressure losses water side

Superheater pressure drop

According to the book of Dubbel [20] the pressure drop of the steam inside the superheater is approximately 10% of the maximal operating pressure. Generally the cheaper the heat exchanger the higher is the pressure drop inside. The pressure drop can be decreased by decreasing the mass flow inside the tube. This implies that more tubes are required since the heat conductivity is

reduced or that finned instead of plain tubes are used. Thus a pressure drop of the steam inside the superheater estimated to be:

$$\Delta p_{sh} = 10\ bar$$

Evaporator pressure drop

Since a natural circulation system is used the pressure loss caused by the evaporator remains zero.

Economizer pressure drop

The pressure-loss always depends on the size of the economizer. Since the quantity of the pressure-loss only influences the required pressure ratio of the feeding-pump the effect on the cycle efficiency is negligible. Hence, the pressure loss of the water inside the economizer is assumed to be:

$$\Delta p_{eco} = 1\ bar$$

3.4.10 Pressure drop gas-side

The quantity of the gas pressure-loss is hardly to predict in a case study since the pressure loss depends mainly on the gas velocity which requires knowledge about the cross-section areas. According to Dubbel [21] a typical fan operating head is $10 \div 60\ mbar$. For that reason a total gas pressure loss of

$$\Delta p_{gas\_total} = 40\ mbar$$

is assumed to be a feasible value.

3.4.11 Fan / Compressor efficiencies

Fan / compressors are required to compensate the pressure loss of the fluidized bed and the pressure loss caused by the heat exchanger. There are two different compressor types:

- Radial ones are used for small power with an isentropic efficiency smaller than $\eta_s \approx 85\%$.
- Axial ones are used for bigger scales with an isentropic efficiency greater than $\eta_s \geq 85\%$.

High-frequency sound and greater wear are the disadvantages of axial ventilator types. This requires bigger silencers which produces an additional pressure drop. According to Dubbel [21] the decision of the type used depends on the volume-flow and the maximal operating pressure.

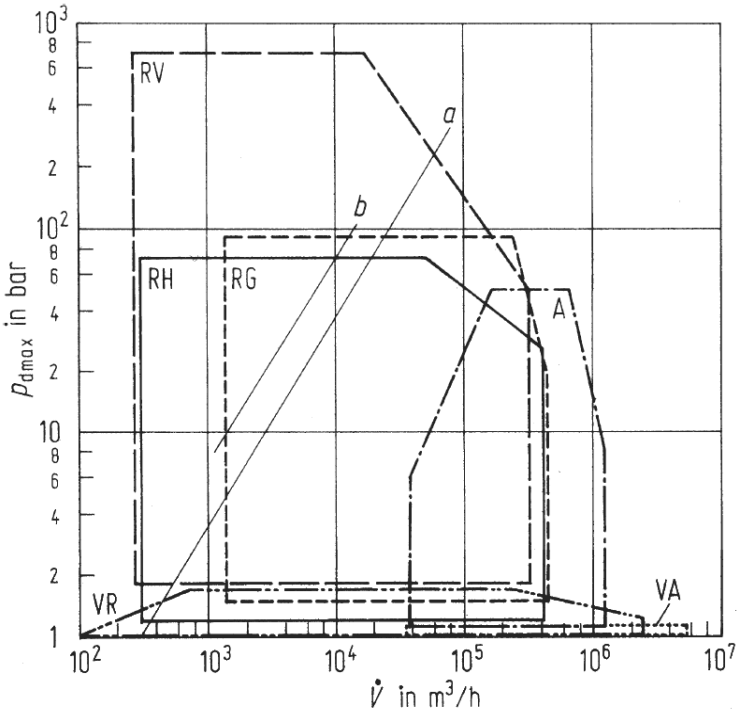

Figure 36 Design chart of the type of a fan / compressor depending of the volume flow and the maximal operation pressure [21]

Declaration of abbreviations:

VR	**ventilator, radial type**
VA	**ventilator, axial type**
RV	**Compressor, radial type, vertical divided casing**
RH	**Compressor, radial type, horizontal divided casing**
RG	**Compressor, radial type with integrated gearbox**
A	**Compressor, axial type**

Estimation of the fan / compressor efficiency

An estimation of the polytropic efficiency the book of Dubbel [21] is used as a reference. Figure 37 is a chart for a fan/compressor. It shows the change of the polytropic efficiency depending on the volume-flow-number

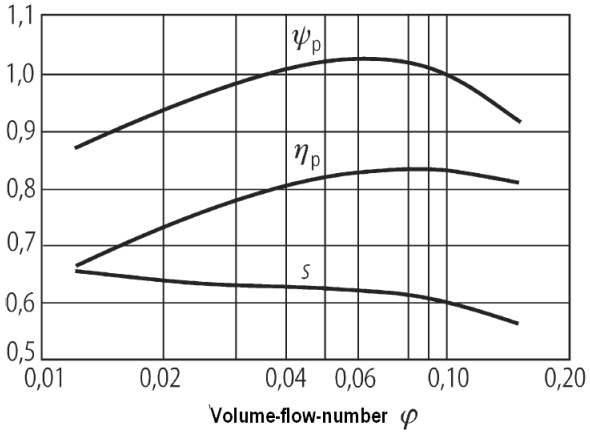

Figure 37 Dependency of the polytropic pressure-number ψ_p, polytropic efficiency η_p, working number s and the volume-flow-number φ of a radial fan / compressor [21].

The volume flow number is defined as follows:

$$\varphi = \frac{4 \cdot \dot{V}}{\pi \cdot d_{c\_out}^2 \cdot u_{c\_out}} \quad \text{(eqn 3-21)}$$

According to [21] the following default values are common.

Default exhaust diameter $d_{c\_out,def} = 400\ mm$

Default exhaust Mach number $M_{u_2,def} = 0{,}7$

With the definition of the Mach number

$$M = \frac{u}{a} \quad \text{(eqn 3-22)}$$

and the speed of sound

$$a = \sqrt{\kappa \cdot R \cdot T} \quad \text{(eqn 3-23)}$$

the exhaust velocity can be calculated from the ideal gas equation:

$$p \cdot v = R \cdot T \quad \text{(eqn 3-24)}$$

The polytropic coefficient can be calculated by the use of the formula for the polytropic change of state:

$$p \cdot v^n = constant \quad \text{(eqn 3-25)}$$

If the state of the fluid before and after the compression is known the polytropic coefficient can be calculated as follows:

$$n = \frac{\ln\left(\frac{p_{c\_in}}{p_{c\_out}}\right)}{\ln\left(\frac{v_{c\_out}}{v_{c\_in}}\right)} \quad \text{(eqn 3-26)}$$

Finally for the isentropic efficiency follows:

$$\eta_s = \eta_p \cdot \frac{\kappa}{\kappa - 1} \cdot \frac{n-1}{n} \cdot \frac{\left(\frac{p_{c\_out}}{p_{c\_in}}\right)^{\frac{\kappa-1}{\kappa}} - 1}{\left(\frac{p_{c\_out}}{p_{c\_in}}\right)^{\frac{n-1}{n}} - 1} \quad \text{(eqn 3-27)}$$

3.5 Modeling parameter constraints for CLR-Hydrogen-Power

3.5.1 Chemical looping steam reforming

Steam reforming

Steam reforming is the most frequently used process for converting hydrocarbons into hydrogen.

Reaction (reac 2-17) represents the steam reforming of methane. It is reversible and strongly endothermic. According to the principle of le Chatelier the reaction must be carried out at a high temperature, high steam to carbon ratio and low pressure to achieve maximum methane conversion. This is shown below. Figure 38 shows that at a constant steam-to-carbon ratio the point with maximum hydrogen yield is moving to higher temperatures with increasing pressure.

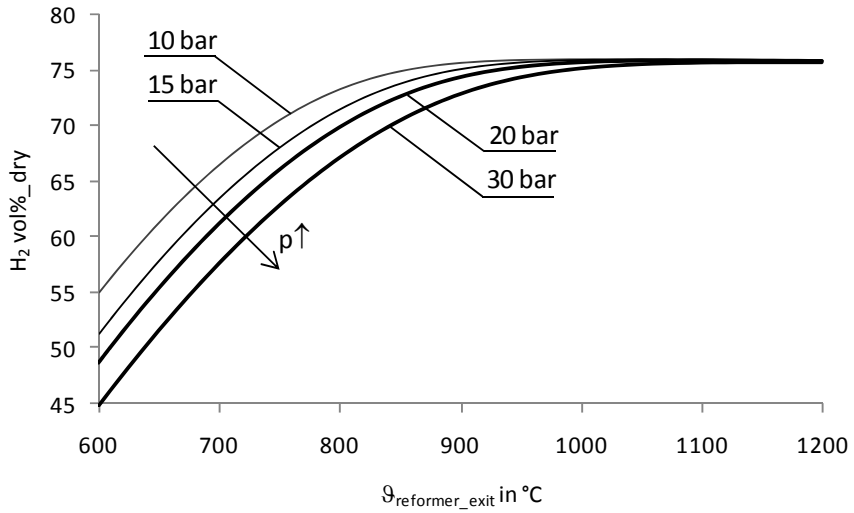

Figure 38 Equilibrium composition of the hydrogen content depending on the reformer exhaust temperature and the reformer pressure at a S/C=2,5 and pure methane in the feed

The maximal possible steam reformer outlet temperature is limited by the melting point of the oxygen carrier and the heat transfer capability of the bubbling bed. Therefore, it is assumed that the minimal temperature difference of the steam reformer exit and the bed material is:

$$\vartheta_{reformer\_min} = 50K.$$

According to le Chatelier's principle and Figure 38 the pressure of the reformer has to be as low as possible for maximum hydrogen yield. Since this study focuses on power production the produced hydrogen should be available at a pressure sufficiently high to be burned in a hydrogen turbine. Typical values for the turbine pressure ratio of state of the art turbines are listed below.

Table 15 Typical pressure ratios of small scale gas turbines [W 9] and [W 8]

Type	Power	Pressure ratio
Siemens		
SGT-100-1S	5,25 $MW(e)$	14,6: 1
SGT-100-2S	4,92 $MW(e)$	13,0: 1
SGT-200-1S	6,75 $MW(e)$	12,2: 1
SGT-200-2S	7,68 $MW(e)$	12,3: 1
SGT-300	7,90 $MW(e)$	13,7: 1
SGT-400	12,9 $MW(e)$	16,8: 1
Alstom		
GT8C2	56,3 $MW(e)$	17,6: 1

Therefore, a hydrogen pressure of

$$p_{H_2} = 18bar(\text{a}).$$

is chosen.

Figure 39 shows the change in the reformer tail-gas composition depending on the reformer temperature and a steam-to-carbon ratio of 2,5 at 18 bar reformer operating pressure. The optimal hydrogen yield would be a at reformer temperature of approximately 1080°C.

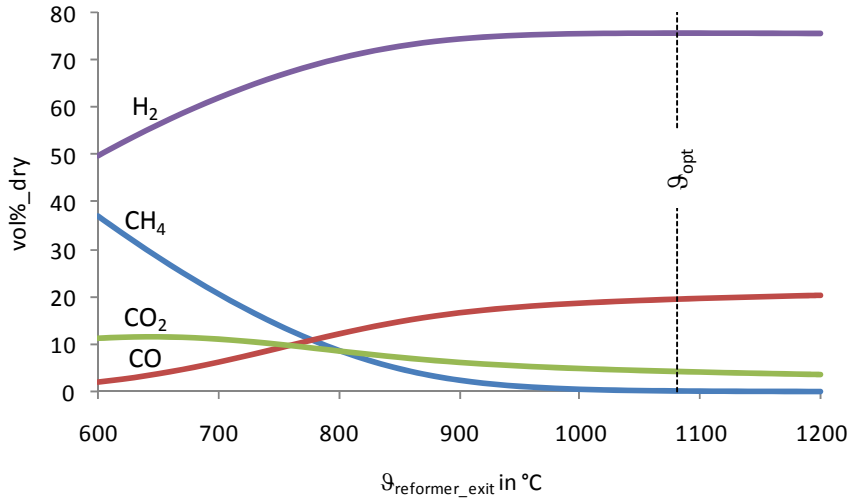

Figure 39 Equilibrium synthesis gas composition depending on the reformer exhaust temperature at 18bar reformer pressure and a S/C-Ratio of 2,5

For the standard case of the simulation to be on the safe side the steam-to-carbon ratio is assumed to be (cf. [25]):

$$S/C = 3$$

CO-Shift

In order to improve the hydrogen yield a carbon monoxide shift reactor is applied utilizing the water-gas-shift reaction.

$$CO + H_2O \longrightarrow CO_2 + H_2 \qquad \text{(reac 3-2)}$$

It is distinguished between three shift reactors depending on the temperature range of the reaction. A CO-shift stage is built up of a fixed bed reactor filled with a special catalyst to achieve maximal hydrogen yield.

- High-temperature (HT)-CO-shift (cf. [27])
  - Operating temperatures: $\vartheta_{out} = 300 \div 530°C$
  - Fast conversion and small volumes of the reactor; equilibrium is not reached
  - Type of catalyst material: Ni/Cr-Oxide, Fe/Cr-Oxide
  - Minimal molar steam to carbon monoxide ratio: $S/CO_{min} = 2 \div 2{,}2$
  - Allowable limits of sulfur: $< 0{,}03\ wt\%$
- Medium-temperature (MT)-CO-shift
  - Operating temperatures: $\vartheta_{in} = 220 \div 270°C$
  - Usually operated isothermal
- Low-temperature (LT)-CO-shift (cf. [27])
  - Operating temperatures: $\vartheta_{out} = 180 \div 270°C$
  - 2nd stage after HT-CO-Shift; equilibrium is almost reached
  - Type of catalyst material: Cu/Zn-Oxide
  - Minimal molar steam to carbon monoxide ratio: $S/CO_{min} = 2 \div 2{,}2$
  - Allowable limits of sulfur: $< 0{,}1\ ppm$
- Typical pressure drop in each reactor: $\Delta p = 0{,}18 \div 0{,}3\ bar$

The equilibrium composition depends on the temperature of the reaction. Typical carbon monoxide contents at the CO-shift outlet depending on the CO-shift outlet temperature are shown below.

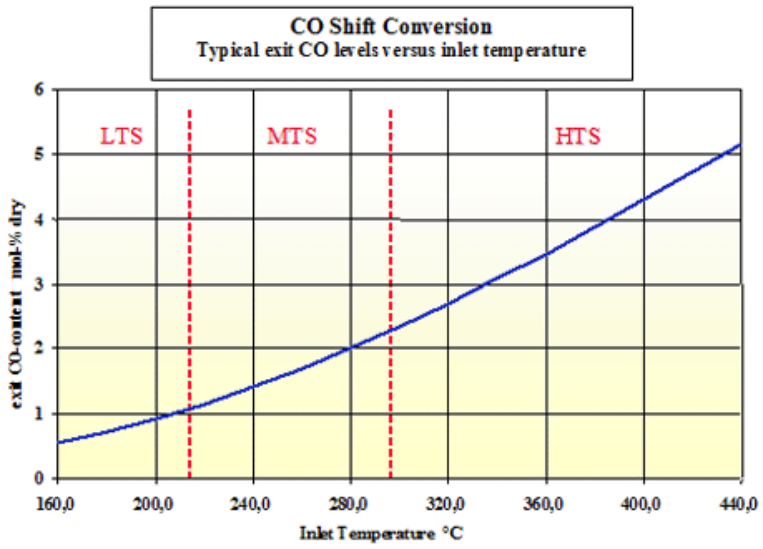

Figure 40 Typical exit CO levels versus inlet temperature. From Linde [W 6]

The use of a HT-CO-shift reactor is state of the art in hydrogen production plants. The hydrogen yield can be increased when using a LT-CO-shift. The additional investment is reasonable for large plants having a capacity above approximately 40.000 Nm³/h H_2 product. For plants having a capacity of above approximately 50.000 Nm³/h H_2 product it is also possible to replace the HT- and LT-CO-shift reactor by one isothermal MT-CO-shift reactor. Three different process configurations for CO-Shift conversion are commercially in use.

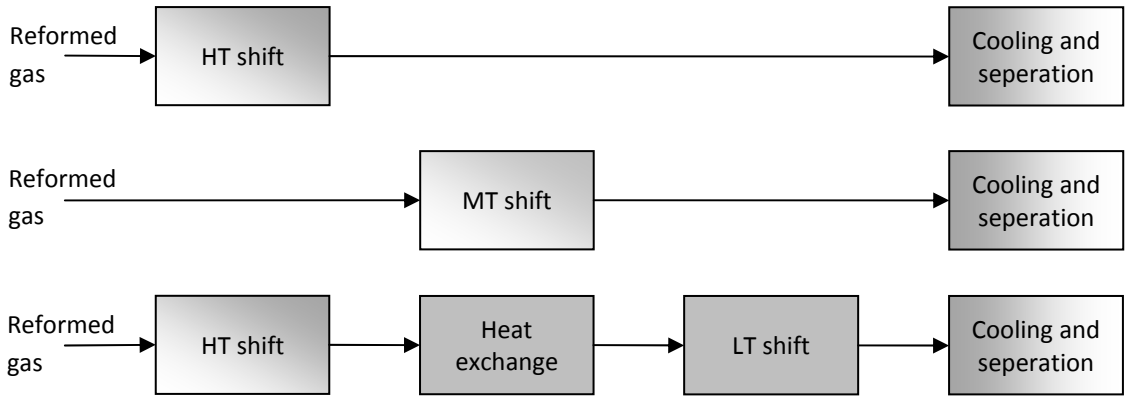

Figure 41 Typical process options for CO shift conversion

For the scale discussed in this thesis it seems to be feasible to use a single high temperature CO-shift reactor.

To identify the state of the CO-shift reaction the CO-conversion across the reactor is used. It is defined as one minus the coefficient of the CO mass flow in the shift outlet and the CO mass flow in the shift inlet.

$$X_{CO} = 1 - \frac{\dot{m}_{CO\_out}}{\dot{m}_{CO\_in}} \qquad \text{(eqn 3-28)}$$

Hydrogen separation process

The choice of the hydrogen purification process depends on the requirements concerning product purity, economics, process flexibility and reliability. The three main hydrogen purification technologies are pressure swing adsorption (PSA), selective permeation using polymer membranes and cryogenic separation. Each of these processes bases on different separation principles and for that reason the process characteristics differ significantly.

Pressure Swing Adsorption (PSA) process

The PSA process is based on the ability of an adsorbent to adsorb greater amounts of impurities at high gas-phase partial pressure than at low partial pressure.

A PSA unit consists of a container filled with adsorbent packets. The packing adsorbs the impurities at high pressure and is desorbed afterwards by decreasing the pressure. The product gas remains at high pressure and high purity H_2 can be achieved. To provide a continuous service usually 4 to 12 PSA columns are operated in parallel.

Since the driving force of the separation is the pressure difference a minimum pressure ratio of approximately 4:1 between the feed and tail-gas is required. To increase the efficiency of the separation the tail-gas pressure has to be as low as possible.

The advantage of a pressure swing adsorption unit is that essentially no hydrogen is adsorbed and the pressure drop of the product gas usually is lower than 0,5bar with hydrogen purities greater than 99vol% (usually 99,999vol% is possible). (cf. [61])

Membrane process

Membrane systems are based on the difference in permeation rates between hydrogen and impurities across a gas-permeable polymer membrane. For permeation, the gas-components have to dissolve into the membrane and then to diffuse through to the permeate side of the membrane. The separation bases on the fact that different components have different solubility and permeability. Gases with high permeability, such as hydrogen, enrich on the permeate side while gases with low permeability enrich on the non-permeate side of the membrane. Hence the first fraction of product gas consists primarily of the component with the highest permeability. The advantage of a membrane separation process is that it is easy to expand and high hydrogen recovery rates achieved. (cf. [61])

Cryogenic process

Cryogenic separation bases on the different boiling temperatures (relative volatility) of the feed components. The feed therefore is cooled by Joule-Thompson refrigeration which is derived from throttling the condensed liquid hydrocarbons or, if required, by external refrigeration packages or by turbo expansion of the hydrogen product. The cryogenic separation unit usually splits the feed into three products: a high purity hydrogen, a methane-rich and a C_2^+ hydrocarbon stream. (cf. [61])

Selection of the hydrogen separation technology

The most-appropriate choice of the separation technology depends on both, performance criteria and operational requirements. The characteristics of the different separation processes are summarized below.

Table 16 Hydrogen separation process comparison. According to [63]

Factors	PSA	Membrane	Cryogenic
Minimum feed H_2 in %	50	15	15
Feed pressure in bar	$10 \div 70$	$13{,}5 \div 135$	$13{,}5 \div 80$
H_2 purity in %	$99{,}9 +$	$max\ 97$	$max\ 98$
H2 recovery up to in %	90	97	98
CO+CO_2 removal	Yes	No	No
H_2 product pressure	Approx. feed	Much less than feed	Approx. feed

Because of the high selectivity towards hydrogen, the capability of CO and CO_2 removal and since a PSA unit is state of the art in almost every hydrogen plant this technology is chosen for the hydrogen separation in this study. Therefore, a pressure swing adsorption unit has been developed for IPSEpro (see A-2 Model of a pressure swing adsorption module for IPSEpro).

Efficiency definitions

Additionally to the efficiency definitions summarized in chapter 2.3.1 the hydrogen production efficiency is expanded. For a better assessment of the single process parts additionally to the hydrogen production efficiency (eqn 2-21) the hydrogen production efficiency of the reformer

$\xi_{reformer}$ is defined. Therefore, the maximal possible hydrogen mass flow is related to the actual amount produced.

$$\xi_{refomer} = \frac{\dot{m}_{H_2\_ref\_out}}{\dot{m}_{H_2\_ref\_out\_max}} \quad \text{(eqn 3-29)}$$

The global hydrogen production efficiency is defined as the coefficient of the produced hydrogen and the maximal producible hydrogen when 100% hydrogen is separated within the PSA-Unit.

$$\xi = \frac{\dot{m}_{H_2}}{\dot{m}_{H_2 max}} \quad \text{(eqn 3-30)}$$

Optimal reactor temperatures

The reactor temperature has to be chosen in order to increase the systems' exergetic output. The system is comparable to the power generation cycle with fluidized bed cooler since the reformer extracts the excessive heat from the reactor system. Therefore, the reactors' exhaust temperatures have to be as low as possible to reduce the amount of unburned fuel in the off-gas. On the other hand decreasing reactor temperatures decrease the heat available for steam reforming which influence the reformer product gas composition (see Figure 39) and might have a negative effect on the process performance. Therefore, the fuel reactor temperature is chosen to be

$$\vartheta_{FR\_exh} = 900°C$$

in the base simulation situation.

3.5.2 Chemical looping autothermal reforming

State of the reactor system

In the case of autothermal reforming the default case was defined by the European Cachet project. The base assumptions in this project are that the water content in the fuel reactor feed has to be 0,25 and the air-to-fuel-ratio has to be 0,3.

$$S/C = 25$$
$$\lambda = 0{,}3$$

Optimal reactor temperature

The optimal reactor temperature for chemical looping autothermal reforming depends on the fuel reactor outlet composition. As mentioned in chapter 2.4, it is the goal to maximize the hydrogen production. Hence, the fuel reactor outlet temperature has to be optimized with respect to maximize the hydrogen yield. On the other hand the reactor temperatures are limited at high temperatures by the physical and at low temperatures by the chemical properties of the oxygen carrier.

To evaluate the optimal reactor temperatures a chemical looping reactor system was modeled with IPSEpro (Figure 42).

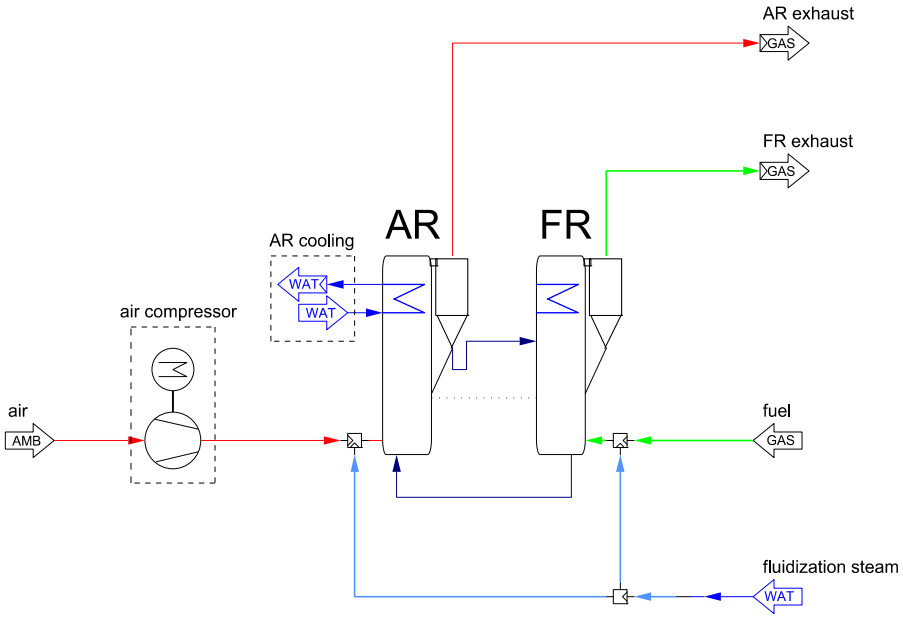

Figure 42 Flow sheet model of a chemical looping reactor system in IPSEpro.

Boundary conditions

For reforming the air reactor has to be modeled in a way that the oxygen in the air and the oxygen carrier (reac 2-11) are in the state of equilibrium. This means that the oxygen is quantitatively consumed in the air reactor. This is an admissible assumption if the reaction time is sufficient (cf. [36]).

The model of the fuel reactor includes the carbon monoxide shift reaction (reac 2-10) in equilibrium and complete methane conversion is assumed. According to Kolbitsch et al. [38] the oxygen carrier shows high methane conversion capability. It is further assumed that the temperature difference of the exhaust gas and the oxygen carrier exiting the reactors are, due to excellent contact and low reaction rate at the top of the reactor, the same. The heat loss is set to zero and the gas pressure drop over the reactors is 0,2 bar. As RedOx system a nickel based oxygen carrier is chosen because of its catalytic behavior. Therefore, complete methane conversion is assumed.

Table 17 Table of settings

Notation	Symbol and Value
Air reactor cooling	$\dot{Q}_{cooling} = 50kW$
Air reactor outlet pressure	$p_{AR\_out} = 1{,}01325\ bar$
Ambient pressure	$p_{amb} = 1{,}01325\ bar$
Ambient relative humidity	$\varphi = 60\%$
Ambient temperature	$\vartheta_{amb} = 25°C$
Fuel	pure methane
Fuel reactor CO-shift equilibrium	$p\delta_{eq\_CO-shift} = 0$
Fuel reactor outlet pressure	$p_{FR\_out} = 1{,}01325\ bar$
Fuel reactor steam-to-carbon ratio	$S/C = 0{,}25$
Methane conversion	$X_{CH_4} = 100\%$
Molar mass of the oxidized oxygen carrier	$M_{ox} = 114{,}26\ kg/kmol$
Molar mass of the reduced oxygen carrier	$M_{red} = 104{,}47\ kg/kmol$
Oxidation state of the oxidized oxygen carrier	$X_{s\_ox} = 27{,}19\%$
Oxidation state of the reduced oxygen carrier	$X_{s\_red} = 14{,}85\%$
Oxygen carrier outlet temperature difference	$\Delta\vartheta_{OC\_out} = 0°C$
Oxygen-oxygen carrier equilibrium	$p\delta_{O_2} = 0$
Pressure drop in the fuel and air reactor	$\Delta p_{gas} = 0{,}2\ bar$
Reactors heat loss	$\dot{Q}_{loss} = 0kW$

Parameter variation

The most important temperature for CLR(a) is the fuel reactor exhaust temperature because it affects the synthesis gas composition. Therefore, it is varied from 700 to 1200°C.

Dependency of the air reactor exhaust temperature

The simulation shows a linear dependency of the air reactor exhaust temperature to the fuel reactor exhaust temperature.

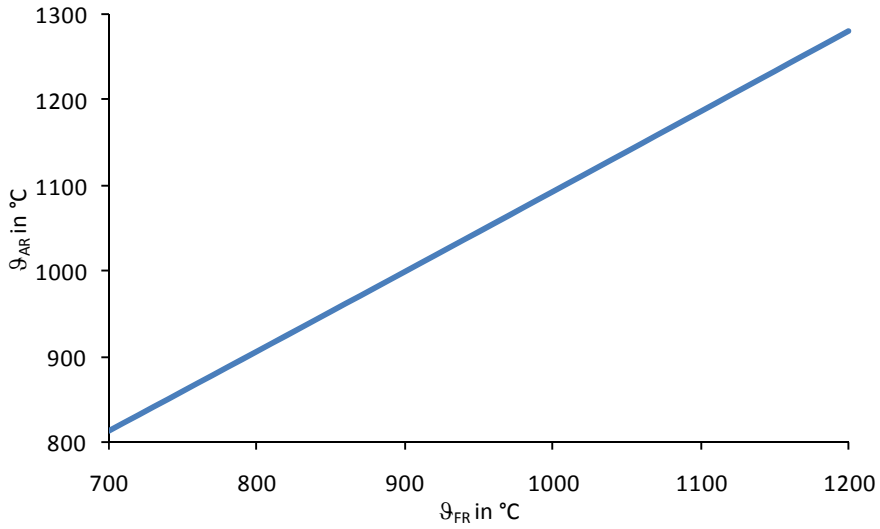

Figure 43 Change of the air reactor temperature depending on the fuel reactor temperature

By assuming that if nickel oxide is used as an oxygen carrier the temperature is limited to 1200°C [47] since the metal tends to agglomeration at high temperature. This leads to a maximum fuel reactor exhaust temperature of approximately 1100°C. On the other hand the temperature is limited by the reduced reactivity of the oxygen carrier inside the fuel reactor. Tests at the chemical looping test rig at the technical university of Vienna showed that a stable operation at fuel reactor temperature of 750°C or even lower is possible.

Dependency of the product gas composition and the LHV and the lambda value

The simulation shows that the lower the fuel reactor exhaust temperature the more hydrogen is produced and the higher is the lower heating value of the product gas. At the same moment the amount of CO_2 and CO and the lambda value decreases.

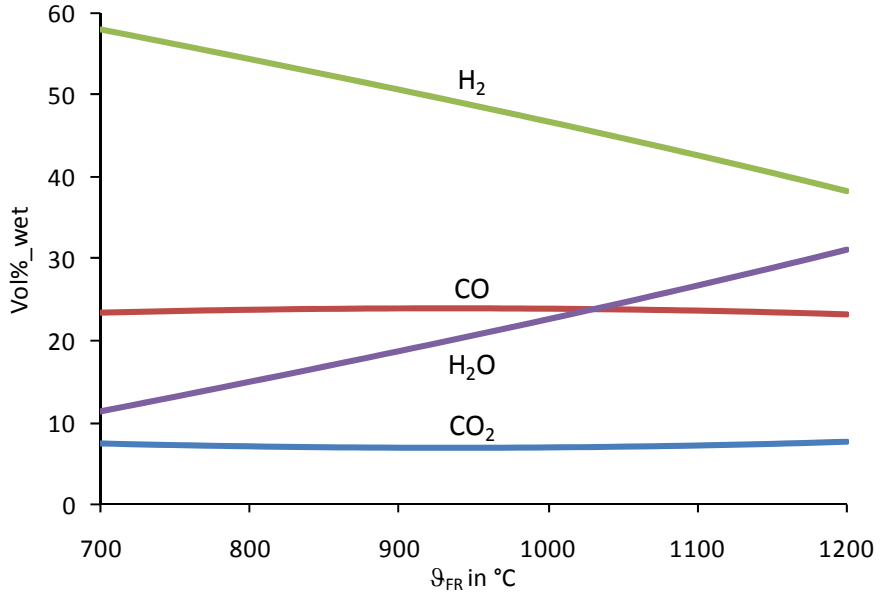

Figure 44 Change of the fuel reactor outlet gas composition depending on the fuel reactor exhaust temperature

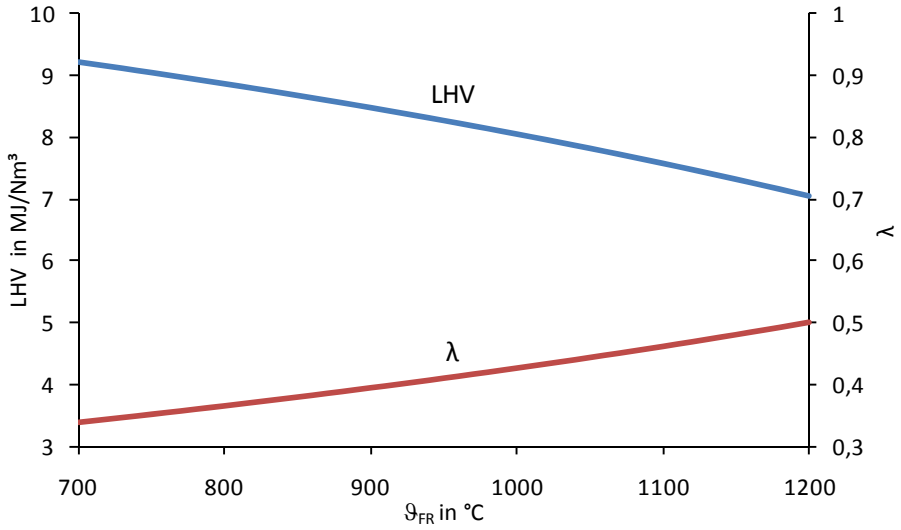

Figure 45 Change of the LHV of the fuel reactor outlet gas and the fuel to air ratio depending on the fuel reactor exhaust temperature

This is the case because at higher temperatures the gas streams have to be heated up more. Hence, additional hydrogen has to be converted to steam (the water content increases) which requires more oxygen and the lambda value increases.

The simulation shows hydrogen production is increased at a low fuel reactor exhaust temperature. Therefore, in the standard case of the simulation the fuel-reactor outlet temperature is assumed to be:

$$\vartheta_{FR\_exh} = 850°C$$

Live steam conditions and steam turbine efficiency

The aim of chemical looping-hydrogen power is to produce as much as possible of the hydrogen. Therefore, high quality live steam conditions and high steam turbine efficiency are not the most important. Consequently the following live steam parameters are chosen:

$$p_{LS} = 80\ bar$$
$$\vartheta_{LS} = 450°C$$

It is proposed to use a simple steam turbine, like a single stage Curtis turbine which is capable to handle large stage work and therefore is simple and inexpensive, with an isentropic efficiency of:

$$\eta_{s,t} = 70\ \%$$

Carbon dioxide separation method

The efforts of the carbon dioxide separation technology for autothermal reforming go in line with the widely discussed post combustion capture technology. (It is proposed that technologies feasible for post capture are also an option for carbon-dioxide removal from the product stream of CLR(a).) For post capture technologies separation principles such as absorption (chemical and physical), adsorption, cryogenic distillation and membranes have been proposed. The selection of the best technology depends on the flue gas properties. The characteristics of CLR(a) product gas are a higher CO_2 content and lower volume flow rates compared to flue gases of conventional combustion.

Gas separation membranes are thin films that are capable to separate certain components with a high selectivity. Gas separation membranes seem to have a great potential but are not commercially available at the moment.

Adsorption with commercially used physical solvents is better suited for applications at high partial pressures of the carbon-dioxide (Figure 46). Since the partial pressure in this application is rather low this technology seems not favorable.

The only commercially available technology capable to separate carbon-dioxide at low partial pressures from flue gases is absorption with chemical solvents (Figure 46). Typical chemical solvents are aqueous solutions of alkanolamines such as monoethanolamine (MEA), diethanolamine (DEA), methyldiethanolamine (MDEA) and the newly developed sterically hindered amines.

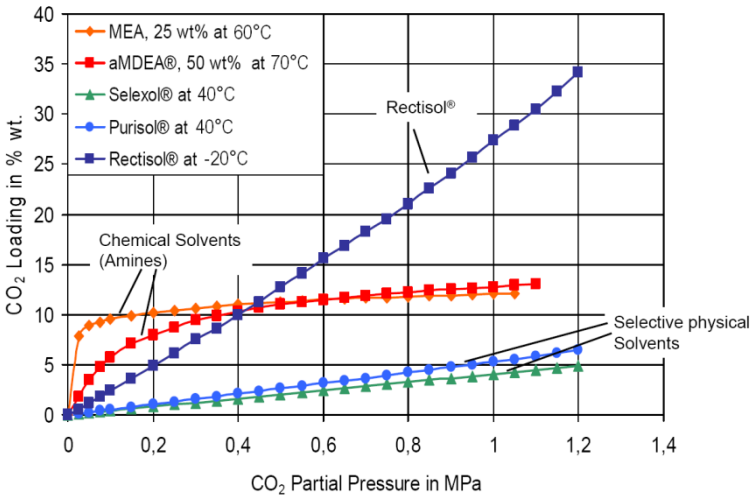

Figure 46 CO_2 loading capacity of chemical solvents [39]

Figure 46 show that monoethanolamine (MEA) are for low CO_2 partial pressure the favorable choice and therefore for processes considered in this study. According to Dang et al. [16] the absorbability of MEA can be increased by a factor of 1,5-2,5 if piperazine is added. Figure 47 shows a typical absorption process.

A typical amine absorption process layout is shown below.

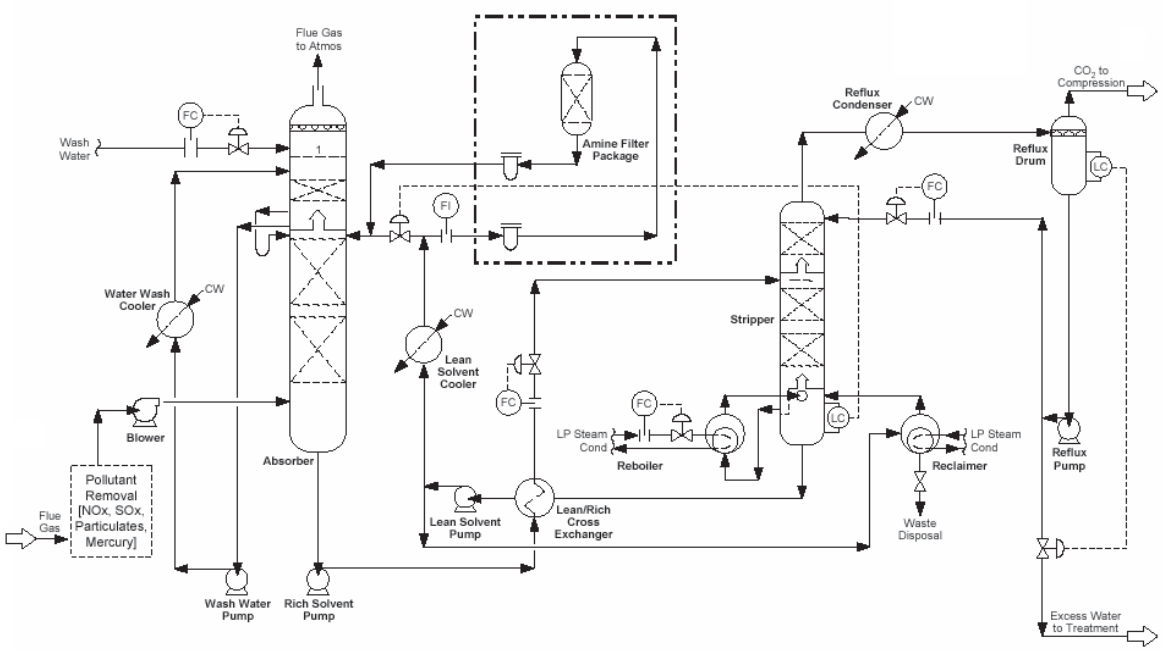

Figure 47 Amine absorption process – basic process layout [14]

The main components of a amine scrubber are the absorber, the desorber or also called stripper, the lean/rich cross heat exchanger and the reflux condenser.

When the flue gas is entering the absorber the lean solvent solution absorbs the gas component which has to be removed. After the enriched solvent is exiting the absorber it passes the lean/rich cross heat exchanger where it is heated up to almost desorber temperature. Then the preheated enriched solvent enters the desorber where the gas component is desorbed. The desorption process is endothermic. The required heat for desorption is applied in the reboiler. The reboiler

heat duty mainly depends on the quality of the lean/rich heat exchanger. Therefore, the lean/rich cross heat exchanger is a very important component.

Amine absorption can be designed to capture 85-95% of the CO_2 in the flue gas with carbon-dioxide purities of over 99,95%. Theoretically both, the level of recovery and purity, are not limited physically but economically. (cf. [14])

A few things have to be taken into account when using an amine scrubber for CO_2 removal from flue gases:

- Flue gas temperature: Limited due to solvent degradation and decreased absorber efficiency.
- Oxygen: Oxygen can increase corrosion and solvent degradation in the absorber system.
- SO_x: SO_x reacts irreversibly with MEA and therefore inhibits the absorption.
- NO_x: Nitrogen-oxides have led to corrosion problems and solvent degradation in some absorption plants.
- $Fly\ ash$: Fly ash may cause solvent foaming.
- Soot: Soot is a special problem in heavy oil fired plants.
- Waste products: Degradation of amine solvent creates a waste product.

For the base case in the simulation the CO_2 separation coefficient is assumed to be (cf. [17]):

$$X_{CO_2} = 60\%$$

According to Desideri et al. [17] the reboiler temperature has to be as high as possible with respect to solvent degradation, corrosion and solvent loss in order to increase the separation efficiency. Generally the reboiler temperature depends on the pressure inside the desorber. Therefore, the higher the desorber pressure is the higher the possible desorption temperature can be.

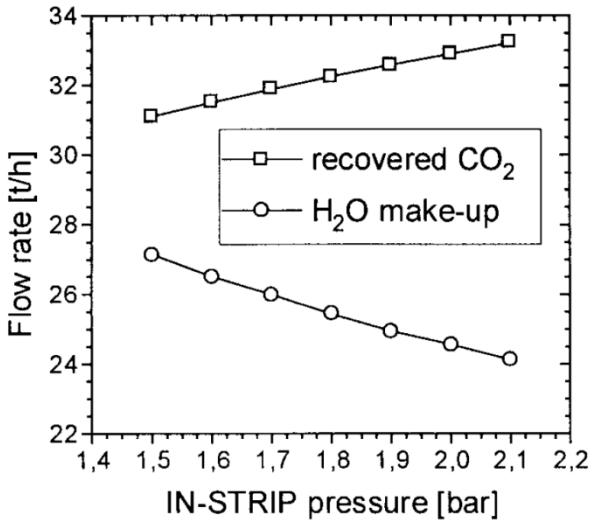

Figure 48 Influence of stripper pressure on recovered CO_2 and water make-up [17]

Hence it is assumed that the desorber pressure is 1,5bar and the reboiler temperature is 120°C. (cf. [17])

$$p_{desorber} = 1{,}5bar$$

$$\vartheta_{reboiler} = 120°C$$

Assuming a temperature difference of the heat releasing condensing steam and the solvent of 10°C (cf. [17]) the saturated steam heating the reboiler has to have a temperature of:

$$\vartheta_{des,steam} = 130°C$$

For desorption of the CO_2 large amounts of low caloric steam is required. Data from the literature vary from 2,76 to 3,95 GJ/tCO_2. According to [17] the required heat consumption for the solvent regeneration is assumed to be:

$$\dot{q}_{CO_2 removal} = 3{,}68\ {}^{GJ}/_{tCO_2}$$

Another important constraint is the absorber inlet temperature. Since a high desorber temperature would increase the loss of solvent the temperature has to be kept as low as possible. Since typical exhaust temperatures in gas powered power plants range from 45 to 65°C and because there are data available for 65°C absorber inlet temperature it is assumed that the gases entering the desorber have got a temperature of: (cf. [17])

$$\vartheta_{desorber\_inlet} = 65°C$$

In addition it is assumed that the scrubber heat loss is zero.

$$\dot{Q}_{scrubber-loss} = 0\ kW$$

4 Results and Discussion

4.1 CLC-Power-Generation

4.1.1 Simulation boundary conditions

With reference to chapter 3.4.2 an isentropic steam turbine efficiency of

$$\eta_{s,t} = 80\%$$

is chosen. According to chapter 3.4.11 a fan / compressor efficiency of

$$\eta_{s,C} = 80\%$$

is chosen. It is assumed that the gas exiting the CO_2-cooler has got a rest-water-content of:

$$y_{H_2O} = 4\%$$

Table 18 Table of set values in case of CLC

Notation	Symbol and Value
Condenser pressure	$p_{co} = 0{,}1\ bar$
CO-shift reaction equilibrium in the fuel reactor	$p\delta_{eq\_CO-shift} = 0$
CO oxidation with metal oxide equilibrium in the fuel reactor	$p\delta_{eq\_CO-CO_2} = 0$
Fuel reactor exhaust temperature	$\vartheta_{FR\_exh} = 900°C$
Isentropic efficiency of the water pumps	$\eta_{s\_waterpump} = 85\%$
Live steam pressure	$p_{LS} = 80\ bar$
Live steam temperature	$t_{LS} = 500°C$
Loop-seal fluidization mass flow relative to gas-mass flow	$\dot{m}_{LS\_fluid\_rel} = 0{,}2\%$
Fuel reactor methane conversion	$X_{CH_4} = 100\%$
Minimal terminal temperature difference air preheater	$\Delta\vartheta_{min\ \_aph} = 25\ °C$
Minimal terminal temperature difference gas-gas heat-exchanger	$\Delta\vartheta_{min\ ,gas\_gas,hx} = 50\ °C$
Minimal terminal temperature difference gas-water heat-exchanger	$\Delta\vartheta_{min\ ,gas\_wat,hx} = 20\ °C$
Minimal terminal temperature difference water-water heat-exchanger	$\Delta\vartheta_{min\ ,wat\_wat,hx} = 10\ °C$
Pressure drop in the fuel and air reactor	$\Delta p_{gas} = 0{,}2\ bar$
Pressure drop of the steam in the superheater	$\Delta p_{sh} = 10\ bar$
Pressure drop of the gas inside the boiler	$\Delta p_{gas\_total} = 40\ mbar$
Applied reactor cooling	$\dot{Q}_{cooling} = 50kW$
Relative heat loss of the CLC reactor system relative to the air mass flow	$\dot{q}_{loss.rel} = 0{,}265\%$
Relative leakage mass flow of the air preheater	$\dot{m}_{rel} = 1{,}5\%$
Stoichiometric ratio (lambda)	$\lambda = 1{,}02$

4.1.2 Chemical looping combustion power cycle with fluidized bed cooler

The process flow sheet of the CLC power cycle with fluidized bed cooler is shown in Figure 50.

The central design elements are the two fluidized bed coolers which are used as evaporator and superheater.

After the gas is leaving the air reactor it first passes an evaporator (evap) and a high pressure economizer (HP ECO). Afterwards it is used for preheating of the compressed air (reg LuVo).

The fuel reactor off gas first passes an evaporator (evap) and then is used for fuel preheating (fuel preheater). Afterwards it passes the low pressure economizer (LP ECO) and is then dried and compressed (CO_2-cooler and FR FAN).

After the produced saturated steam passes the superheater (SH) it is expanded to condenser pressure in the steam turbine. Bleed steam is used for fluidization of the loop-seals, for deaeration (deaerator) and for recuperative feedwater preheating (rek.preheater). After leaving the condenser the saturated water is compressed to atmospheric pressure (FWP 1) and feeding-water is added. Then the water is compressed to deaerator pressure (FWP 2), preheated in a low pressure economizer (LP ECO) and afterwards deaerated (deaerator). Finally, the feed water is compressed to evaporator pressure (FWP 3), preheated in the recuperative preheater (rek.preheater) and after passing the high pressure economizer (HP ECO) re-introduced into the evaporator system.

Reactor exhaust temperature

The reactor exhaust temperatures are limited by the properties of the oxygen carrier. If the temperature is too high the oxygen carrier tends towards agglomeration while a too low temperature will decrease the reactivity of the oxygen carrier. To show optimization potential towards oxygen carrier mixtures the fuel reactor exhaust temperature is varied from 750 to 1100°C.

The simulation shows (Figure 49) that with increasing fuel reactor exhaust temperature the H_2O and CO_2 content decreases slightly while the H_2 and CO content increases. This behavior reflects the assumption of thermodynamic equilibrium at the fuel reactor exit. In reality, fuel conversion may as well be limited by reactivity. In this case the H_2 and CO concentrations decrease with increasing temperature.

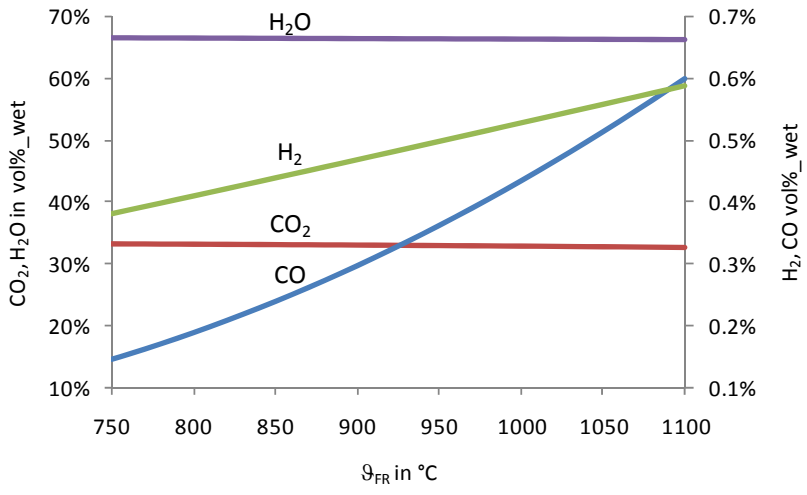

Figure 49 Fuel reactor exhaust composition depending on the fuel reactor exhaust temperature

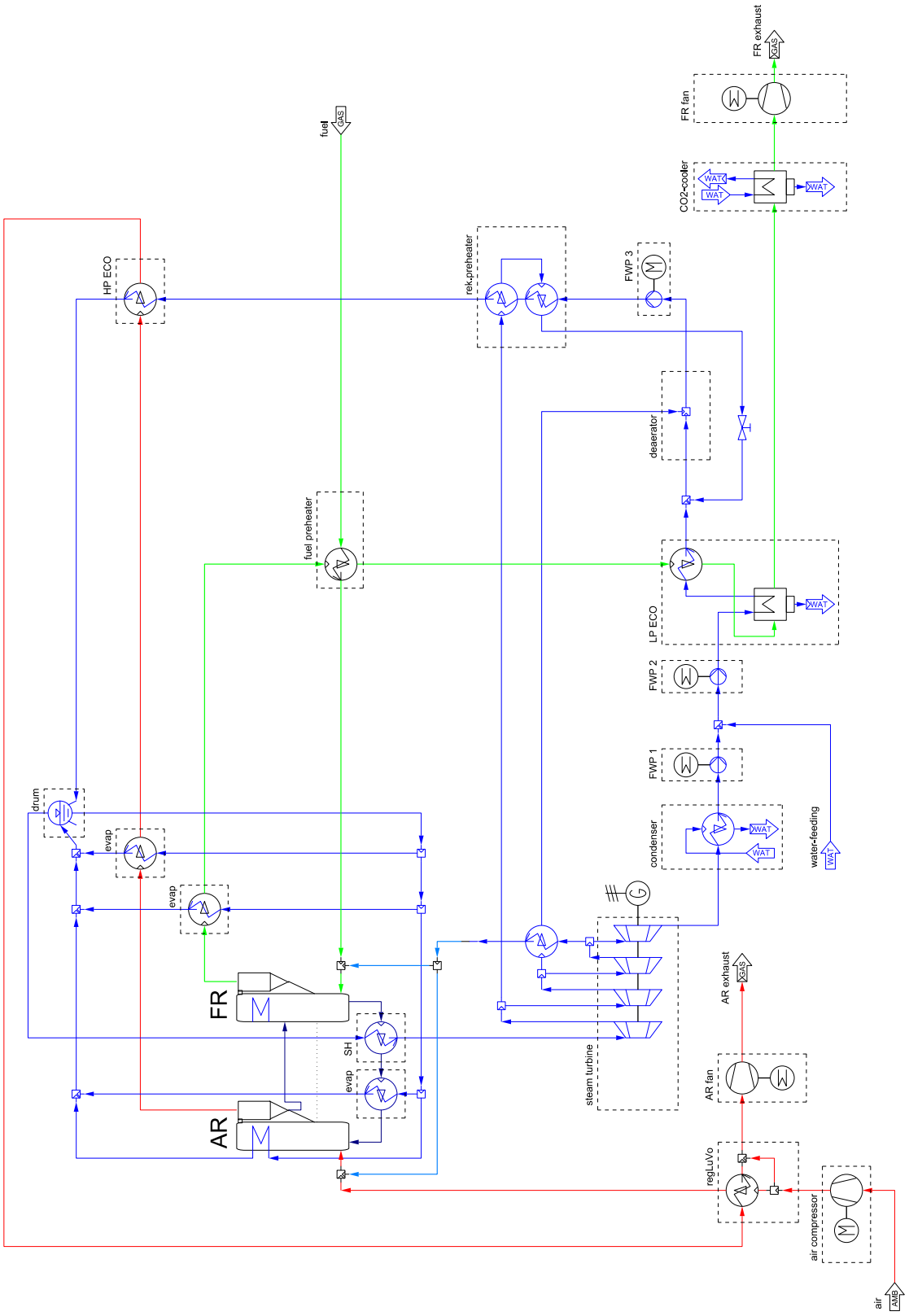

Figure 50 Flow sheet of the chemical looping power cycle with fluidized bed cooler

Increasing amount of CO and H_2 means that unburned fuel is released. Hence, the simulation shows (Figure 51) that the exergetic efficiency ζ increases with decreasing fuel reactor exhaust temperature.

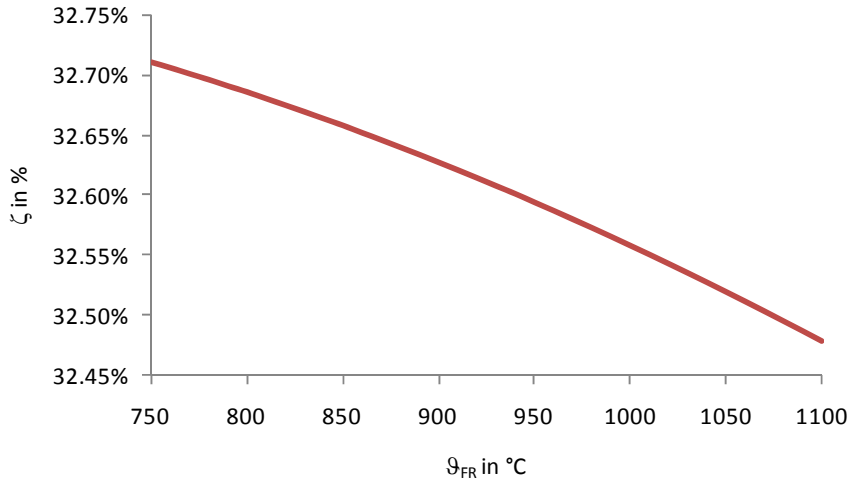

Figure 51 Exergetic efficiency of the cycle depending on the fuel reactor temperature

Therefore, the oxygen carrier could be optimized towards reactivity at low temperatures to enable chemical looping combustion at low reactor temperature.

Optimal deaerator pressure and preheater temperature

The deaerator pressure and the preheater temperature have to be selected in favor of increased cycle efficiency. This is achieved by a minimization of the exergy-loss. The exergetic efficiency of the steam generator ζ_{SG} is defined as the coefficient of the exergy difference of the live steam and the feeding water divided by the supplied fuel exergy.

$$\zeta_{SG} = \frac{E_{LS} - E_{FW}}{E_{fuel}} \qquad \text{(eqn 4-1)}$$

The exergetic efficiency of the steam generator increases with an increasing deaerator pressure. This implies a higher deaeration temperature and an increased preheater temperature.

The exergetic efficiency of the process which is defined as the sum of exergy produced in the process divided by the applied exergy.

$$\zeta_P = \frac{P_{ST} - P_{water,pump}}{E_{LS} - E_{FW}} \qquad \text{(eqn 4-2)}$$

The exergetic efficiency of the process decreases with increasing deaerator pressure or the temperature of preheating.

The exergetic efficiency of the cycle is derived by multiplying the steam generator by the process exergetic efficiencies.

$$\zeta = \zeta_{SG} \cdot \zeta_P \qquad \text{(eqn 4-3)}$$

Since the absolute changes are rather low the relative increase, referred to an arbitrary chosen reference, of the exergetic cycle efficiency is calculated.

$$\zeta_{rel} = \frac{\zeta - \zeta_0}{\zeta_0} \qquad \text{(eqn 4-4)}$$

Influence of the deaerator pressure on the exergetic efficiency of the cycle

The deaerator pressure is varied from 5 to 12 bar and the exergetic efficiencies of the steam generator, process, power cycle and the relative change are plotted in Figure 52.

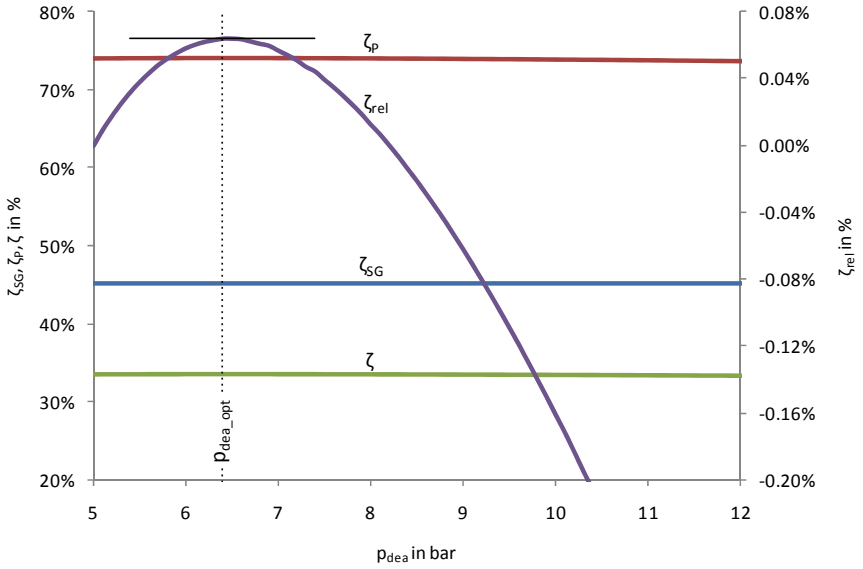

Figure 52 Dependency of the exergetic efficiencies and the deaerator pressure

The variation shows that the cycle performance is the best if the deaerator operates at a pressure of:

$$p_{dea\_opt} = 6{,}4\ bar$$

Influence of the preheater temperature on the exergetic efficiency of the cycle

The preheater temperature is varied from 200 to 260°C and the exergetic efficiency of the steam generator, process, power cycle and the relative change is plotted in Figure 53.

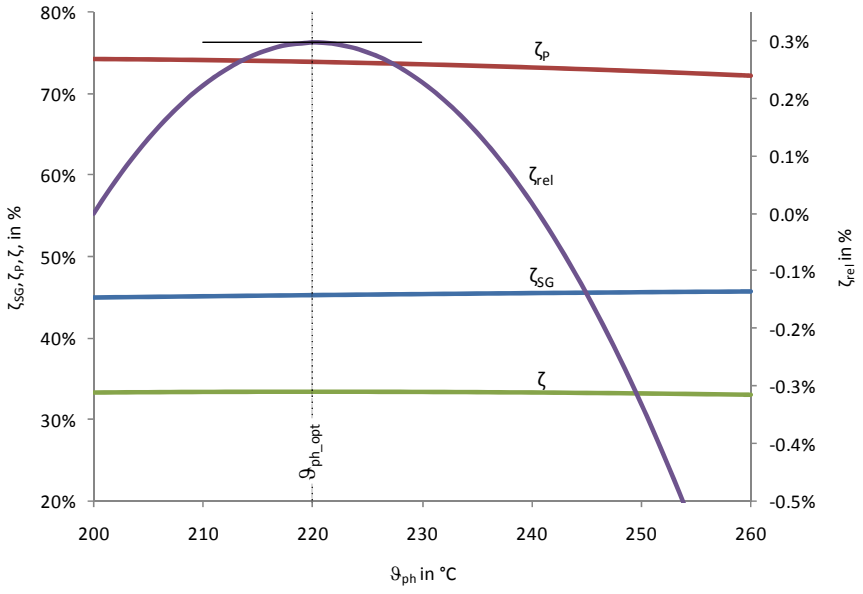

Figure 53 Dependency of the exergetic efficiencies and the preheater temperature.

The variation shows that the cycle performance has a maximum at:

$$\vartheta_{ph\_opt} = 220°C$$

Q-T-Diagram

The Q-T-Diagram is a tool for graphical presentation of heat-exchanger systems. It is commonly used for the design of such systems. It offers the possibility of the graphical evaluation of the efficiency of such systems. Therefore, the resulting Q-T-Diagram at a fuel reactor exhaust temperature of 900°C, a deaerator pressure of 6,4 bar and a feed water preheating temperature of 220°C is shown below.

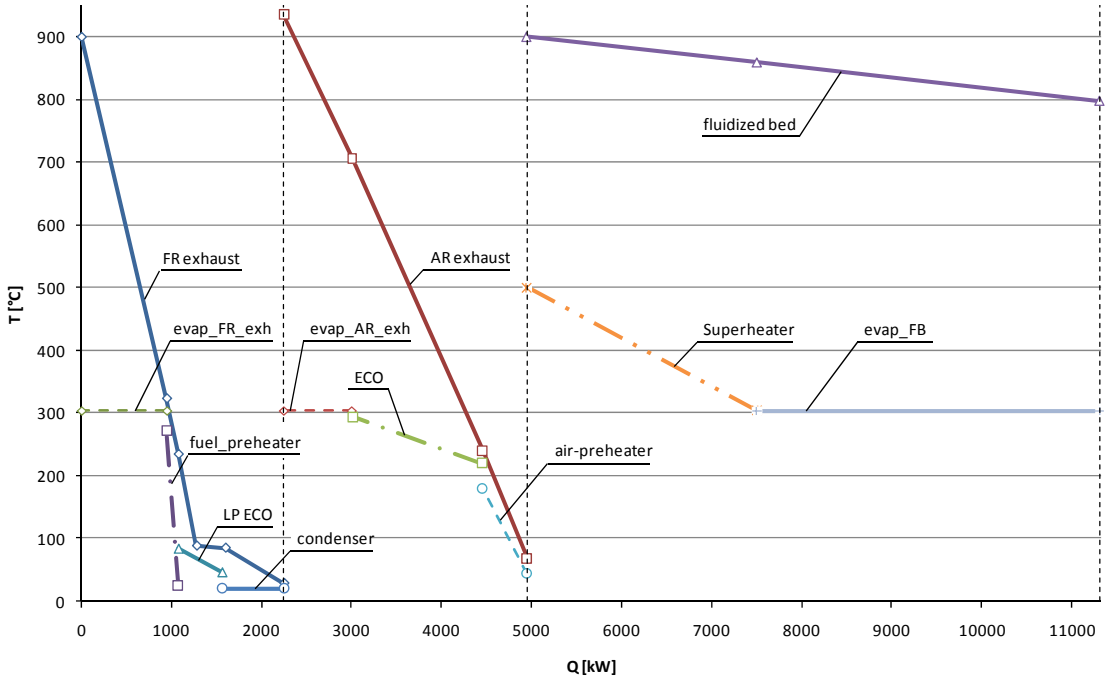

Figure 54 Q-T-Diagram of the process design with fluidized bed cooler

Efficiency of the cycle

The energetic and exergetic efficiency and the loss due to unburned fuel are calculated according to chapter 2.3.1 at a fuel reactor exhaust temperature of 900°C, a deaerator pressure of 6,4 bar and a feed water preheating temperature of 220°C.

Energetic or thermal efficiency:

$$\eta_{th} = \frac{P_{gen} - P_{compressor} - P_{pump}}{\dot{m}_{fuel} \cdot H_u} = 33{,}7\%$$

Exergetic efficiency:

$$\zeta = \frac{P_{gen} - P_{compressor} - P_{pump}}{E_{fuel}} = 32{,}8\%$$

Loss due to unburned fuel:

$$l_u = 1 - \frac{\dot{m}_f \cdot LHV_f - \dot{m}_{off\_gas} \cdot LHV_{off\_gas}}{\dot{m}_f \cdot LHV_f} = 0{,}00738$$

4.1.3 Chemical looping combustion power cycle with fluidized bed cooler simple

The design is similar to the more complex one. The only differences are that no air preheater and no feed water preheater are used. Additionally, the low pressure economizer is moved to the high pressure section (FR_ECO). Furthermore, the fluidization steam is produced separately instead of using bleed steam (FS). The flow sheet is shown below.

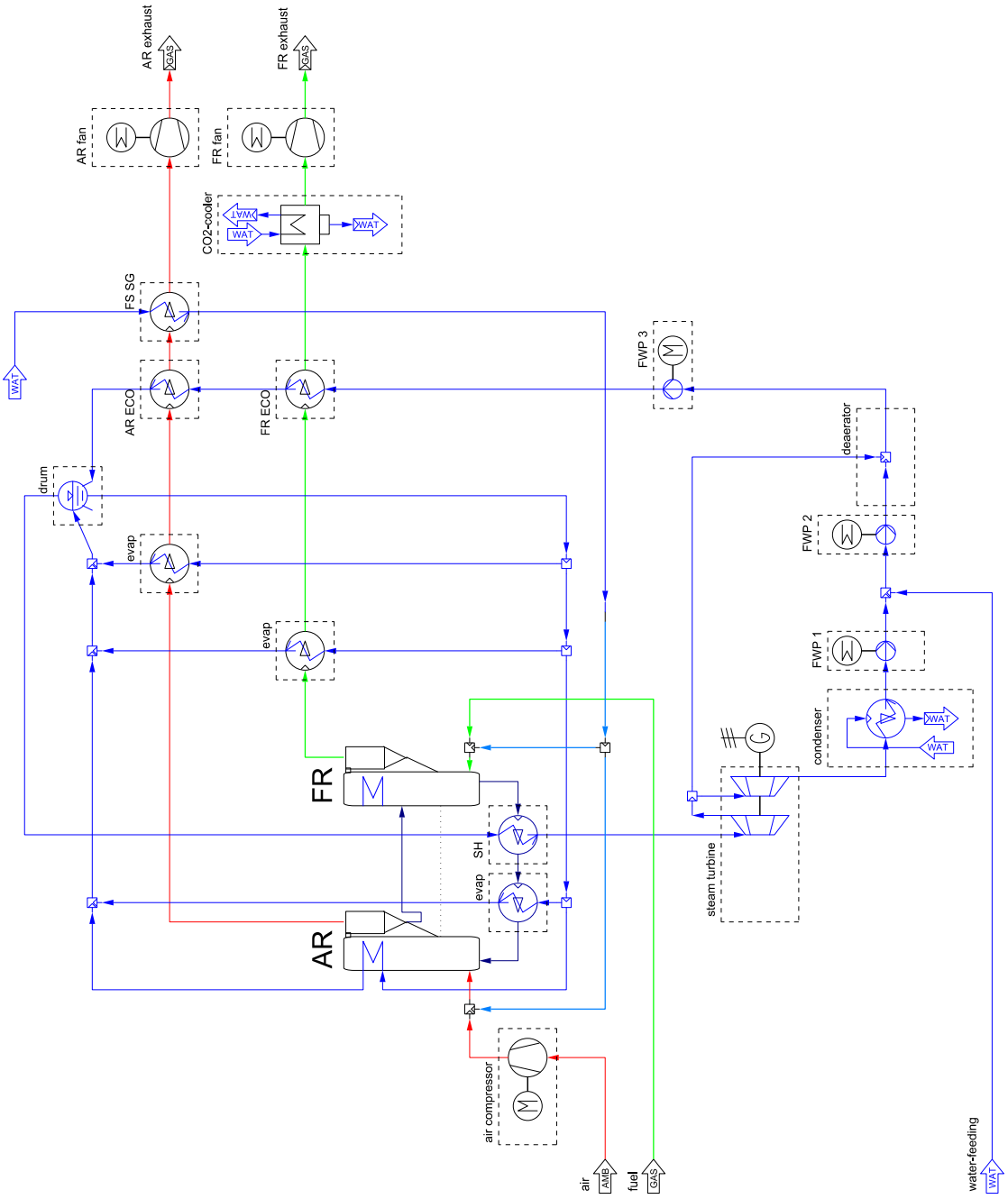

Figure 55 Flow sheet of the chemical looping power cycle with fluidized bed cooler simple

Reactor exhaust temperature and gas composition

The simple process configuration shows the same dependencies of the exhaust gas composition on the fuel reactor temperature as the more complex one. This is because there are no differences in the way the CLC reactor system is operated.

Optimal deaerator pressure

The optimal deaerator pressure is determined like in the design case with fluidized bed cooler. The resulting optimal deaerator pressure is:

$$p_{dea\_opt} = 3{,}4\ bar$$

Q-T-Diagram

The resulting Q-T-Diagram at a fuel reactor exhaust temperature of 900°C and a deaerator pressure of 3,4 bar is shown below.

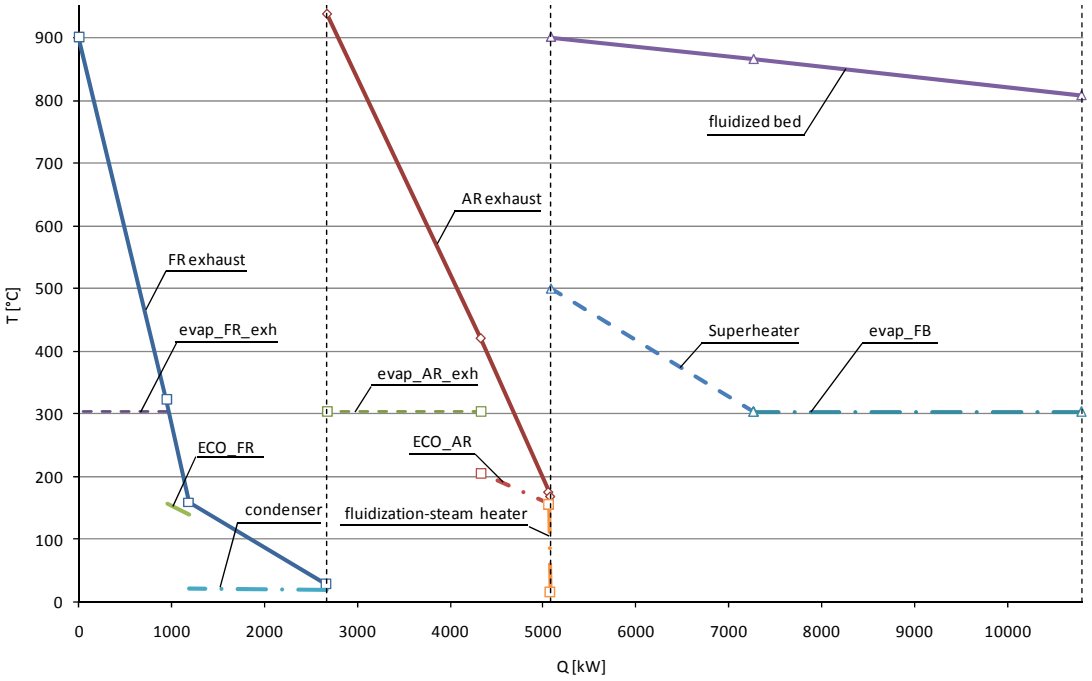

Figure 56 Q-T-Diagram of the process design with fluidized bed cooler simple

Efficiency of the cycle

The energetic and exergetic efficiency and the loss due to unburned fuel are calculated according to chapter 2.3.1 at a fuel reactor exhaust temperature of 900°C and a deaerator pressure of 3,4 bar.

Energetic or thermal efficiency:

$$\eta_{th} = \frac{P_{gen} - P_{compressor} - P_{pump}}{\dot{m}_{fuel} \cdot H_u} = 30{,}6\%$$

Exergetic efficiency:

$$\zeta = \frac{P_{gen} - P_{compressor} - P_{pump}}{E_{fuel}} = 29{,}7\%$$

Loss due to unburned fuel:

$$l_u = 1 - \frac{\dot{m}_f \cdot LHV_f - \dot{m}_{off\_gas} \cdot LHV_{off\_gas}}{\dot{m}_f \cdot LHV_f} = 0{,}00738$$

4.1.4 Chemical looping combustion power cycle λ-cooled

The flow sheet of the CLC power λ-cooled power cycle is shown in Figure 58.

The design focuses on a simple reactor system. Therefore, no fluidized bed cooler is used and the produced heat is withdrawn by excessive air passing through the air reactor.

The flow sheet looks very similar to the complex one with fluidized bed cooler. The only difference is that the superheater (SH) is a gas water heat exchanger placed in the air reactor exhaust gas instead of using a fluidized bed cooler. Therefore, the reactor system has got no internal parts.

Reactor exhaust temperature

The change of the fuel reactor exhaust composition remains the same as in the design case with fluidized bed cooler (compare Figure 49 and Figure 57).

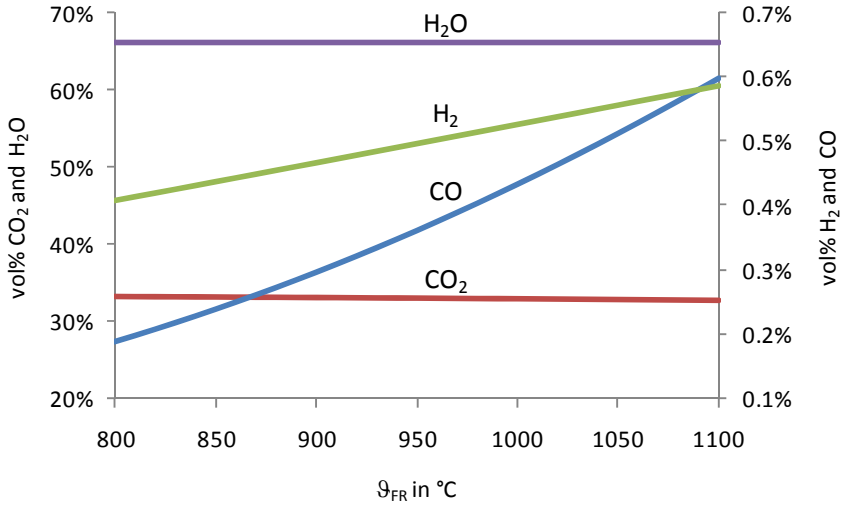

Figure 57 Fuel reactor exhaust composition depending on the fuel reactor exhaust temperature

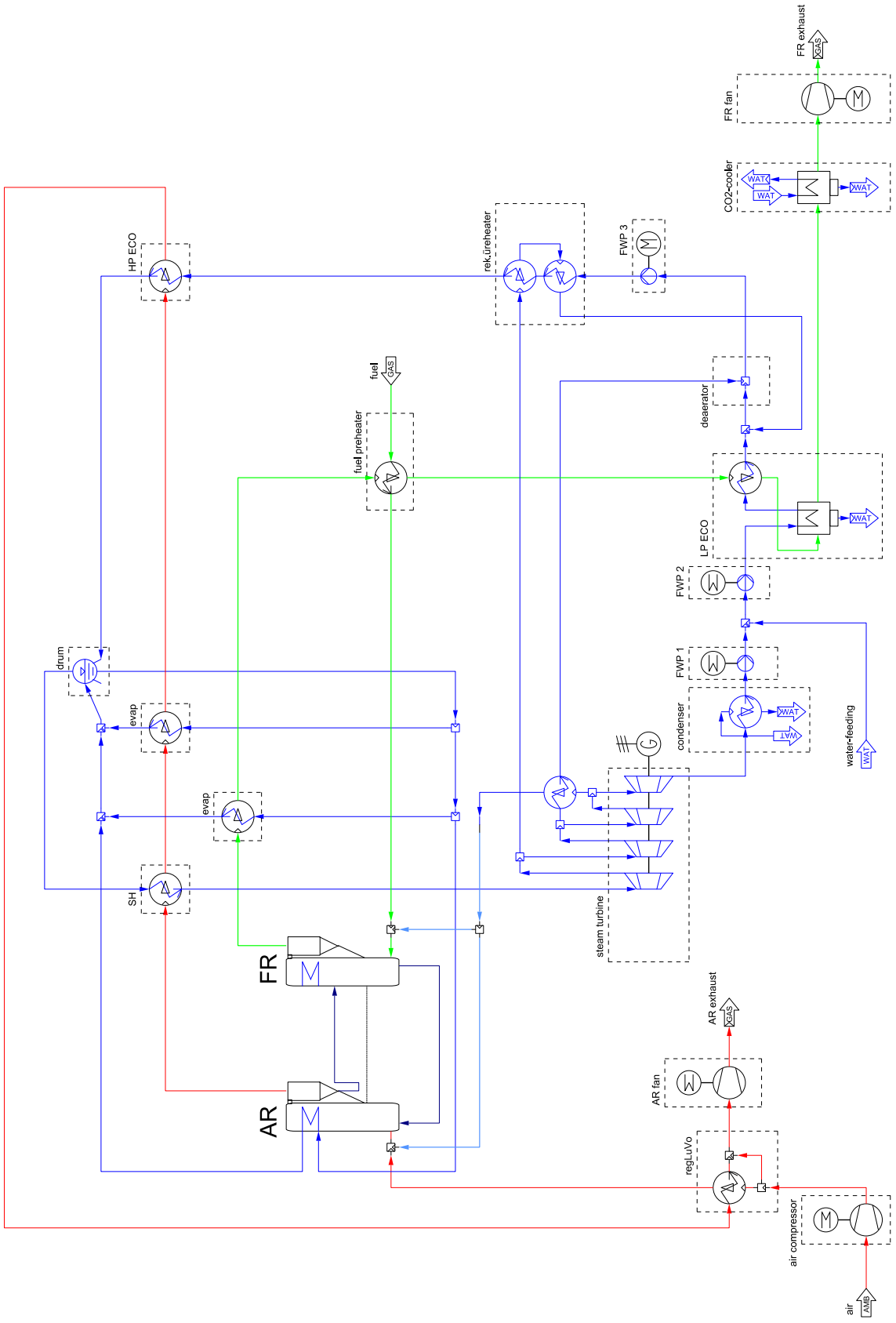

Figure 58 Flow sheet of the chemical looping power cycle λ-cooled

The simulation shows that increasing fuel reactor exhaust temperature leads to greater exergetic efficiency ζ (Figure 59).

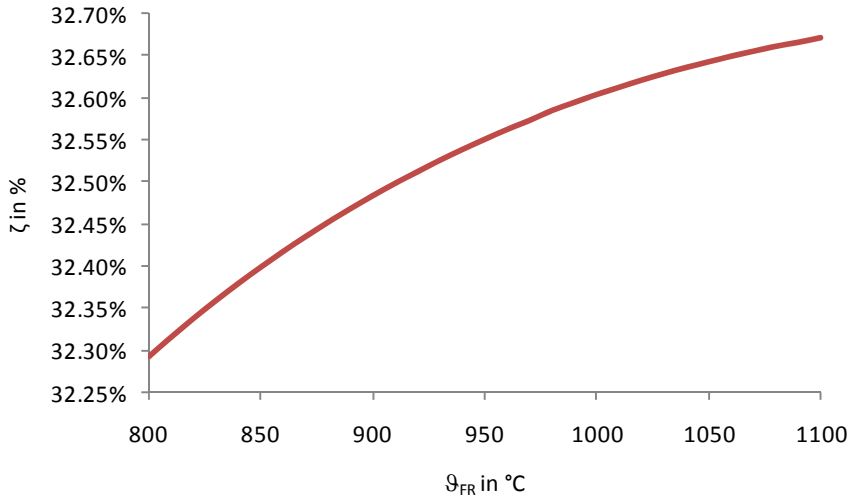

Figure 59 Exergetic efficiency of the cycle depending on the fuel reactor temperature

While in the case with fluidized bed cooler lower reactor temperatures lead to a better process performance (see Figure 49) the simulation shows in the λ-cooled case that higher reactor outlet temperatures are favorable (see Figure 59). This is the case although the loss due to unburned fuel increases with increasing fuel reactor exhaust temperature.

Optimal deaerator pressure and preheater temperature

The optimal deaerator pressure and preheater temperature are determined like in the design case with fluidized bed cooler. The resulting optimal deaerator pressure is

$$p_{dea\_opt} = 6{,}1\ bar$$

The resulting optimal preheater temperature is

$$\vartheta_{ph\_opt} = 216°C$$

Q-T-Diagram

The resulting Q-T-Diagram at a fuel reactor exhaust temperature of 900°C, a deaerator pressure of 6,1 bar and a feed water preheating temperature of 216°C is shown below.

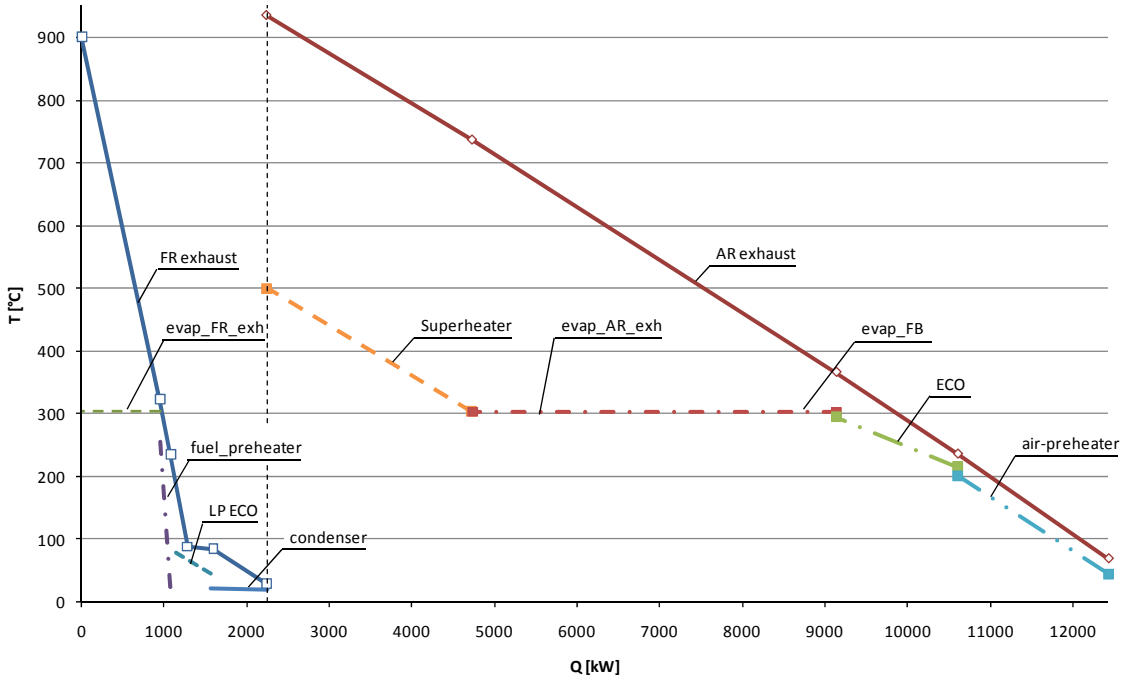

Figure 60 Q-T-Diagram of the λ-cooled process design

Efficiency of the cycle

The energetic and exergetic efficiency and the loss due to unburned fuel are calculated according to chapter 2.3.1 at a fuel reactor exhaust temperature of 900°C, a deaerator pressure of 6,1 bar and a feed water preheating temperature of 216°C.

Energetic or thermal efficiency:

$$\eta_{th} = \frac{P_{gen} - P_{compressor} - P_{pump}}{\dot{m}_{fuel} \cdot H_u} = 31{,}1\%$$

Exergetic efficiency:

$$\zeta = \frac{P_{gen} - P_{compressor} - P_{pump}}{E_{fuel}} = 30{,}2\%$$

Loss due to unburned fuel:

$$l_u = 1 - \frac{\dot{m}_f \cdot LHV_f - \dot{m}_{off\_gas} \cdot LHV_{off\_gas}}{\dot{m}_f \cdot LHV_f} = 0{,}00738$$

4.1.5 Summary and conclusion for CLC power generation

The process simulation with IPSEpro shows that chemical looping combustion is a carbon dioxide sequestration ready power generation technology.

The theoretical considerations (see chapter 2.3.2) that if a fluidized bed cooler is used the process efficiency increases due to decreased air reactor off-gas mass flow which decreases the so-called stack loss have been confirmed.

The simulation also shows that if no fluidized bed cooler is used the thermal efficiency of the process increases with increasing reactor temperature although the amount of unburned fuel increases. This is graphically explained by using the Q-T-diagram (Figure 60). Increasing reactor exhaust temperatures lead to exhaust gas graphs with greater inclination because the total amount of heat input remains the same. Therefore, at a fixed evaporation pressure and pinch-point temperature the amount of producible steam increases. In the design case with fluidized bed cooler decreasing reactor temperatures will lead to a Q-T-diagram (Figure 54) where the graphs of the exhaust gases are moving down and the graph of the bed flattens. This means that heat is moved from the exhaust gases to the bed at lower reactor temperatures. Therefore, the amount of steam producible remains almost constant while the loss due to unburned fuel decreases. This has positive effects not only on the amount of steam producible but also on the loss due to unburned fuel.

The calculated process efficiencies at a fuel reactor exhaust temperature of 900°C (and the calculated optimal deaerator pressure and feed water preheating temperature) are summarized in Table 19.

Table 19 Summary of the process efficiencies

	η_{th} in %	ζ in %	l_u
with fluidized bed cooler	33,7	32,8	0,00738
with fluidized bed cooler simple	30,6	29,7	0,00738
λ-cooled design	31,1	30,2	0,00738

The idealized flow-sheet simulation shows that the loss due to unburned fuel is higher than in a conventional oil or gas fired power plant (typical losses due to unburned fuel l_u=0-0,005 [29]) but lower than in coal fired power plants (typical losses due to unburned fuel $l_u \geq$0,01 [29]). Mention, this is only true if the modeled reactions are in equilibrium which is only theoretically possible.

It is proposed to use fluidized bed coolers to increase the thermal efficiency of the power generation cycle. Therefore, oxygen carriers with high reactivity at lower temperatures are required. A future step to decrease the loss due to unconverted carbon monoxide and hydrogen might be to include a polishing step or to switch to another (see Figure 14) or mixtures of oxygen carrier materials. The polishing step can be an afterburner which uses pure oxygen or a separation step which separates the burned from the unburned gases and recycles the unburned gases (compare Figure 11 bleed stream).

4.2 CLR-Hydrogen-Power

4.2.1 Chemical looping steam reforming

4.2.2 Simulation boundary conditions

The steam reformer is assumed to operate ideally which means that the methane conversion (reac 2-7) and the CO-shift (reac 2-10) equilibrium is reached.

$$p\delta_{ref,eq\_CO-CO_2} = 0$$

$$p\delta_{ref,eq\_CO-shift} = 0$$

Also it is assumed that the steam reformer heat loss and the pressure drop are zero

$$\dot{Q}_{ref,loss} = 0\ kW$$

$$\Delta p_{ref} = 0\ bar$$

and that the fuel-steam mixture is preheated to (cf. [57])

$$\vartheta_{ref,in} = 650°C$$

and the steam for steam reforming has got a temperature of:

$$\vartheta_{ref,steam} = 600°C$$

The steam-to-carbon ratio in the reformer inlet is assumed to be:

$$S/C = 3$$

It is assumed that the temperature difference steam reformer outlet to bed is:

$$\Delta\vartheta_{\mathrm{ref}} = 50°\mathrm{C}$$

The CO-shift reactor also is modeled ideally which means that the CO-shift reaction is in equilibrium and no methanation occur.

$$p\delta_{eq\_CO-shift} = 0$$

$$X_{CO-shift,CH_4} = 0\%$$

Furthermore it is assumed that the heat loss is zero and the pressure drop is 0,2 bar (cf. [27]).

$$\dot{Q}_{CO-shift,loss} = 0\ kW$$

$$\Delta p_{CO-shift} = 0{,}2\ bar$$

In the standard case a CO-shift inlet temperature of

$$\vartheta_{CO-shift,in} = 450°C$$

is chosen. Also the PSA-unit is modeled ideally which means that the exergy loss is zero.

$$E_{PSA,loss} = 0\ kW$$

According to [61] a PSA product gas pressure drop of:

$$\Delta p_{PSA,product} = 0{,}5\ bar$$

and a product pressure of

$$p_{H_2} = 18\ bar(a)$$

is chosen. It is assumed that the synthesis gas entering the PSA has got a temperature of:

$$\vartheta_{PSA,in} = 40°C$$

For all other assumptions refer to chapter 4.1.1.

4.2.3 Chemical looping steam reforming with CO-shift

The flow-sheet of the CLR(s) process with CO-shift is shown in Figure 61.

The central design elements are the steam reformer (reformer), the CO-shift reactor (CO-shift) and the PSA-unit (PSA). The process is designed in a way that the hydrogen separation coefficient of the PSA-unit is calculated based on the energy requirement of the CLC system to heat the steam reformer.

In this process design the AR off gas is used for superheating of the steam (SH) and for steam production (evap). Finally, it is used for air preheating (regLuVo).

After preheating (FS PH) the fuel is conducted to the steam reformer (reformer) where it is oxidized. The produced synthesis gas is afterwards used for superheating of the steam for reforming (RS SH) and for steam production (evap). Then the synthesis gas is upgraded by the use of a CO-shift reactor (CO-shift). The hydrogen enriched CO-shift product gas then passes an evaporator (evap), the high pressure economizer (HP ECO) and a low pressure economizer (SR LP ECO). Finally, the gas is used for production of the loop-seal fluidization steam (fl.st.H) and is cooled down to PSA inlet temperature. Afterwards hydrogen is separated from the synthesis gas in the PSA unit. The cold PSA tail gas is transmitted, via the recycle loop, after preheating (rec.g.PH) to the fuel reactor. After the oxidized recycle gas is leaving the fuel reactor it is used for fuel preheating (FS PH) and for preheating of the recycle gas (rec. PH). Then it passes a low pressure economizer (FR LP ECO) and is then cooled down (CO2-cooler) to compression temperature.

Parameter variations

For the design it is assumed that the fuel reactor exhaust, the CO-shift and the reformer inlet temperature are the values which influence the efficiency of the process the most. Therefore, the influences of these parameters on the process are studied in more detail.

Optimal deaerator pressure

The optimal deaerator pressure is calculated like in the CLC design case. The optimal deaerator pressure if all other parameters are set to standard values is:

$$p_{dea\_opt} = 12{,}8\ bar$$

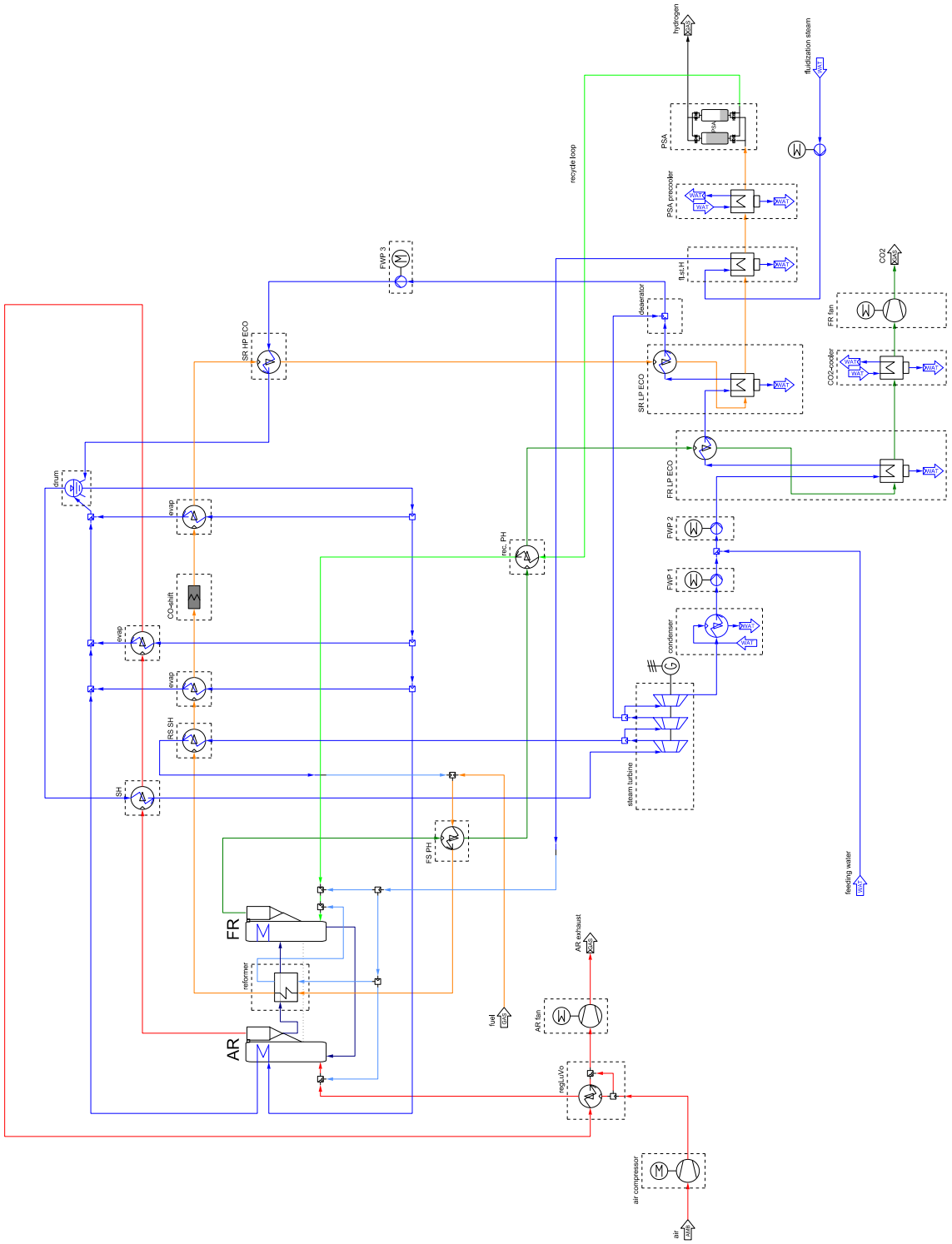

Figure 61 Flow sheet of the chemical looping steam reforming cycle with CO-shift

Variation of the fuel reactor exhaust temperature

The fuel reactor exhaust temperature influences the air reactor and the reformer outlet temperature. This is caused by the direct link of the reactor system via the oxygen carrier with a fixed oxidation state difference (see chapter 3.3.3). Therefore, the air reactor and reformer outlet temperatures increase with increasing fuel reactor outlet temperature (Figure 62).

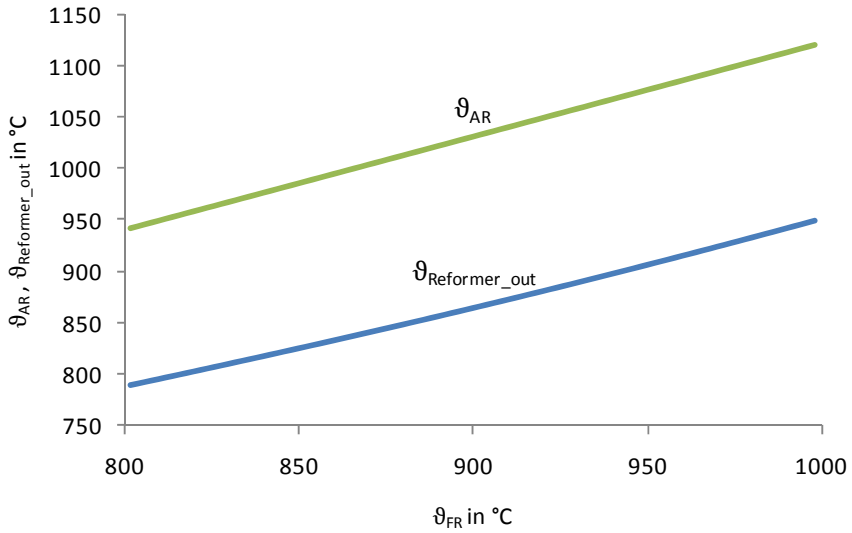

Figure 62 Change of the air reactor and the reformer outlet temperature depending on the fuel reactor exhaust temperature

With changing fuel reactor outlet temperature also the composition changes. The simulation shows that with increasing fuel reactor exhaust temperature the CO and the H_2 content increases while the CO_2 content decreases slightly (Figure 63).

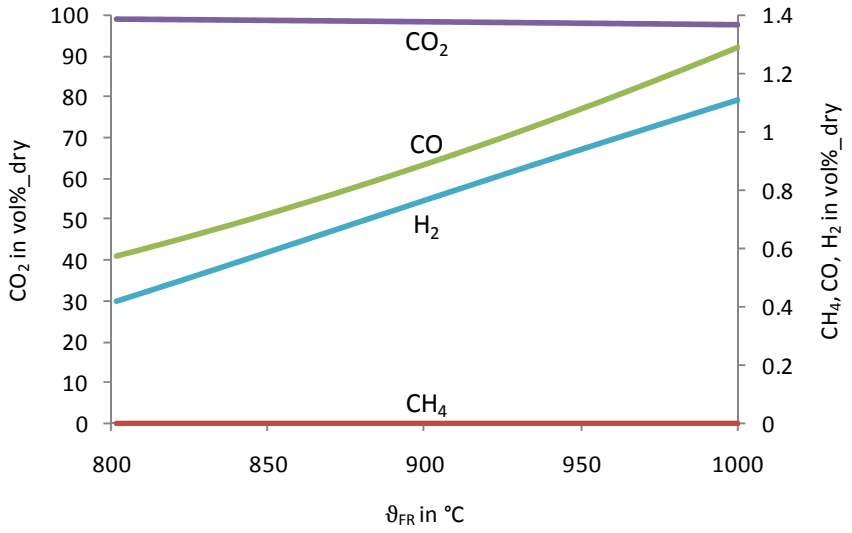

Figure 63 Change of the fuel reactor exhaust composition depending on the fuel reactor exhaust temperature

Increasing fuel reactor exhaust temperature implying increasing reformer outlet temperature promotes hydrogen and carbon monoxide production (Figure 64). This is because the products of the steam reforming reaction (reac 2-7) are preferred at higher temperature while the CO-shift reaction (reac 2-10) is acting vice versa.

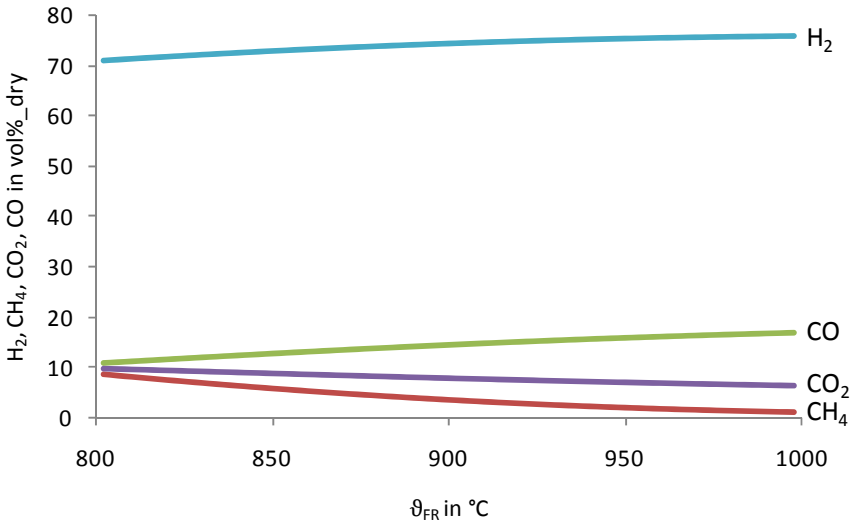

Figure 64 Change of the steam reformer exhaust composition depending on the fuel reactor exhaust temperature

The simulation shows that if more hydrogen is produced the hydrogen separation coefficient X_H_2 of the PSA-unit decreases (Figure 65). This is caused by connection of the hydrogen separation coefficient to the amount of heat required in the reactor system. If the fuel reactor temperature increases the amount of heat required in the chemical looping system increases. Additionally the produced amount of hydrogen in the steam reformer increase. Hence, the hydrogen separation coefficient of the PSA unit decreases. The system reaches its critical point when the PSA-unit has to separate 100 percent of the produced hydrogen. This happens at a fuel reactor exhaust temperature of:

$$\vartheta_{FR\_exh\_critical} = 801{,}8°C$$

The according maximal hydrogen product mass-flow is:

$$\dot{m}_{H_2\_max} = 239{,}3\ \frac{kg}{h}$$

The total hydrogen production efficiency is calculated referring to this value.

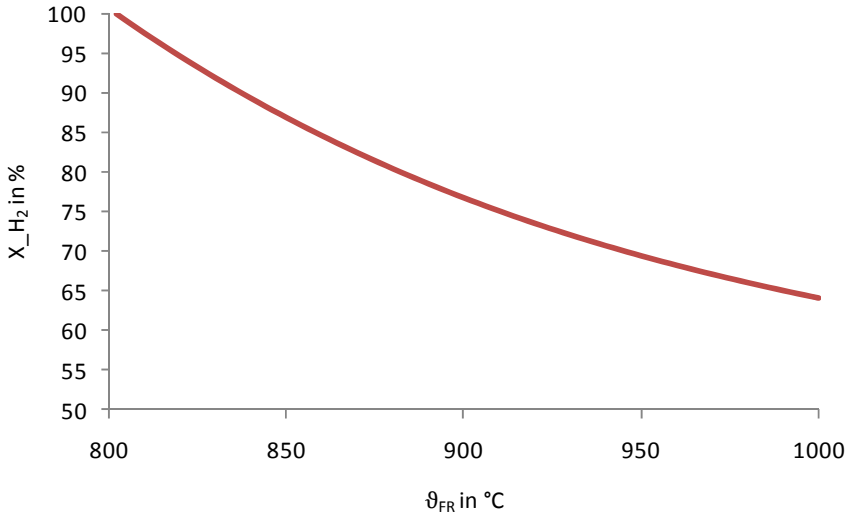

Figure 65 Change of the hydrogen separation coefficient depending on the fuel reactor exhaust temperature

Furthermore with changing hydrogen separation coefficient the recycle gas composition changes.

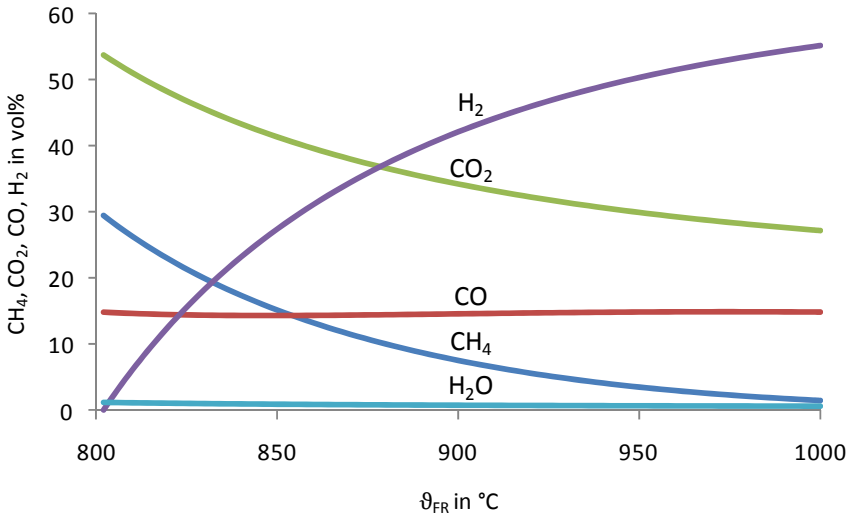

Figure 66 Change of the recycle gas composition respectively fuel reactor inlet composition depending on the fuel reactor exhaust temperature

Summary

Increasing fuel reactor temperature results in increasing heat required to fulfill the energy balance. This requires that more fuel is offered to the CLC system and the PSA unit has to separate less hydrogen. Additionally, the amount of hydrogen in the reformer product gas increases. This is contra productive since the hydrogen, which needed much energy to be produced, is used to feed the inefficient heating process. In addition increasing reactor temperature increases the amount of unburned fuel which makes the efficiency of the chemical looping system even worse.

The simulation shows that although the steam reformer efficiency $\xi_{reformer}$ increases with increasing fuel reactor temperature the exergetic efficiency of the overall process ζ decreases. Vice versa the exergetic efficiency increases with increasing total hydrogen production efficiency ξ. This is shown in Figure 67.

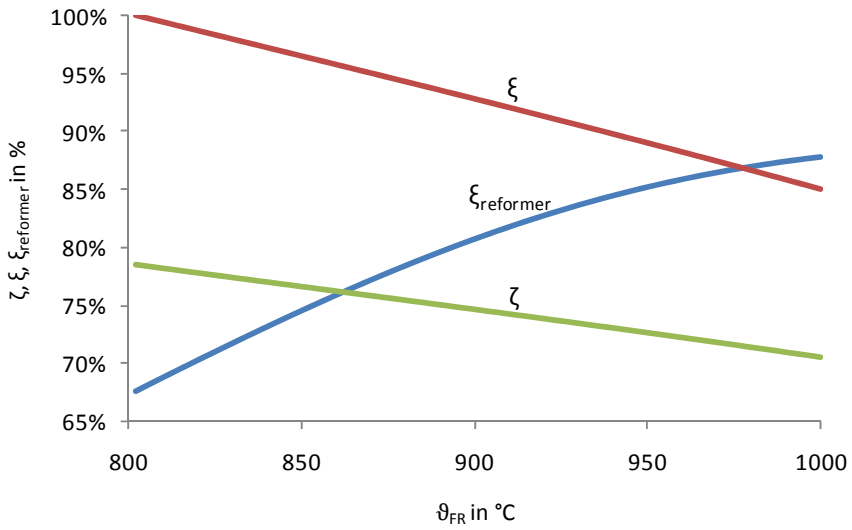

Figure 67 Change of the exergetic efficiency of the process and the hydrogen production efficiency of the reformer and the process depending on the fuel reactor exhaust temperature

CO-Shift temperature variation

The CO-shift equilibrium composition depends on the CO-shift reactor temperature (see Figure 40). This is shown in Figure 68. With decreasing CO-shift reactor inlet temperature the change of the H_2 (ΔH_2) and the change of the CO_2 (ΔCO_2) content increases (the products of the CO-shift reaction increase) while the change of the CO (ΔCO) and the change of the CH_4 (ΔCH_4) decreases. This is because the products of the CO-shift reaction (reac 2-10) are preferred at lower temperatures. Although the volumetric methane content changes its' mass content remains constant because no reaction of methane has been assumed (see chapter 4.2.2).

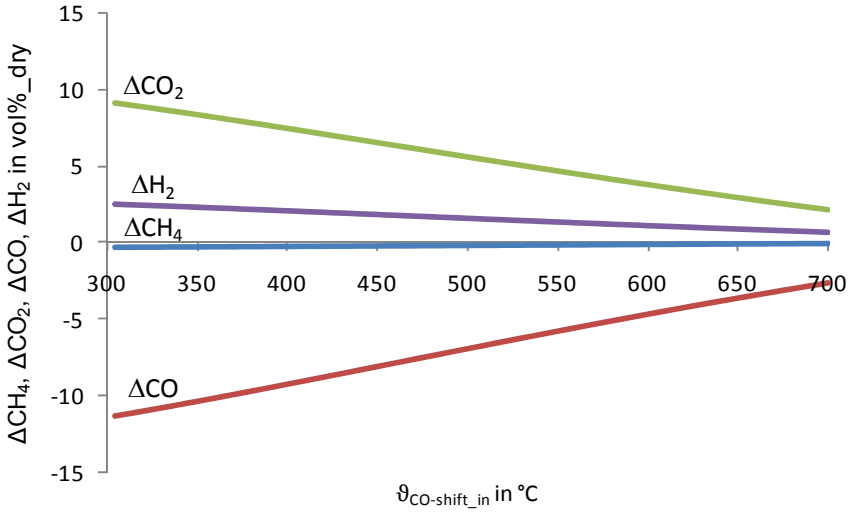

Figure 68 Change of the gas composition over the CO-shift-reactor depending on the CO-shift-reactor inlet temperature

These facts can be also seen when looking at the CO-conversion across the CO-shift reactor. Figure 69 shows that with increasing CO-shift reactor inlet temperature the CO-conversion decreases which means that the effectiveness of the CO-shift decreases.

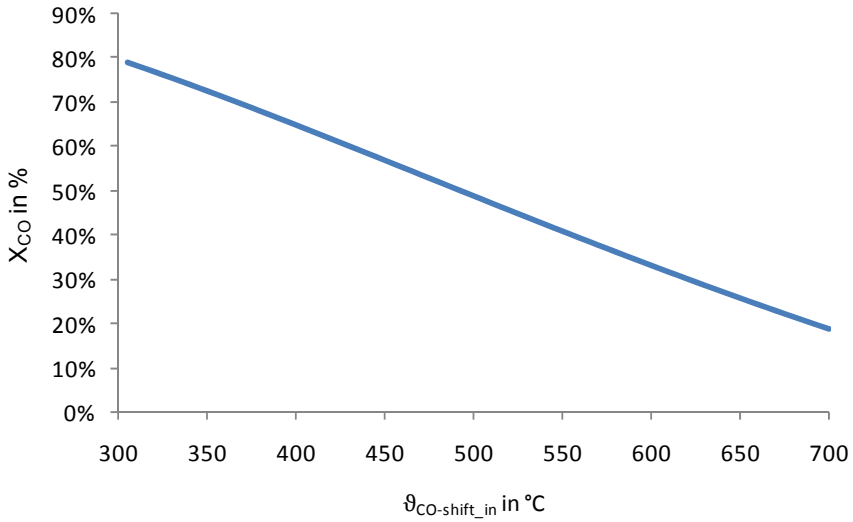

Figure 69 Change of the CO-conversion across the CO-shift reactor depending on the CO-shift-reactor inlet temperature

Similarly to the relations in the case of fuel reactor temperature variation increasing hydrogen content in the shift reactor exhaust requires that a smaller amount of hydrogen has to be separated in the PSA-unit and more hydrogen is recycled. This means that the hydrogen separation coefficient X_H_2 and the mass flow of the total produced hydrogen ($m°_{H2}$) must increase with increasing CO-shift inlet temperature (Figure 70).

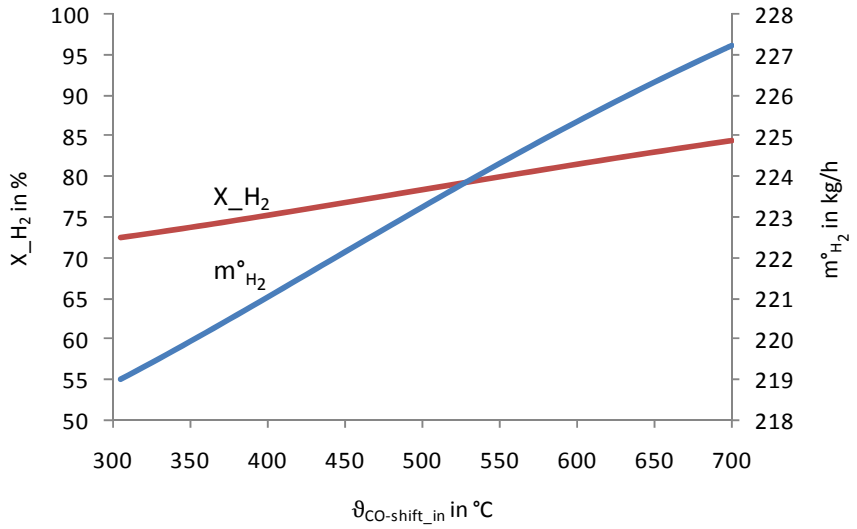

Figure 70 Change of the hydrogen separation coefficient and the produced hydrogen mass-flow depending on the CO-shift-reactor inlet temperature

Summary

The simulation shows that an increased CO-shift reactor inlet temperature results in a decreasing amount of hydrogen in the CO-shift tail-gas. Therefore, more hydrogen can be separated by the separation unit and less hydrogen is recycled. Hence, increasing the CO-shift reaction temperature will result in an increasing process efficiency ζ due to higher total hydrogen output (Figure 71).

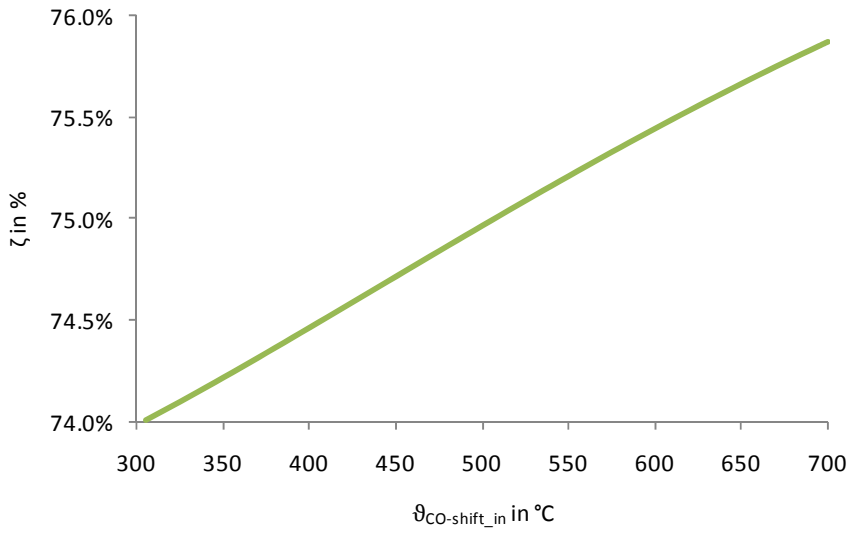

Figure 71 Change of the exergetic efficiency of the process and the hydrogen production efficiency of the reformer and the process depending on the CO-shift-reactor inlet temperature

It is proposed to skip the CO-shift reactor to increase the efficiency of the cycle. This is the case because at higher (approximately 800°C) CO-shift inlet temperature the temperature difference across the shift reactor gets nearly zero while the exergetic efficiency increases.

Reformer feed-gas temperature variation

In conventional steam reforming plants the feed-gas is preheated to a temperature of up to 650°C (cf. [57]) in order to increase the hydrogen output. This is obtained because the required heat for steam reforming is reduced and so the reformer can operate at a higher efficiency which leads to a higher hydrogen output.

The simulation shows that with increasing steam reformer inlet temperature the steam reformer outlet temperature increases (Figure 72).

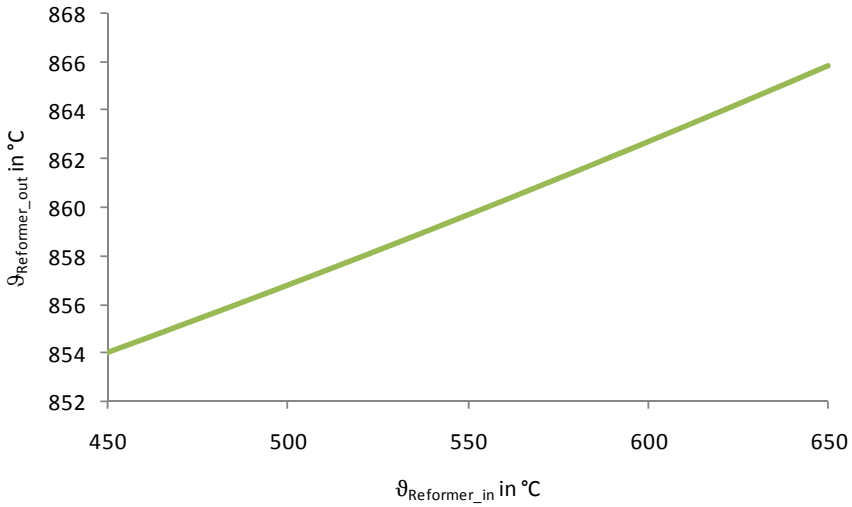

Figure 72 Change of the steam reformer outlet temperature depending on the steam reformer inlet temperature

At higher temperature the equilibrium of the steam reforming reaction (reac 2-7) is, according to Le Chatelier, on the product side of the reaction. Hence, the simulation shows that with increasing

steam reformer inlet temperature the H_2 and CO increases while the CH_4 and CO_2 content in the reformer outlet decreases (Figure 73).

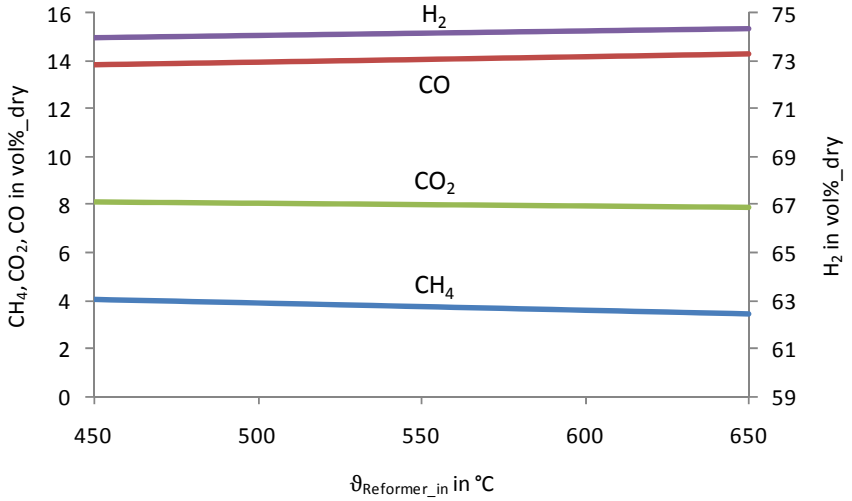

Figure 73 Change of the steam reformer tail-gas-composition depending on the steam reformer inlet temperature

Thus the hydrogen content in the fuel reactor inlet slightly increases and the effect on the fuel reactor off-gas composition is very low too (Figure 74).

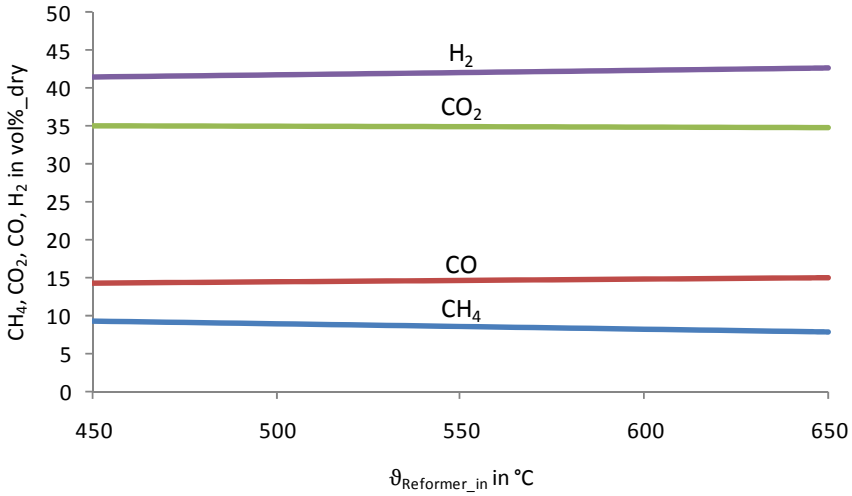

Figure 74 Change of the recycle gas or the fuel reactor inlet gas-composition respectively depending on the steam reformer inlet temperature

Summary

The simulation shows that a good fuel preheating leads to a higher steam reformer efficiency $\xi_{reformer}$ and that more hydrogen has to be recycled. This results in higher process efficiency ζ which has been the opposite in the previous variations (Figure 75).

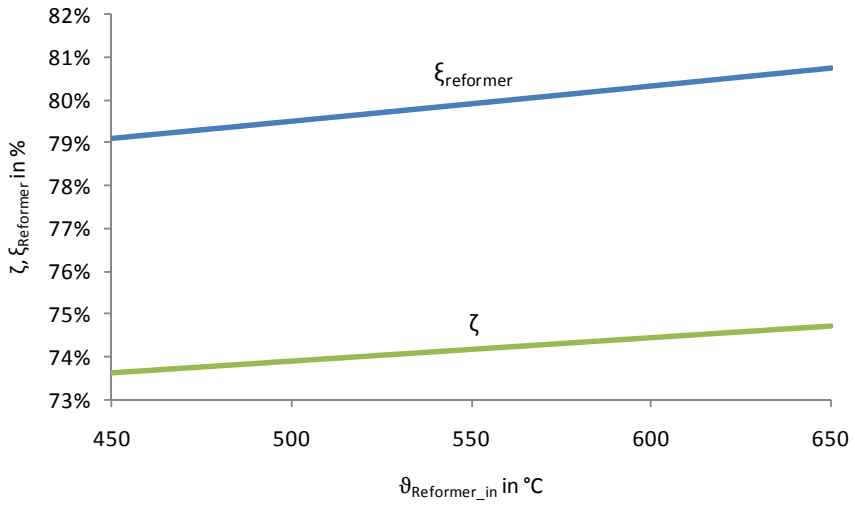

Figure 75 Change of the exergetic efficiency of the process and the hydrogen production efficiency of the reformer and the process depending on the steam reformer inlet temperature

This might be astonishing at the first moment but the effect of a higher steam reformer inlet temperature leads to less heat required and the overall performance is better although high quality product-gas is used for heating the reactor system.

Therefore, it is proposed to preheat the fuel as much as possible to increase the process efficiency. It has to be noticed that this is only a viable strategy for high performance applications because the absolute influence on the total hydrogen production efficiency is rather low. In return the high investment costs of a high quality gas-gas heat exchanger are only an option for large scale hydrogen production facilities.

Comparison of the design with or without CO-shift

Skipping the CO-shift reactor seems to have a big advantage for the total hydrogen production efficiency. This can be seen in Figure 71 where the exergetic efficiency increases with increasing CO-shift inlet temperature while the effectiveness of the CO-shift reactor decreases (see Figure 68).

The parameter variations in the previous chapter show that the amount of hydrogen recycled has a direct impact on the efficiency. In this study it is assumed that a nickel based oxygen carrier is used which has shown in experiments that it is very attractive when methane is used as fuel (cf. [36]). Therefore, it has been assumed that the methane conversion is hundred percent. Since nickel based oxygen carriers are very expensive the substitution of nickel by other metals seems to be a very attractive option to reduce the investment costs. Another reason is that nickel is very toxic and therefore it has to be the aim to use a harmless substitute. Such oxygen carriers would not be able to sustain a high methane conversion while the conversion of hydrogen in general is very high. Therefore, the impact of the methane conversion capability on the total hydrogen output is simulated.

The simulation shows that at a constant fuel reactor exhaust and CO-shift reactor temperature with increasing methane conversion capability X_{CH4} the total produced hydrogen mass flow $m°_{H2}$ increases in both cases.

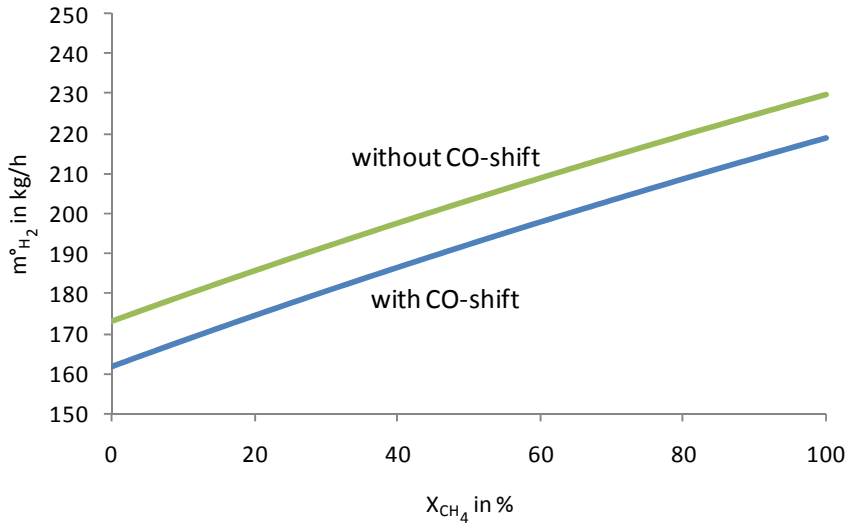

Figure 76 Change of the total hydrogen produced depending on the oxygen carrier methane conversion capability

Figure 76 shows that even if an oxygen carrier with poor methane conversion is used the design without a CO-shift is the superior one. This is a quite surprising result since the use of a CO-shift reactor increases the amount of hydrogen re-circled which is the superior propellant if a cheap oxygen carrier is used. This result can be explained by looking at the fuel reactor inlet composition at constant fuel reactor and CO-shift temperature (Figure 77).

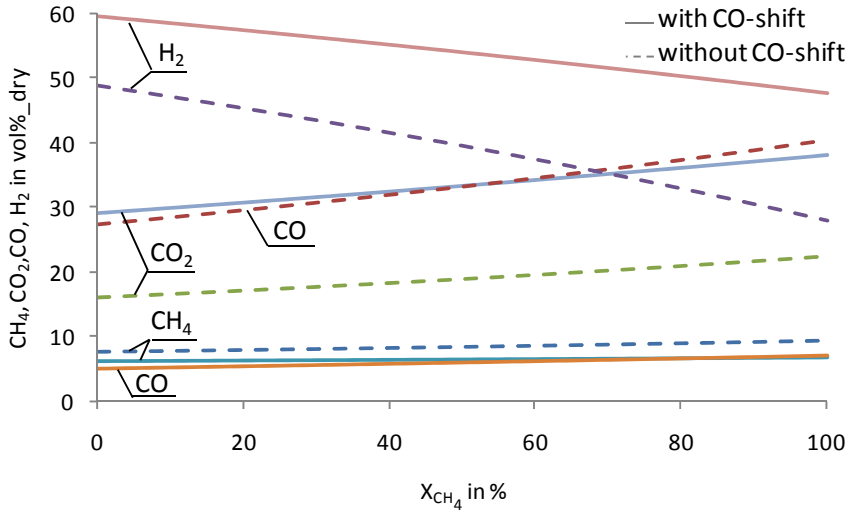

Figure 77 Change of the fuel reactor inlet gas composition depending on the methane conversion capability of the oxygen carrier

While the methane content in the gas stream is approximately 2% higher the impact on the CO_2, CO and H_2 content is much larger in case of no CO-shift. As expected the simulation shows that the H_2 and CO_2 content are higher and the CO content is lower in the CO-shift design case (caused by the CO-shift reactor). The greater amount of CO_2 content decreases the efficiency of the reactor system since the inert carbon dioxide has to be reheated without contributing to the heat input. Anyhow, this seems to be not the reason for the significant inferiority of the design with CO-shift since in both cases the amount of carbon cycling has to be the same. Therefore, the influence of recycling carbon on the heat reactor energy balance has to be in both cases approximately the same.

It is adopted that the reason for the discrepancy is justified by simulation boundary conditions. In this case the simulation doesn't depict the reality since different oxygen carrier materials also have got a different catalytic activity towards CO-shift conversion and different reactivity towards the gas-solid reaction.

Therefore, it is proposed that representative CO-shift, methane conversion capabilities and gas-solid reactivity of different oxygen carriers have to be evaluated and implemented into the model for a correct prediction. The assumption that a higher hydrogen content in the fuel reactor inlet would lead to better process efficiencies if using cheep oxygen carriers may be a point.

The simulation shows that the use of a CO-shift is disadvantageous for a high system performance at least when using high quality oxygen carriers. The calculated exergetic efficiencies are summarized below.

Design case	Exergetic efficiency ζ in %
with CO-shift	74,8 %
without CO-shift	76,5 %

4.2.4 Chemical looping autothermal reforming

Simulation boundary conditions

The simulation boundary conditions are summarized in Table 20. All other settings refer to chapter 4.1.1 and 4.2.2.

Table 20 Table of set values in case of CLR(a)

Notation	Symbol and Value
Chemical scrubber carbon dioxide separation coefficient	$X_{CO_2} = 60\%$
Chemical scrubber inlet temperature	$\vartheta_{scrubber,in} = 65°C$
Chemical scrubber outlet temperature	$\vartheta_{scrubber,out} = 65°C$
Fuel reactor exhaust temperature	$\vartheta_{FR\_exh} = 850°C$
Fuel reactor inlet temperature	$\vartheta_{FR-inlet} = 300°C$
Gas pressure drop in the chemical scrubber	$\Delta p_{scrubber} = 0\ bar$
Heat loss of the chemical scrubber	$\dot{Q}_{scrubber-loss} = 0\ kW$
Isentropic efficiency of the steam turbine	$\eta_{s,t} = 70\%$
Live steam pressure	$p_{LS} = 80\ bar$
Live steam temperature	$t_{LS} = 450°C$
Reboiler pressure drop	$\Delta p_{Reboiler} = 0\ bar$
Reboiler relative heating duty	$\dot{q}_{Reboiler} = 3{,}68\ GJ/tCO_2$
Reboiler temperature	$\vartheta_{Reboiler} = 120°C$
Reflux condenser outlet temperature	$\vartheta_{reflux-out} = 90°C$
Scrubber product outlet pressure	$p_{scrubber-product} = 1{,}5\ bar(a)$
Steam-to-carbon ratio in the fuel reactor feed gas	$S/C_{FR-in} = 0{,}25$
Stoichiometric ratio	$\lambda = 0{,}3$

Process layouts

The process is built up in a way that the carbonaceous fuel is converted to hydrogen and carbon dioxide as far as possible. Therefore, the CO_2 (chem.scrubber) and the H_2 (PSA) is separated from the fuel reactor off gas and the remaining tail gas is recycled and brought back to the fuel reactor. The process schemes differ by the placement of the CO-shift reactor (CO-shift).

Because carbon is looping in a process internal circle a bleed is required so that inert contents cannot accumulate inside the cycle. In the case if pure methane is used as fuel the bleed mass-flow could be theoretically set to zero. Due to numerical inaccuracy a certain amount of gas has to be released by the bleed to ensure convergence. Therefore, the bleed mass-flow in the simulation is set to:

$$\dot{m}_{bleed} = 10\,kg/h$$

The required heat for separation of the CO_2 is produced inherent and is offered to the chemical scrubber by the produced steam.

Chemical looping autothermal reforming with HT-CO-shift

The process flow-sheet of the CLR(a) cycle wit HT-CO-shift is shown in Figure 78.

Central design element of the design case is that the CO-shift reactor is placed in between the fuel reactor and the chemical scrubber.

After the gas is leaving the fuel reactor it is cooled down (evap) and upgraded by the CO-shift reactor (CO-shift). After the gas is used for the production of the steam required for the shift reaction (shift ST evap 1&2), to preheat the fuel-recycle gas mixture (fuel-rec.PH) and for production of the fluidization steam (FS PH) it is conducted to the chemical scrubber (chem..scrubber) at atmospheric pressure (FR fan 1). In the chemical scrubber a part of the CO_2 is removed from the gas. After leaving the chemical scrubber the CO_2 depleted gas is compressed to PSA inlet pressure (PSA compressor) and cooled down to PSA inlet temperature (PSA precooler). Then a part of the hydrogen is removed from the gas by the use of the PSA unit (PSA). The remaining H_2 and CO_2 depleted tail gas is conducted to the recycle loop. In the recycle loop the gas is mixed with the fuel after bleeding. After preheating (fuel-rec.PH) the fuel-recycle gas mixture is mixed with water and injected into the fuel reactor.

Chemical looping autothermal reforming after CO_2 separation CO-shift

The process flow-sheet of the CLR(a) cycle wit CO-shift after CO_2 separation is shown in Figure 79.

The process layout is similar to the previous one. The only difference is that the CO-shift reactor is placed downstream of the chemical scrubber.

Chemical looping autothermal reforming with no CO-shift

The process flow-sheet of the CLR(a) cycle with no CO-shift is shown in Figure 80.

The process layout is similar to the previous designs. The only difference is that no CO-shift reactor is used.

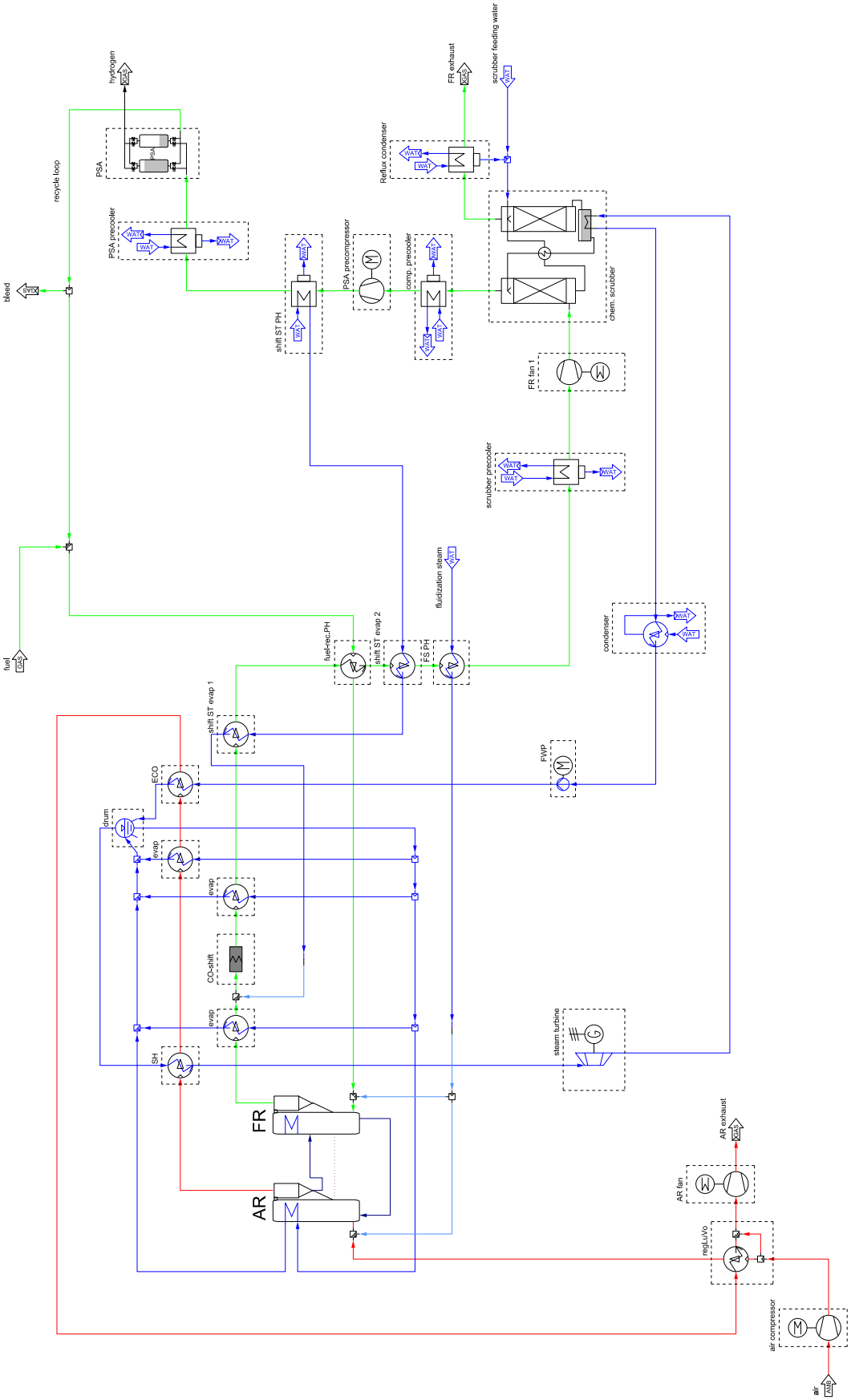

Figure 78 Flow sheet of the chemical looping autothermal reforming cycle with HT-CO-shift

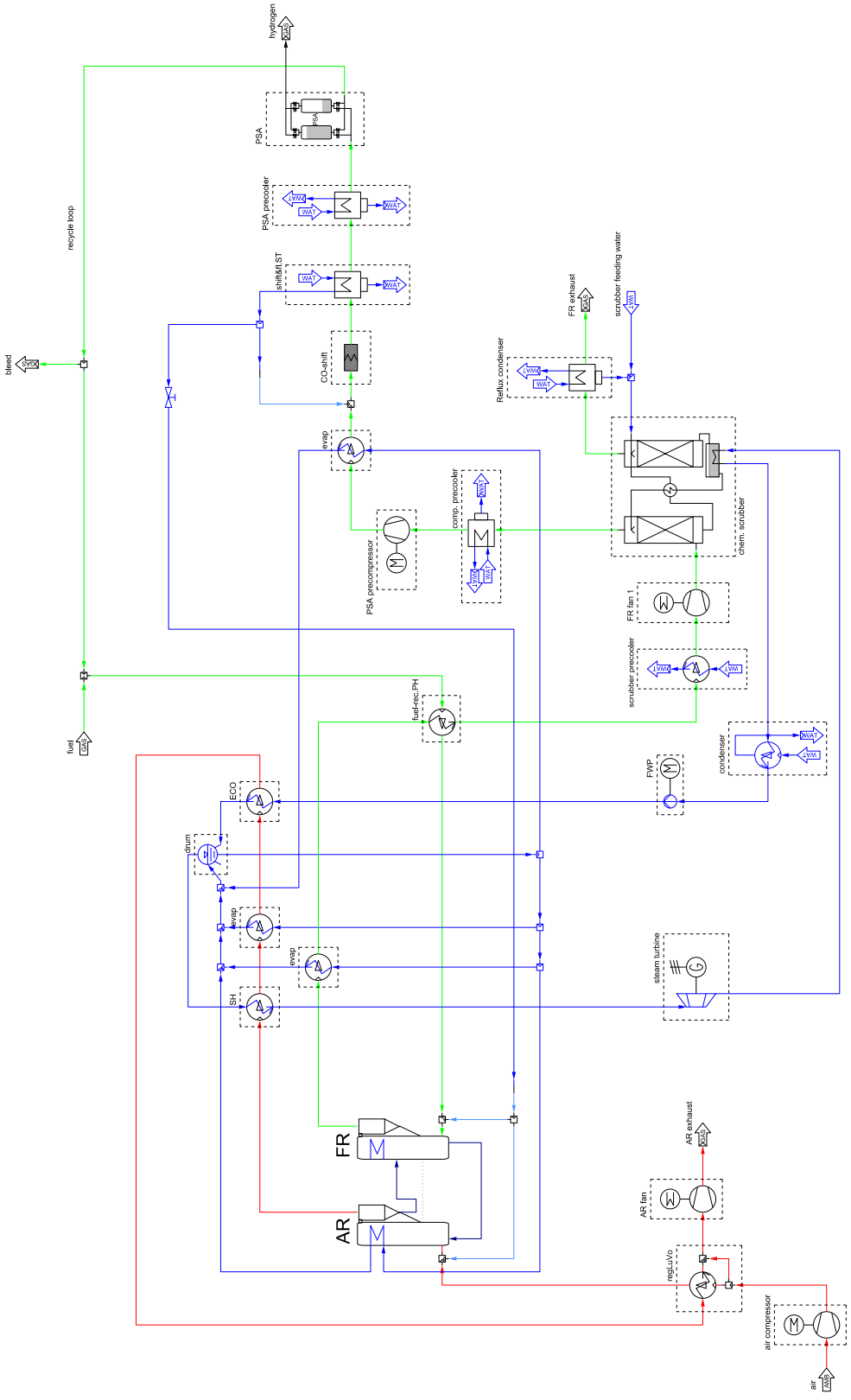

Figure 79 Flow sheet of the chemical looping autothermal reforming cycle with CO-shift after CO_2 separation

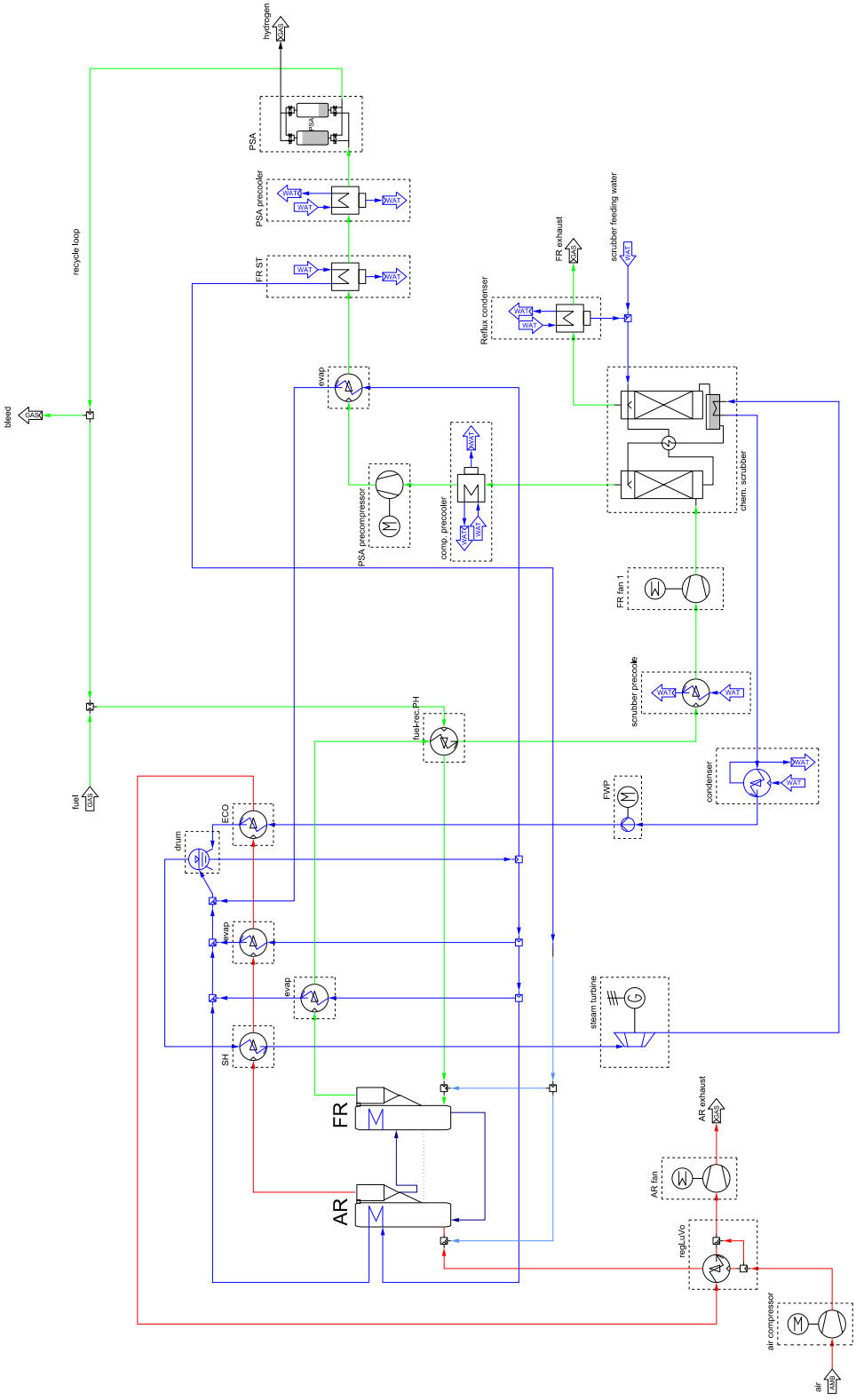

Figure 80 Flow sheet of the chemical looping autothermal reforming cycle with no CO-shift

Comparison of process designs

The simulation shows the following efficiencies for the different cycle options with the boundary conditions mentioned before:

Table 21 Summary of the calculated process efficiencies

Design case		no CO-shift	HT-CO-shift	CO-shift after CO_2 separation
Exergetic efficiency	ζ	48,7%	58,5%	42,1%
Hydrogen mass-flow	ξ_{H_2}	161,0 kg/h	195,2 kg/h	146,9 kg/h

Hence, the use of a HT-CO-shift reactor is the most favorable design choice in order to increase the exergetic efficiency and the amount of hydrogen produced.

Placing a CO-shift before the hydrogen separation unit increases the amount of hydrogen available for separation. This has got a positive effect on the hydrogen separation capability of the PSA unit due to higher hydrogen partial pressure and also affects the amount of hydrogen which can be separated instead of recycling unconverted methane.

Table 22 Simulated hydrogen content in the feed-gas of the H_2 separation unit

Design case	Hydrogen content in the hydrogen separation unit feed-gas
No CO-shift	36,0 $vol\%\_dry$
HT-CO-shift	75,8 $vol\%\_dry$
CO-shift after CO_2 separation	61,3 $vol\%\_dry$

Although, this is also the fact when the CO-shift reactor is placed immediately in front of the PSA-unit the simulation shows that this design approach has got the lowest efficiency. This seems to be the case as the additionally produced hydrogen cannot be separated because it is required for re-heating the not separated carbon dioxide in the recycle loop when passing through the fuel reactor.

By placing the CO-shift in front of the carbon dioxide separation unit the partial pressure of the CO_2 increases. Therefore, the chemical scrubber is working with higher efficiency or it even might be possible to switch to other less heat demanding solvents or to replace it by a more efficient separation process (eg. Rectisol ®).

Table 23 Simulated carbon dioxide content in the feed-gas of the CO_2 separation unit

Design case	Carbon dioxide content in the CO_2 separation unit feed-gas
No CO-shift	24,3 $vol\%\_dry$
HT-CO-shift	27,9 $vol\%\_dry$
CO-shift after CO_2 separation	23,1 $vol\%\_dry$

Hence, the design case with a HT-CO-shift in front of the CO_2 and H_2 separation unit is not only the best choice for the efficiency of the process but it is also favorable for both separation units.

As a consequence this process design approach is going to be discussed in detail.

Detailed discussion of the design approach HT-CO-shift

Improvement of the carbon dioxide separation unit

The heat supply is essential for a CO_2 separator which uses chemical absorption. Therefore, the heat supplied to the chemical scrubber system should be optimized. In the proposed design the separation reaches an optimum when the supplied saturated steam is completely condensed. This means that the steam content of the heating fluid has to be zero. This is unfavorable in practice. Therefore, it is proposed to leave a rest steam content in the reboiler outlet. It is assumed that the rest content of steam has to be:

$$x_{steam} = 5\ \%$$

The additional heat supply to the chemical scrubber increases the CO_2 separation coefficient from 60 to 69,5% at the basic simulation settings.

Fuel-reactor exhaust temperature variation

To study the influence of changing fuel-reactor exhaust temperature the temperature is varied from 750°C to 900°C.

Although the opposite has been expected (compare to chapter 3.5.2 Optimal reactor temperature) the simulation shows that with increasing temperature the H_2 content increases while the CO_2 and CO content decreases. The methane content is zero because complete methane conversion has been assumed (Figure 81).

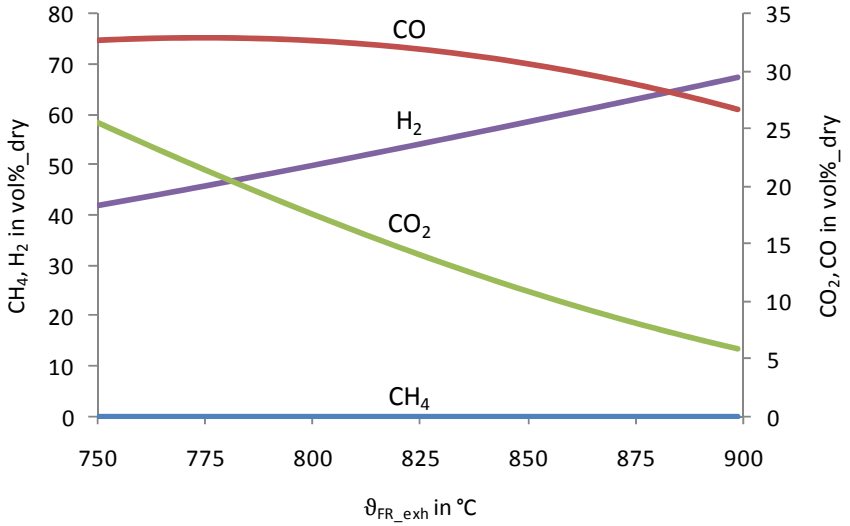

Figure 81 Change of the fuel reactor exhaust gas composition depending on the fuel reactor exhaust temperature

The reason is that the fuel reactor inlet gas in the simulation in chapter 3.5.2 consists only of methane while in this design the gas is a mixture of recycle gas and fuel.

The H_2 content increases and the CO and CO_2 content decrease at the scrubber inlet (Figure 82). This is caused by the CO-shift in-between the fuel reactor and the scrubber.

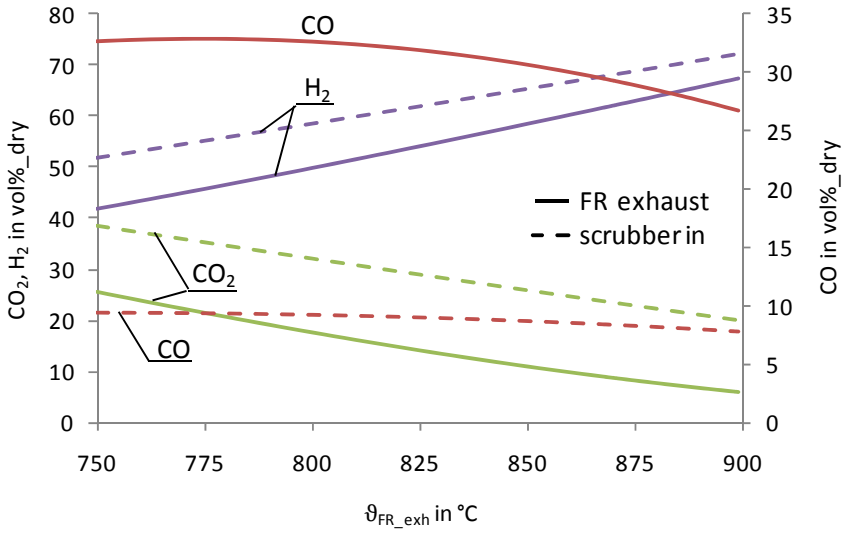

Figure 82 Change of the gas composition at the fuel reactor exit and the scrubber inlet depending on the fuel reactor exhaust temperature

After removal of carbon dioxide the depleted tail-gas of the scrubber respectively PSA inlet shows that the CO_2 content decreases while the H_2 and CO content increases. The point where the CO_2 content gets zero in the PSA inlet (respectively the scrubber outlet) is a theoretic operation point which would require infinite contact areas of the chemical scrubber (Figure 83).

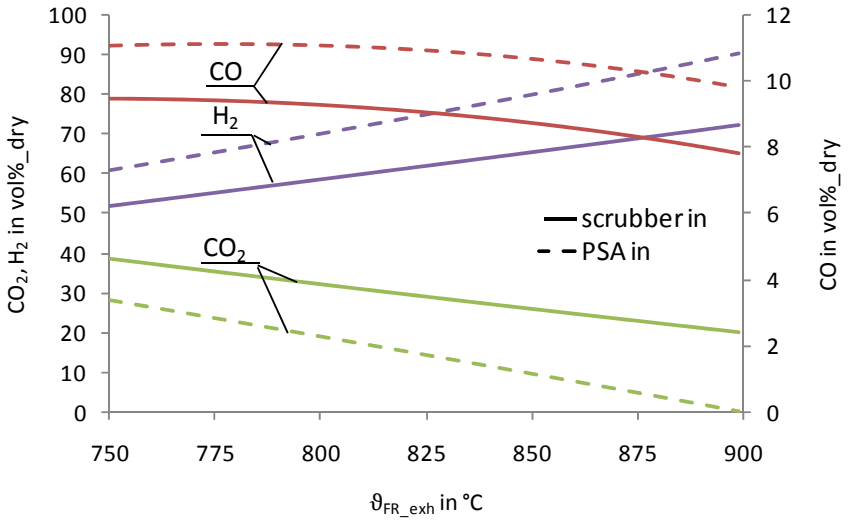

Figure 83 Change of the PSA inlet gas composition depending on the fuel reactor exhaust temperature

After passing the PSA the hydrogen depleted recycle gas has got a decreased H_2 content but an increased CO_2 and CO content (Figure 84).

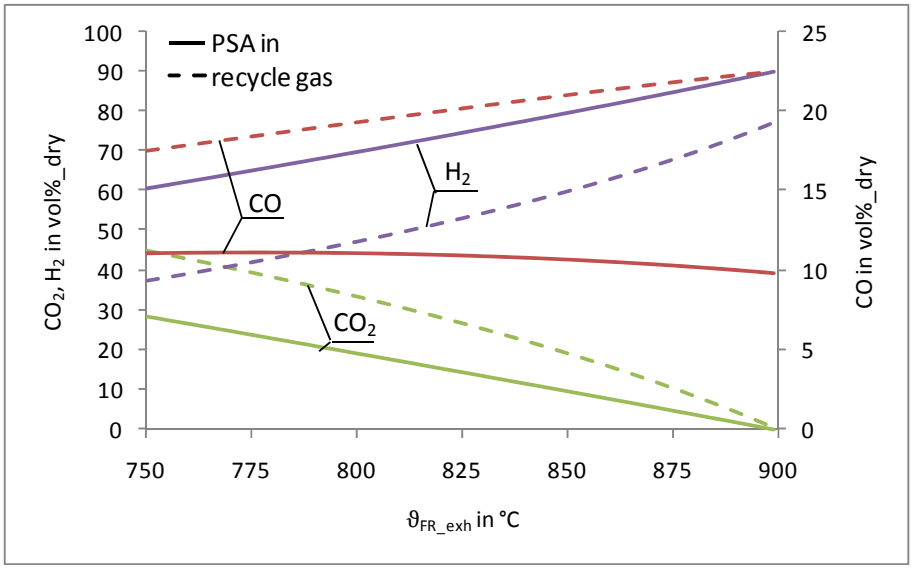

Figure 84 Change of the fuel recycle-gas gas composition depending on the fuel reactor exhaust temperature

Summary and conclusion

The simulation shows the expected effect on the gas-composition on the scrubber and PSA feed-gas when using a CO-shift (the CO_2 and the H_2 content increases at the scrubber and PSA inlet). Nevertheless the fuel-reactor acted in an unexpected way compared to the simulation in chapter 3.5.2 because the hydrogen content increases with increasing reactor temperature. This is caused by the different fuel reactor inlet gas composition. While in chapter 3.5.2 pure methane has been used in this case the fuel reactor inlet gas consists mainly of hydrogen and carbon monoxide.

The simulation shows, that at a temperature of approximately 900°C the CO_2 content at the scrubber tail gets zero because the scrubber removes the complete amount of the CO_2 (X_CO_2 gets 100%) which is only theoretical possible. Additionally the hydrogen separation coefficient X_H_2 of the PSA unit is almost constant (Figure 85).

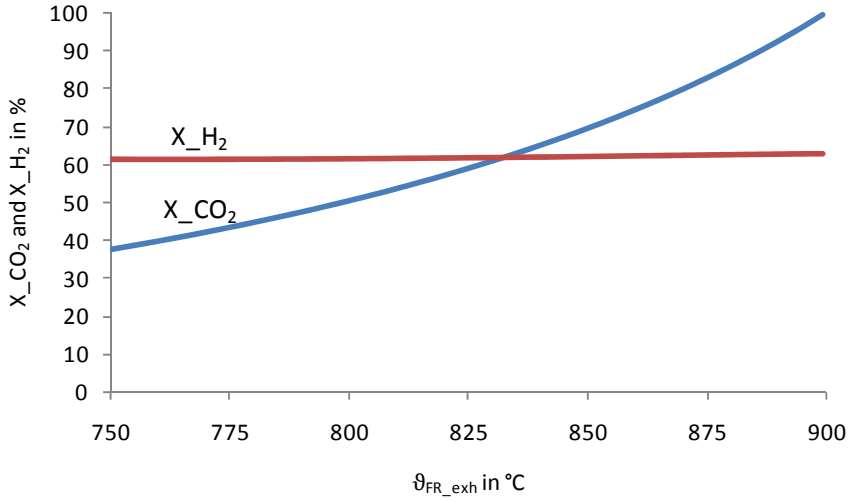

Figure 85 Change of the CO_2 and the H_2 separation coefficient depending on the fuel reactor exhaust temperature

Therefore, with an increasing fuel reactor temperature the amount of hydrogen produced increases and the amount of carbon dioxide in the recycle loop which otherwise would have had

to be reheated decreases. On the other hand the carbon monoxide content in the recycle loop increases so does the amount of carbon released from the bleeding.

This leads to the conclusion that increasing the fuel reactor temperature increases the exergetic efficiency of the process ζ although the loss of carbon l_C increases (Figure 86).

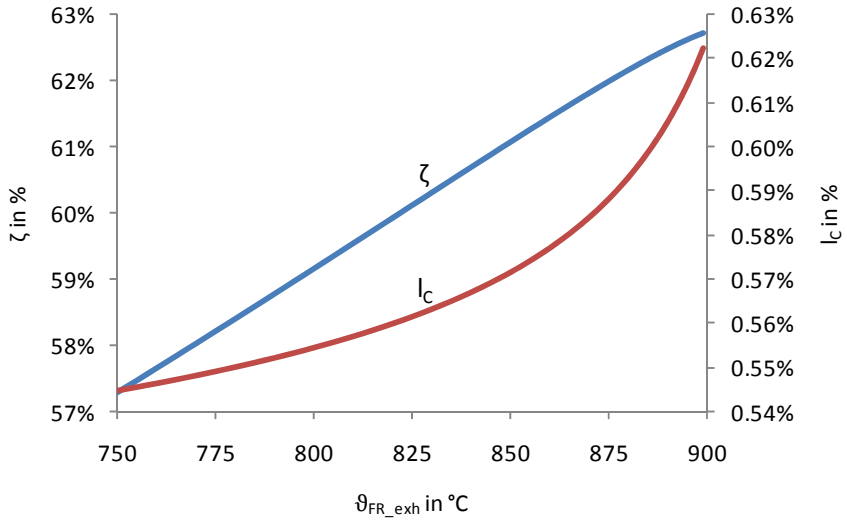

Figure 86 Change of the exergetic efficiency and the loss of carbon depending on the fuel reactor exhaust temperature

CO-shift inlet temperature variation

In order to study the influence of the CO-shift reactor inlet temperature the temperature is varied from 300 to 450°C.

According to the CO-shift reaction (reac 2-10) carbon monoxide is converted to hydrogen supported by steam. With decreasing CO-shift reactor inlet temperature the products of the CO-shift equation are favored by equilibrium. Therefore, the H_2 and CO_2 content should increase while CO should decrease. Actually the simulation does not show this. The simulation shows that with decreasing CO-shift inlet temperature the change of CO_2 and CO content increases while the change of the H_2 content decreases.

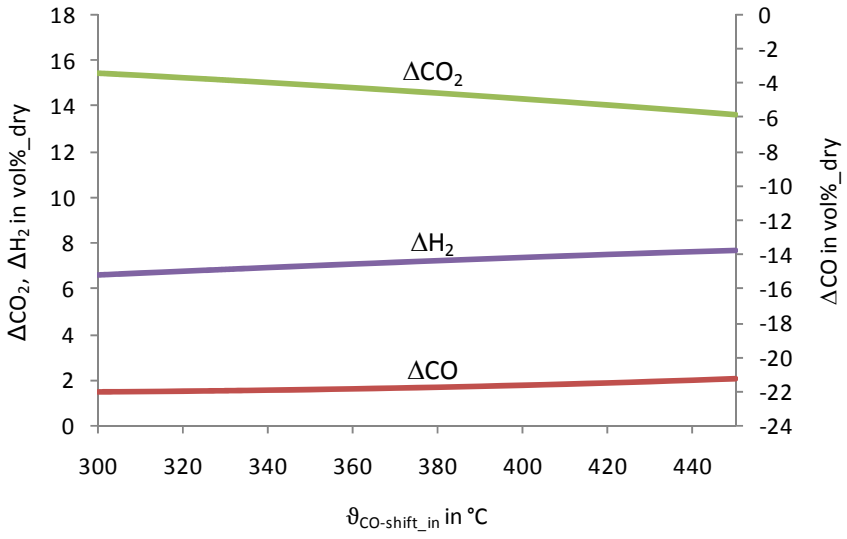

Figure 87 Change of the gas composition along the CO-shift depending on the CO-shift inlet temperature

This is caused by changing CO-shift reactor inlet composition. The simulation shows that with decreasing CO-shift inlet temperature the hydrogen content increases while the CO and CO_2 content decreases in the CO-shift reactor inlet. Decreasing CO influences the CO-shift reaction equilibrium in a way that the reactant side of the reaction is preferred. Hence, the change of H_2 content across the CO-shift reactor decreases with decreasing CO-shift reactor inlet temperature.

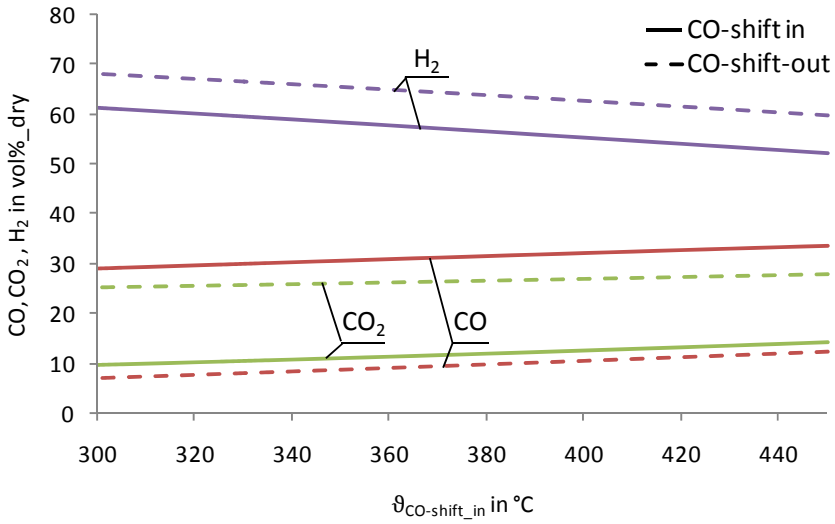

Figure 88 Change of the CO-shift inlet gas composition depending on the CO-shift inlet temperature

Summary and conclusion

Decreasing the CO-shift inlet temperature increases the hydrogen content in the PSA feed gas and the carbon dioxide content in the scrubber feed gas. As a consequence the CO_2 separation coefficient X_CO_2 increases with decreasing CO-shift inlet temperature while H_2 separation coefficient X_H_2 remains almost constant (Figure 89).

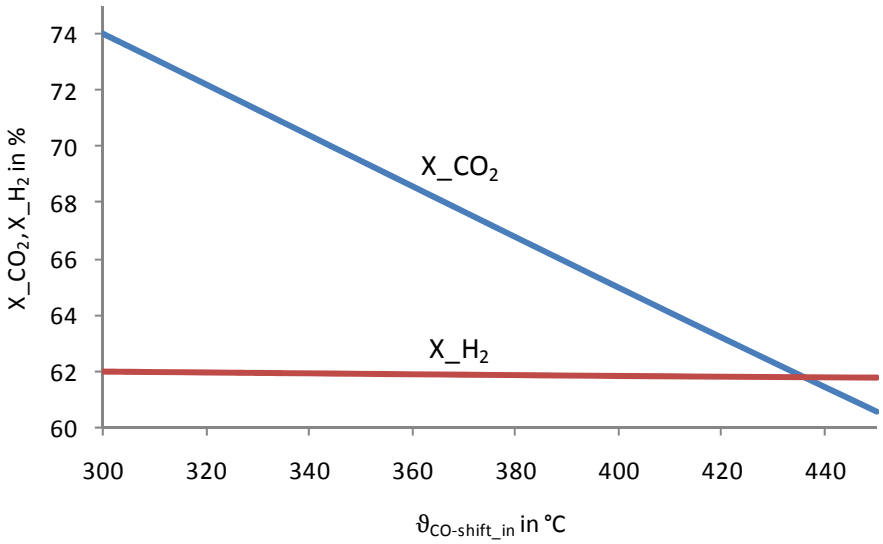

Figure 89 Change of the CO_2 and the H_2 separation coefficient depending on the CO-shift inlet temperature

With increasing carbon dioxide separation efficiency the exergetic efficiency increases. This is because otherwise the CO_2 would have to be reheated. Additionally, the carbon loss decreases since less carbon is in the recycle gas stream (Figure 90).

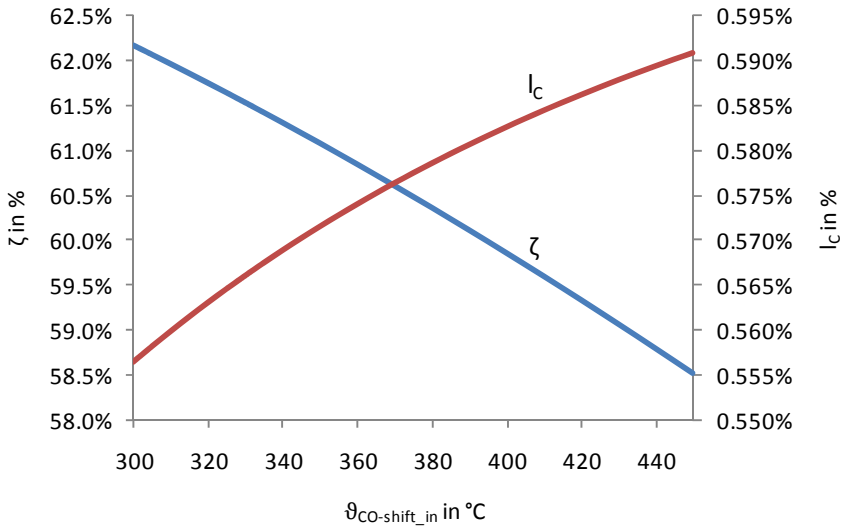

Figure 90 Change of the exergetic efficiency and the loss of carbon depending on the CO-shift inlet temperature

Influence of inert gases in the fuel

The presence of inert gases in the fuel leads to an accumulation of the inerts in the cycle. Therefore a certain amount of gas has to be released by the use of a bleed valve. The bleed mass flow is increased from 10 kg/h to:

$$\dot{m}_{bleed} = 50\,kg/h$$

In order to predict the influence of inert gas components in the fuel the inert gas content in the fuel is varied from 0 to 1,5 vol%.

The simulation shows that with increasing amount of inert gas in the fuel the CO_2, CO and H_2 content in the recycle gas decreases while the inert content increases (Figure 91).

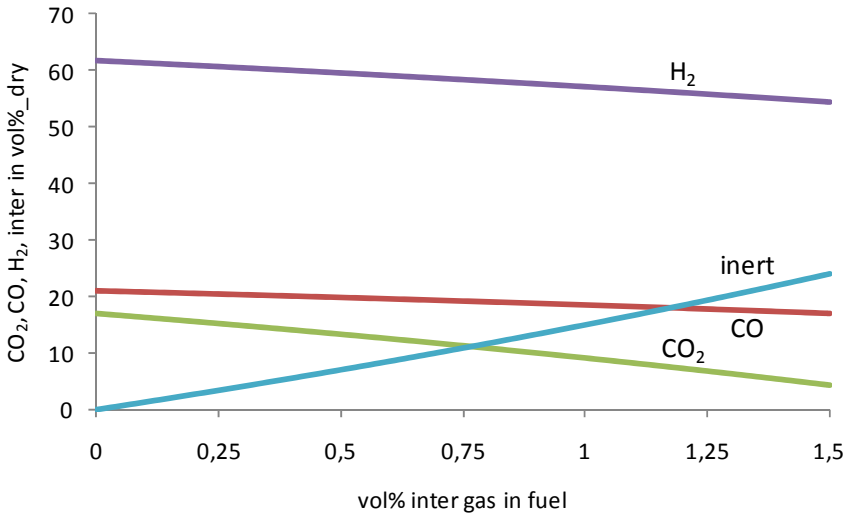

Figure 91 Change of the recycle-gas gas composition depending on the amount of inert gas in the fuel

An increasing amount of inert gas recycled has to result in decreased process exergetic efficiency ζ and a decreased loss of carbon l_C. The simulation shows that the exergetic efficiency actually increases while the loss of carbon decreases (Figure 92).

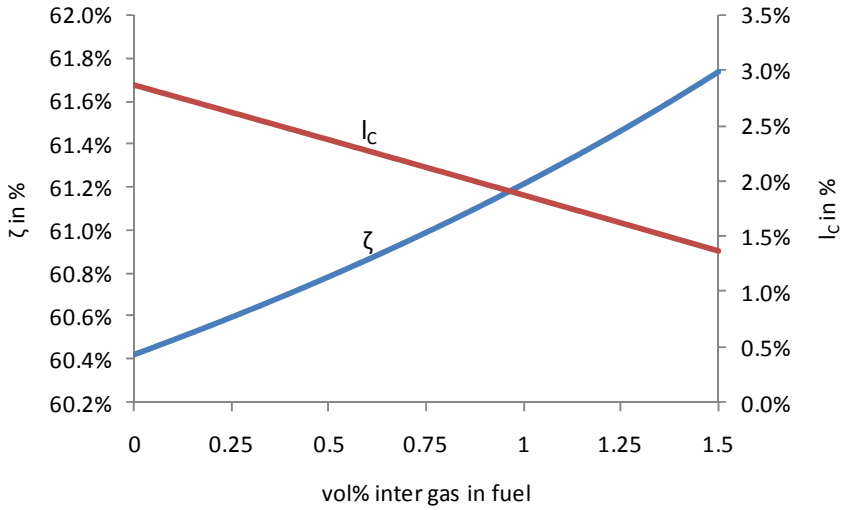

Figure 92 Change of the exergetic efficiency and the loss of carbon depending on the amount of inert gas in the fuel

This interesting and unexpected result is caused inherently by the design of the flow-sheet. As assumed before the steam content in the reboiler exit has to be 5%. As a result the CO_2 separation coefficient increases if a larger amount of steam is produced. Greater amounts of inert gases lead to a higher gas mass flow and therefore the quantity of steam produced increases when the fuel reactor exhaust temperature is kept constant. Hence, more carbon dioxide (X_CO_2 increases) and more hydrogen (X_H_2 increases) can be separated (Figure 93).

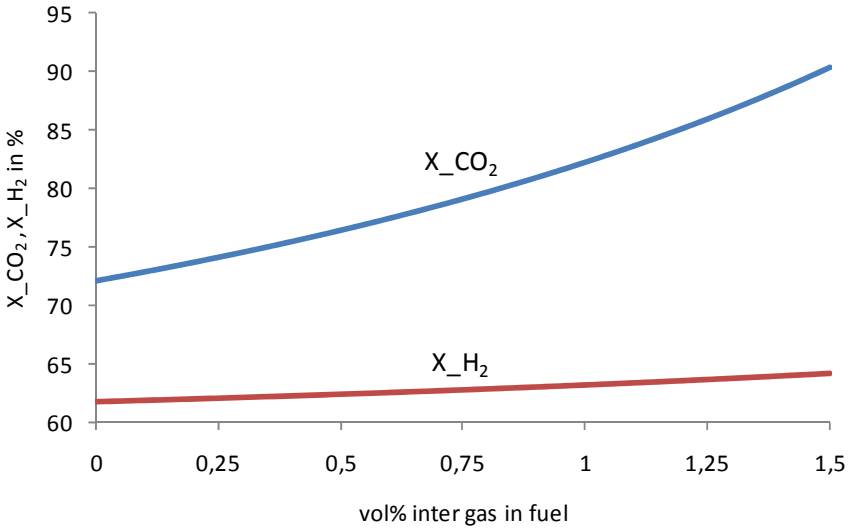

Figure 93 Change of the CO_2 and the H_2 separation coefficient depending on the amount of inert gas in the fuel

This means that the process efficiency has to decrease if the carbon dioxide separation coefficient is kept constant. This fact is shown in Figure 94, where the loss of carbon l_C and the exergetic efficiency ζ decreases with increasing inert gas in the fuel adapts to the CO_2 separation coefficient set.

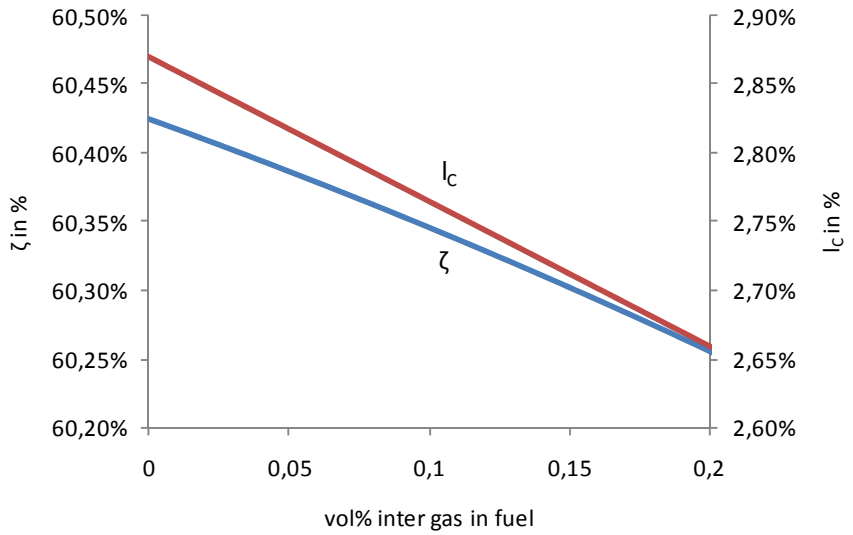

Figure 94 Change of the exergetic efficiency and the loss of carbon depending on the amount of inert gas in the fuel at constant CO_2 separation coefficient

The variation of the inert gas content in fuel shows that the optimum has to be evaluated for each application separately depending on the real amount of inert gas in the fuel.

5 Conclusion

The integration of chemical looping into a power (CLC) and hydrogen (CLR) cycle have been simulated in order to find the potential and constraints of such processes.

It has been assumed that:

- A nickel based oxygen carrier is used which is theoretically capable to convert the complete amount of methane and the CO-shift (reac 2-10) and CO oxidation with metal oxide (reac 3-1) equilibrium inside the fuel reactor is reached.
- The CO-shift equilibrium is reached if a CO-shift reactor is used.
- A carbon dioxide separator using chemical absorption by aqueous MEA is used.
- A pressure swing adsorption (PSA) is used for hydrogen separation.

It has been found out that in case of chemical looping power generation that:

- Chemical looping combustion shows potential for power generation even at small scale or simple applications.
- Using a fluidized bed cooler is essential in a chemical looping combustion system to increase the efficiency of the cycle at decreased fuel reactor temperature.
- If the reactor design is done properly and when using high quality oxygen carriers the loss due to unburned fuel is significant and will require an additional gas treatment.

In case of chemical looping hydrogen power steam reforming it has been found out that:

- The use of a CO-shift decreases the overall hydrogen production.
- Fuel preheating increases the process efficiency but is only a viable strategy in large scale applications.
- It is preliminary that using a CO-shift reactor is a good strategy when oxygen carriers with low methane conversion capability are used.

And in case of autothermal reforming:

- Placing the CO-shift in front of the carbon dioxide and hydrogen separation unit increases the process efficiency by increasing the amount of CO_2 and H_2 which can be separated and the process efficiency increases.
- If there are inert gases in the fuel bleeding is required.
- For the prediction of the specific effect of inert gas on the process a detailed study at a given amount of inert is required.
- If the process is operated “stand-alone” a solvent with lower heat requirement would increase the efficiency of the process.

Future investigations have to be carried out to study the effect of methane conversion capability when nickel substitutes are used as oxygen carrier.

6 Nomenclature

Symbol	Notation	Dimension
λ	Air/fuel ratio or stoichiometric ratio	$-$
a	Speed of sound	m/s
A_i	Species i in reaction	$-$
c_{in}	Inlet velocity	m/s
c_{out}	Outlet velocity	m/s
$d\omega/dt$	Deviation of the mass conversion of the OC	$\%/s$
d_{C_out}	Exhaust diameter	m
D_m	Particle size	mm
dq	Change of the relative heat	J/kg
ds	Change of the relative entropy	$J/kg \cdot K$
ds_{irr}	Change of the relative irreversible entropy	$J/kg \cdot K$
ds_q	Change of the relative entropy of heat	$J/kg \cdot K$
du	Change of the relative value of the Inner Energy	J/kg
dw	Change of the relative technical work	J/kg
$E_{applied}$	Applied exergy	W
E_{fuel}	Exergy of the fuel	W
e_f	Relative exergy of the fuel	W
E_{FW}	Exergy of the feed water	W
E_{LS}	Exergy of the live steam	W
e_{LS}	Relative exergy of the live steam	W
e_{LS}	Relative exergy of the live steam	W
e_{ph}	Relative exergy of the feeding water after preheating	W
e_{ph}	Relative exergy of the feed water	W
$E_{produced}$	Produced exergy	W
$G(p,T)$	Absolute value of the Gibbs function	W
$dG(p,T)$	Deviation of the absolute Gibbs function	
$g(T,p)$	relative value of the Gibbs function	J/kg
$G_R^0(T)$	Gibbs free enthalpy of reaction	$J/mole$
h	Relative Enthalpy	J/kg
h_{LS}	Relative enthalpy of the live steam	J/kg
h_{ph}	Relative enthalpy of the feeding water after preheating	J/kg
$K_P(T)$	Equilibrium constant	$bar^{\Sigma \nu_i}$
l_u	loss due to unburned fuel	$-$
l_C	Loss of carbon	$-$
LHV	Lower Heating Value of the fuel	J/kg
LHV_{fuel}		
LHV_f		

Symbol	Notation	Dimension
$LHV_{off_{gas}}$	Lower heating value of the off-gas	J/kg
l_{min}	Air demand for oxidation	kg/kg
l_{RC}	Relative radiation an convection loss	$-$
M	March Number	$-$
m	Actual mass of the OC	kg
$\dot{m}_0$	stoichiometric mass flow of oxygen needed for complete conversion	kg/s
m_{bed}	Mass of the bed material	kg
$\dot{m}_{C\_feed}$	Mass flow of carbon in the feed	kg/s
$\dot{m}_{C\_lost}$	Mass flow of lost carbon	kg/s
$\dot{m}_{CO\_in}$	Mass flow of carbon monoxide in the inlet stream	kg/s
$\dot{m}_{CO\_out}$	Mass flow of carbon monoxide in the outlet stream	kg/s
$\dot{m}_{off_{gas}}$	Mass flow of the off-gas	kg/s
$\dot{m}_{f0}$	Brutto fuel mass flow	kg/s
$\dot{m}_{feedwat}$	Feeding Water Mass Flow	kg/s
$\dot{m}_{fluid-steam}$	Mass flow of the fluidization steam	kg/s
$\dot{m}_{fuel}$, $\dot{m}_f$	Net fuel mass-flow	kg/s
$\dot{m}_{H_2}$	Hydrogen mass flow	kg/s
$\dot{m}_{H_2\_ref\_out\_max}$	Maximal reformer outlet hydrogen mass flow	kg/s
$\dot{m}_{H_2\_ref\_out}$	Reformer outlet hydrogen mass flow	kg/s
$\dot{m}_{H_2max}$	Maximal hydrogen mass flow	kg/s
$\dot{m}_{LS}$	Live steam mass flow	kg/s
$\dot{m}_{LS\_fluid\_rel}$	Relative fluidization mass flow	kg/s
$mole\ C$	Mole fraction of C	mol/kg
$mole\ H_2O$	Mole fraction of H_2O	mol/kg
m_{ox}	Mass of the completely oxidized particle	kg
M_{ox}	Molar mass of the oxidized oxygen carrier	$kg/kmol$
$\dot{m}_{H_2prod}$	Mass flow of the produced hydrogen	kg/s
$\dot{m}_{H_2max}$	Mass flow of the hydrogen maximal producible	kg/s
$\dot{m}_{reac-inlet}$	Reactor inlet mass flow	kg/s
$\dot{m}_{rel}$	Relative leakage mass flow of the air preheater	%
m_{red}	Mass of the completely reduced particle	kg
M_{red}	Molar mass of the reduced oxygen carrier	$kg/kmol$
$\dot{m}_{sol}$	Oxygen carrier circulation rate	kg/s
n	Polytrophic coefficient	$-$
O_{min}	O_2 demand for oxidation	kg/kg
p	Pressure	bar
p_{amb}	Ambient pressure	bar
$P_{applied}$	Power applied	W

Symbol	Notation	Dimension
P_c	Power of the Turbine at the Clutch	W
p_{c_in}	Compressor inlet pressure	bar
p_{co}	Condenser pressure	bar
$P_{compressor}$	Power of the compressor	W
p_{c_out}	Compressor outlet pressure	bar
$p_{desorber}$	Desorber pressure	bar
p_{dea_opt}	Optimal deaerator pressure	bar
$p\delta_{eq}$	Logarithmic deviation of the equilibrium	$-$
$p\delta_{eq\_CO-CO_2}$	Logarithmic deviation of equilibrium of the CO oxidation with metal oxide reaction	$-$
$p\delta_{eq\_CO-shift}$	Logarithmic deviation of equilibrium of the CO-shift reaction	$-$
P_{el}	Electrical power	kW
P_{fuel}	Fuel Power	W
P_{gen}	Power of the generator	W
p_{H_2}	Hydrogen pressure	bar
p_i	Partial pressure of the component i	bar
p_i^*	Equilibrium partial pressure of the component i	bar
p_{LS}	Pressure of the live steam	bar
$P_{produced}$	Power delivered	W
P_{pump}	Power of the pump	W
P_{ST} , P_t	Power output of the steam turbine	W
$P_{water,pump}$	Power required for the water pumps	W
$\dot{q}_{CO_2removal}$	Required heat for CO_2 removal	GJ/tCO_2
$\dot{Q}_{RC}$	Radiation and convection loss	W
$\dot{Q}_{scrubber-loss}$	Scrubber heat loss	W
$\dot{Q}_u$	Usable heat release	W
R	Ideal gas Constant	$J/kg \cdot K$
R_0	Oxygen ratio	%
$R_{0,OC}$	Oxygen ratio of the oxygen carrier batch	%
ρ_a	Apparent density	kg/m^3
s	Relative Enthropy	$J/kg \cdot K$
S/C	Steam to Carbon ratio	$-$
s_{LS}	Relative enthropy of the live steam	$J/kg \cdot K$
s_{ph}	Relative entropy of the feed water	$J/kg \cdot K$
T	Absolute Temperature	K
T_{amb}	Absolute Temperature of the ambient	K
ϑ_{amb}	Ambient temperature	$°C$
T_{AR}	Temperature air reactor	K
t_{co}	Condenser temperature	$°C$
T_{FR}	Temperature fuel reactor	K

Symbol	Notation	Dimension
$T_{heat-removal}$	Temperature of heat removal	K
$T_{heat-supply}$	Temperature of heat supply	K
t_{LS} , ϑ_{LS}	Live steam temperature	$°C$
T_m^*	Rectified thermodynamic mean temperature	K
t_{pinch}	Pinch-Point Temperature	K
u	Relative value of the Inner Energy	J/kg
U	circulation ratio	$-$
u_{C_out}	Exhaust velocity	m/s
$\dot{V}$	Volume flow	m^3/s
v	Specific density	m^3/kg
v_i	Stoichiometric coefficient of the component i	$-$
w_t	Technical work	J/kg
$w_{t,FWP}$	Technical work of the feed water pump	J/kg
$w_{t,ST}$	Technical work of the steam turbine	J/kg
X	Degree of oxidation	$-$
x	Steam mass fraction	$-$
X_{CH_4}	Methane conversion rate	$-$
X_{CO_2}	Carbon dioxide separation coefficient	%
X_{H_2}	Hydrogen separation coefficient	%
x_{MeO}	Mass fraction of metal oxide in the fully oxidized state	kg/kg
X_{s_ox}	Oxidation state of the oxidized oxygen carrier	$-$
X_{s_red}	Oxidation state of the reduced oxygen carrier	$-$
y_{CH_4}	Mass content of methane	$-$
y_{CO}	Mass content of carbon monoxide	$-$
y_{CO_2}	Mass content of carbon dioxide	$-$
y_{H_2O}	Mass content of water	%
$\Delta\omega$	Difference of ω between FR and AR	%
η_c	Clutch Efficiency	$-$
η_{el}	Electric efficiency	$-$
η_i	Inner Turbine Efficiency	$-$
η_m	Mechanical Turbine Efficiency	$-$
η_p	Polytrophic efficiency	$-$
η_s	Isentropic efficiency	$-$
$\eta_{s,t}$	Isentropic Turbine Efficiency	$-$
η_{SG}	Thermal Steam Generator efficiency	$-$
η_{th}	thermal efficiency	$-$
$\vartheta_{des,steam}$	Temperature of the desorber supply steam	$°C$
ϑ_{FR_exh}	Temperature of the fuel reactor exhaust	$°C$
ϑ_{ph_opt}	Optimal pre-heating temperature	$°C$

Symbol	Notation	Dimension
$\vartheta_{reboiler}$	Reboiler temperature	$°C$
ξ	hydrogen produced	$-$
$\xi_{refomer}$	Hydrogen production efficiency of the reformer	$-$
φ	Volume flow number	$-$
φ	Relative Humidity	$\%$
ω_{AR}	Mass conversion of the OC at the AR exit	$\%$
ω	Mass conversion of the oxygen carrier	$\%$
Δh	Change of the relative enthalpy	J/kg
Δp_{eco}	Pressure drop inside the economizer	bar
Δp_{gas_total}	Total pressure drop of the gas	bar
Δp_{sh}	Pressure drop inside the superheater	bar
$\Delta\vartheta_{min,gas-water,htx}$	Minimal temperature difference for gas-water heat exchange	$°C$
$\Delta\vartheta_{\mathrm{min,gas-gas,htx}}$	Minimal temperature difference for gas-gas heat exchange	$°C$
$\Delta\vartheta_{OC\_out}$	Oxygen carrier outlet temperature difference	$°C$
$\vartheta_{reformer\_min}$	Minimal temperature difference in the reformer	$°C$
$\vartheta_{desorber\_inlet}$	Desorber inlet temperature	$°C$
η_C	Efficiency of the Carnot process	$-$
ζ	exergetic efficiency	$-$
ζ_0	Reference exergetic efficiency	$-$
ζ_P	Exergetic efficiency of the process	$-$
ζ_{rel}	Relative change of the exergetic efficiency	$-$
ζ_{SG}	exergetic efficiency of the steam generator	$-$

7 References

7.1 Articles and books

[1] Abad A., Adànez J., García-Labiano F., de Diego L.F., Gayán P., Celaya J., *Mapping of the range of operational conditions for Cu-, Fe-, and Ni-based oxygen carriers in chemical-looping combustion*, Chemical Engineering Science 62 (2007), pp 533-549

[2] Abad A., García-Labiano F., Adánez J., de Diego L.F., Gayán P., Celaya J., 8th International conference on greenhouse gas control technologies, 19-22 June 2006a, Trondheim, Norway

[3] Abramowitz, Milton, *Handbook of mathematical function.* National Bureau of Standards, Washington, DC1972, 10th print with corrections

[4] Atkins P.W., *Elements of Physical Chemistry*. 3rd Edition, Oxford University Press, 1993

[5] Barnola J.M., Raynaud D., Korotkevich Y.C., Lorius C., *Vostok ice core provides 160,000-year record of atmospheric CO_2*, Nature 1987 v329, pp 408-414

[6] Beebe R., Aust FIE., CP. Eng, April 1998, *Condition Monitoring of Steam Turbines by Performance Analysis*. 52nd Conference of the Machinery Failure Prevention Society, Virginia Beach, April 1998

[7] Blood D., Simpson S., and Harries R., Dillon D., Mitsui Babcock Energy Ltd; A Weekes, ME Engineering Ltd 2003. *HEAT RECOVERY STEAM GENERATORS FOR POWER GENERATION AND OTHER INDUSTRIAL APPLICATIONS*. Report No. COAL R232, DTI/Pub URN 03/804, March 2003

[8] Bolhàr-Nordenkampf J., Pröll T., Kolbitsch P., Hofbauer H., *Performance of a NiO-based oxygen carrier for chemical looping combustion and reforming in a 120kW unit.* Energy Procedia 00 (2008) 000–000

[9] Buhre B.J.P., Elliott L.K., Sheng C.D., Gupta R.P., Wall T.F., *Oxy-fuel combustion technology for coal-fired power generation.* Progress in Energy and Combustion Science 31 (2005) pp.283–307

[10] Casarosa C., Donatini F., Franco A., *Thermoeconomic optimization of heat recovery steam generators operating parameters for combined plants*. Energy 29 (2004) pp.389–414

[11] *CHP QA GUIDANCE NOTE* 28. Final GN28-V1

[12] *Climate Change 2001*. Intergovermental Panel on Climate Change. Cambridge University Press, 2001.

[13] *Climate Change 2007*. Intergovermental Panel on Climate Change. Cambridge University Press, 2007.

[14] *CO_2 Capture and Storage*. A VGB Report on the State of the Art 2004

[15] Dahmen W., Reusken A., *Numerik für Ingenieure und Naturwissenschaftler,* Springer Berlin Heidelberg, German 2006

[16] Dang H., Rochelle G.T., *CO2 Asorption Rate and Solubility in Monoethanolamine/Piperazin/Water.* First National Conference on Carbonn Sequestration Washington, DC, May 14-17, 2001

[17] Desideri U., Paolucci A., *Performance modelling of a carbon dioxide removal system for power plants*. Energy Conversion & Management 40 (1999) pp 1899-1915

[18] Diego de L.F., Gayán P., García-Labiano F., Celaya J., Abad A., and Adánez J., *Impregnated CuO/Al_2O_3 oxygen carriers for chemical-looping combustion: avoiding fluidized bed agglomeration*. Energy Fuels 19 (2005), pp 1850-1856

[19] Dietzel F., *Dampfturbinen - Berechnung, Konstruktion, Teillast und Bertiebsverhalten, Kondensation*. Carl Hanser Verlag München Wien 1980, 3rd press

[20] Dubbel, *Taschenbuch für den Maschinenbau*. Springer Berlin Heidelberg, 21th press, 2005

[21] Dubbel, *Taschenbuch für den Maschinenbau*. Springer Berlin Heidelberg, 22th press, 2007

[22] Dybkjaer Ib, *Tubular reforming and autothermal reforming of natural gas - an overview of available processes.* Fuel Processing Technology 42 (1995) 85-107

[23] Effenberg H., *Dampferzeugung,* Springer Verlag Berlin 2000, German

[24] Energy Nexus Group 2002, *Technology Characterization: Steam Turbines*. Publication by the Energy Nexus Group, March 2002

[25] *Enery Bulletin on REFORMERS*. Confederation of Indian Industry, Energy Management Cell

[26] Fathi M., Bjorgum E., Viig T., Rokstad OA, Partial oxidation of methane to synthesis gas: elimination of gas phase oxygen, Catal Today 2000 v63 pp489-97

[27] Göttlicher G., *CO2 Capture From IGCC Power Plants.* Laboratory of Energy Engineering and Environmental Protection, presentation 2003

[28] Grace J.R., *Contacting modes and behaviour classification of gas-solid and other two-phase suspensions.* Can. J. Chem. Engng 64 (1986), pp. 353–363.

[29] Haider M., *Skriptum zur Vorlesung Konstruktion und Berechnung wärmetechnischer Anlagen*. Technical University of Vienna Eigenverlag 2007

[30] Hofbauer H., *Skriptum zur Vorlesung: Wirbelschichttechnik.* Technical University of Vienna Eigenverlag 4th ed

[31] Huckle H., Schneider S. 2006, 2nd press; *Numerische Methoden.* Springer Berlin Heidelberg, German

[32] IPCC Special Report on *"Carbon Capture and Storage"* 2005 Published by Cambridge University Press, New York

[33] Ishida M., Zheng D., Akehata T. Energy 12 (1987), pp. 147-154

[34] Johansson M., Mattisson T., Rydén M. and Lyngfelt A., *Carbon capture via Chemical-Looping Combustion and Reforming*. Rio de Janeiro, October 2006

[35] Knoche K.F., Richter H., *Brennsoff-Wärme-Kraft* 20 (1968), pp. 205-210

[36] Kolbitsch P., *Chemical looping combustion for 100% carbon capture - Design, operation and modeling of a 120kW pilot rig.* PhD-Thesis at the University of Technology Vienna

[37] Kolbitsch P., Bolhàr-Nordenkampf J., Pröll T., Hofbauer H., *DESIGN OF A CHEMICAL LOOPING COMBUSTOR USINF A DUAL CIRCULATING FLUIDIZED BED (DCFB) REACTOR SYSTEM*. Technical University of Vienna

[38] Kolbitsch P., Pröll T., Bolhar-Nordenkampf J, Hofbauer H., *Characterization of Chemical Looping Pilot Plant Performance via Experimental Determination of Solids Conversion.* Energy & Fuels in proceeding

[39] Koss U., M. Meyer Lurgi Oel.Gas.Chemie GmbH, *Zero Emission IGCC with Rectisol® technology*. Presentation at the GTC 2002 in San Francisco

[40] Lewis and Gilliland, *Production of pure carbon dioxide*. Patent number 2665972, 1954

[41] Lnygfelt A., Leckner B., Mattisson T., *A fluidized-bed combustion process with inherent CO2 separation; application of chemical-looping combustion*. Chemical Engineering Science 56 (2001), pp 3101-3113

[42] Magnus R., Anders L., MattissonT., *Synthesis gas generation by chemical-looping reforming in a continously operating laboratory reactor*. Fuel 85 (2006), pp 1631-1641

[43] Magnus R., Anders L., *Using steam reforming to produce hydrogen with carbon dioxide capture by chemical-looping combustion*. International Journal of Hydrogen Energy 31 (2006), pp 1271-1283

[44] Magnus R., *Hydrogen production from fossil fuels with carbon dioxide capture, using chemical-looping technologies.* PhD thesis Chalmers University of Technology

[45] Mattison T., Lyngfelt A., *Application of chemical-looping combustion with capture of CO2. Proceedings of the seconf nordic minisymposium on carbon dioxide capture and storage*. Göteborg, Sewden; 2001

[46] Mattisson T., Järdnäs A., Lyngfelt A., *Reactivity of Some Metal Oxides Supported on Alumina with Alternating Methane and Oxygen-Application for Chemical-Looping Combustion.* Energy & Fuels 2003, 17, pp 643-651

[47] Mattissona T., Johanssonb M., Lyngfelt A., *The use of NiO as an oxygen carrier in chemical-looping combustion.* Fuel 85 (2006) 736–747

[48] Menny K., *Dampfturbinen und Dampfkraftanlagen*. Teubner 2007, 5th pub, German

[49] Müller K.J., Willinger R., Haselbacher H., *Skriptum zur Vorlesung Grundzüge der Thermischen Turbomaschinen*. Technical University of Vienna Eigenverlag 2001

[50] Nogueira M., Mamora D., *Effect of Flue-Gas Impurities on the Process of Injection and Storage of CO_2 in Depleted Gas Reservoirs.* Journal of Energy Resources Technology, March 2008, Vol. 130 / 013301, ASME

[51] Oi L. E., *Aspen HYSYS Simulation of CO_2 Removal by Amine Absorption from a Gas Based Power Plant*. SIMS2007 Conference, Göteborg, October 30-31st 2007

[52] Opfer G., *Numerische Mathematik für Anfänger*. Vieweg Verlag, 4.Auflage 2002, German

[53] Plato, Robert, *Concise Numerical Mathematics, Graduate Studies in Mathematics Volume 57.* American Mathematical Society 2003

[54] Pröll T., Bolhár-Nordenkampf J., Kolpitsch P. and Hofbauer H. *Comprehensive modelling tool for chemical looping based processes*. Vienna University of Technology, Institute of Chemical Engineering

[55] Richard A., Zahoransky, *Energietechnik - Systeme zur Energieumwandlung. Kompaktwissen für Studium und Beruf*. Vieweg Sudium und Technik, 3.Auflage 2007

[56] Romeo L.M., Bolea I., Escosa J.M., *Integration of power plant and amine scrubbing to reduce CO_2 capture costs*. Applied Thermal Engineering 28 (2008) pp. 1039-1046

[57] Rostrup-Nielsen J.R., Rostrup-Nielsen T., *Large-scale hydrogen production*. CATTECH Volume 6, no. 4, (2002) 150-159

[58] Schaback R., Wendland H., 2005. *Numerische Mathematik*. Springer-Verlag Berlin Heidelberg New York, 4. Auflage, German

[59] Scheffknecht G., *Wege zum CO_2-freien Kohlekraftwerk.* Lecture at the University of Vienna at class "Ausgewählte Kapitel in der Energietechnik" in German November 2007

[60] Stobbe ER., De Boer BA., Geus JW., *The reduction and oxidation behavior of manganese oxides*. Catal Today 1999;47:161-7

[61] Strauß K., *Kraftwerkstechnik zur Nutzung fossiler, nuklearer und regenerativer Energiequellen*. VDI-Buch, Springer Berlin Heidelberg, 2006, (German)

[62] *VDI-Wärmeatlas, Berechnungsblätter für den Wärmeübergang.* VDI Gesellschaft, Springer Verlag Berlin, 10.Auflage, German

[63] Whysall M.,.Picioccio K.W. *Selection and Revamp of Hydrogen Purification Processes*. Presentation at the 1999 AIChE Spring Meeting, Texas Houston

[64] Willinger R., *Skritpum zur Vorlesung Grundzüge der Thermischen Energieanlagen*. Technical University of Vienna Eigenverlag, 2004

7.2 Web links

[W 1] http://jasaaman.com/

[W 2] http://www.airpreheatercompany.com/

[W 3] http://www.dresser-rand.com/

[W 4] http://www.elliott-turbo.com/

[W 5] http://www.epa.gov/solar/

[W 6] http://www.linde-le.com

[W 7] http://www.manturbo.com/

[W 8] http://www.power.alstom.com/

[W 9] http://www.powergeneration.siemens.de/

[W 10] http://www.seed.slb.com/en/scictr/watch/climate_change/weyburn.htm

[W 11] http://www.simtechnology.com/

[W 12] http://www.snm.co.jp/

[W 13] http://www.trivenigroup.com/

[W 14] http://www.wienenergie.at

8 Table of figures

9 Table of tables

APPENDIX

A-1 Gas analysis of Vienna in German language from [W 14]

	Probennahme	Analyse
DATUM:	31.12.2007	31.12.2007
UHRZEIT:	23:59	23:59
ORT:	Wien	VA
NAME:	Meinolf	Meinolf

WIEN ENERGIE GASNETZ

GASANALYSE

GAS: G 20

ERDGAS H Jahresanalyse 2007 vom Versorgungsgebiet Wien

Gaszusammensetzung:

Komponenten	Vol%
CH_4	97.1354
C_2H_6	1.0089
C_3H_6	0.0000
C_3H_8	0.2873
C_4H_8	0.0000
i-C_4H_{10}	0.0523
n-C_4H_{10}	0.0567
i-C_5H_{12}	0.0190
n-C_5H_{12}	0.0125
C_6H_{14}	0.0168
C_2+	0.0000
C_7+	0.0000
H_2	0.0000
CO	0.0000
CO_2	0.3950
N_2	1.0161
O_2	0.0000
SUMME	100.0000

GASKENNWERTE:

Brennwert	Ho=	11.086	kWh/m³
	Ho=	39.908	MJ/m³
Heizwert	Hu=	9.996	kWh/m³
	Hu=	35.985	MJ/m³
Wobbeindex	Wo=	14.638	kWh/m³
	Wo=	52.696	MJ/m³
relative Dichte	d=	0.574	(Luft=1)

VERBRENNUNGSKENNWERTE:

Theoretische Abgasmenge und Abgaszusammensetzung

Bestandteil	Abgas feucht		Abgas trocken	
	m³/m³	Vol%	m³/m³	Vol%
CO_2	1.010	9.616	1.010	11.752
H_2O	1.908	18.173	0.000	0.000
N_2	7.582	72.211	7.582	88.248
SUMME	10.500	100.000	8.592	100.000
Theoretischer Luftbedarf L min.=			9.582	m³/m³

Alle Mengenangaben für Gas in m³ beziehen sich auf den Normzustand (0 °C, 1013,25 mbar)

Wien Energie Gasnetz GmbH, DVR: 0563747 v 1.1 / 01 - 2003 STAATL. AKKR. PRÜF- UND VERSUCHSANSTALT

A-2 Model of a pressure swing adsorption module for IPSEpro

Icon:

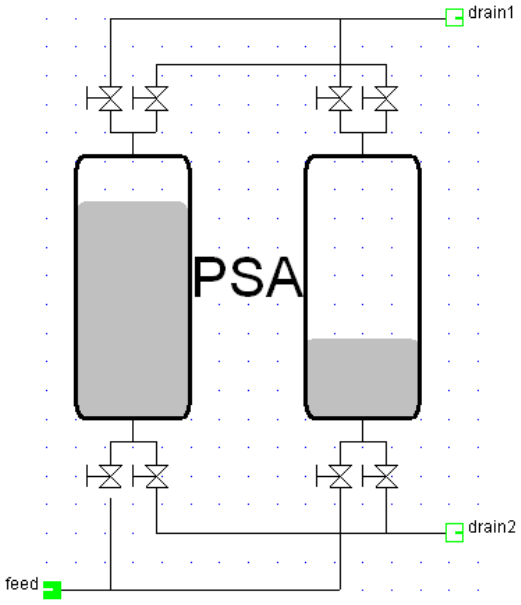

Unit syntax:

```
# ************************************************************************
# ********************      EQUATION SECTION      ********************
# ************************************************************************
# Mass balance gas
# The mass balance for the gas has been omitted, since it is automatically satisfied by fmolsum inside the g_cmp_gas_ model
# Energy balance
        fh_total:       drain1.h_total*drain1.massflow + drain2.h_total*drain2.massflow +
                        Q_loss = feed.h_total*feed.massflow;
# Pressure drop drain1
        fp1:            feed.p= dp_1 + drain1.p;
# Pressure drop drain2
        fp2:            feed.p = dp_2 + drain2.p;
#Temperature drop drain1
        ft1:            feed.t= dt_1 + drain1.t;
#Temperature drop drain2
        ft2:            feed.t= dt_2 + drain2.t;
# Exergy loss
        f_E_loss:       drain1.Exergy + drain2.Exergy + E_loss = feed.Exergy;
# Equations for the components of the Gas global (g_cmp_gas_)
# If all three streams use the same Gas global, no additional equations are required!
# Case 1: All three Gas objects are different
ifl     ref(drain1.Gas) != ref(drain2.Gas) && ref(drain1.Gas) != ref(feed.Gas)
        && ref(drain2.Gas) != ref(feed.Gas)
```

```
then
        f1wAr:      feed.massflow * feed.Gas.wAr = drain1.massflow * drain1.Gas.wAr +
                    drain2.massflow * drain2.Gas.wAr;
        f1wC2H4:    feed.massflow * feed.Gas.wC2H4 = drain1.massflow * drain1.Gas.wC2H4
                    + drain2.massflow * drain2.Gas.wC2H4;
        f1wC2H6:    feed.massflow * feed.Gas.wC2H6 = drain1.massflow * drain1.Gas.wC2H6
                    + drain2.massflow * drain2.Gas.wC2H6;
        f1wC3H8:    feed.massflow * feed.Gas.wC3H8 = drain1.massflow * drain1.Gas.wC3H8
                    + drain2.massflow * drain2.Gas.wC3H8;
        f1wCH4:     feed.massflow * feed.Gas.wCH4 = drain1.massflow * drain1.Gas.wCH4 +
                    drain2.massflow * drain2.Gas.wCH4;
        f1wCO:      feed.massflow * feed.Gas.wCO = drain1.massflow * drain1.Gas.wCO +
                    drain2.massflow * drain2.Gas.wCO;
        f1wCO2:     feed.massflow * feed.Gas.wCO2 = drain1.massflow * drain1.Gas.wCO2 +
                    drain2.massflow * drain2.Gas.wCO2;
        f1wH2:      feed.massflow * feed.Gas.wH2 = drain1.massflow * drain1.Gas.wH2 +
                    drain2.massflow * drain2.Gas.wH2;
        f1wH2O:     feed.massflow * feed.Gas.wH2O = drain1.massflow * drain1.Gas.wH2O +
                    drain2.massflow * drain2.Gas.wH2O;
        f1wH2S:     feed.massflow * feed.Gas.wH2S = drain1.massflow * drain1.Gas.wH2S +
                    drain2.massflow * drain2.Gas.wH2S;
        f1wHCl:     feed.massflow * feed.Gas.wHCl = drain1.massflow * drain1.Gas.wHCl +
                    drain2.massflow * drain2.Gas.wHCl;
        f1wHCN:     feed.massflow * feed.Gas.wHCN = drain1.massflow * drain1.Gas.wHCN +
                    drain2.massflow * drain2.Gas.wHCN;
        f1wN2:      feed.massflow * feed.Gas.wN2 = drain1.massflow * drain1.Gas.wN2 +
                    drain2.massflow * drain2.Gas.wN2;
        f1wN2O:     feed.massflow * feed.Gas.wN2O = drain1.massflow * drain1.Gas.wN2O +
                    drain2.massflow * drain2.Gas.wN2O;
        f1wNH3:     feed.massflow * feed.Gas.wNH3 = drain1.massflow * drain1.Gas.wNH3 +
                    drain2.massflow * drain2.Gas.wNH3;
        f1wNO:      feed.massflow * feed.Gas.wNO = drain1.massflow * drain1.Gas.wNO +
                    drain2.massflow * drain2.Gas.wNO;
        f1wO2:      feed.massflow * feed.Gas.wO2 = drain1.massflow * drain1.Gas.wO2 +
                    drain2.massflow * drain2.Gas.wO2;
        f1wSO2:     feed.massflow * feed.Gas.wSO2 = drain1.massflow * drain1.Gas.wSO2 +
                    drain2.massflow * drain2.Gas.wSO2;
endifl
# Separation coefficients
        f1sepCO:    feed.massflow * feed.Gas.wCO * sep_coef_CO/100 = drain1.massflow *
                    drain1.Gas.wCO;
        f1sepH2:    feed.massflow * feed.Gas.wH2 * sep_coef_H2/100 = drain1.massflow *
                    drain1.Gas.wH2;
# Always separated from H2 stream
        fsepAr:     drain1.Gas.wAr = 0;
```

```
        fsepC2H4:       drain1.Gas.wC2H4 = 0;
        fsepC2H6:       drain1.Gas.wC2H6 = 0;
        fsepC3H8:       drain1.Gas.wC3H8 = 0;
        fsepCH4:        drain1.Gas.wCH4 = 0;
        fsepCO2:        drain1.Gas.wCO2 = 0;
        fsepH2O:        drain1.Gas.wH2O = 0;
        fsepH2S:        drain1.Gas.wH2S = 0;
        fsepHCl:        drain1.Gas.wHCl = 0;
        fsepHCN:        drain1.Gas.wHCN = 0;
        fsepN2:         drain1.Gas.wN2 = 0;
        fsepN2O:        drain1.Gas.wN2O = 0;
        fsepNH3:        drain1.Gas.wNH3 = 0;
        fsepNO:         drain1.Gas.wNO = 0;
        fsepO2:         drain1.Gas.wO2 = 0;
        fsepSO2:        drain1.Gas.wSO2 = 0;
# ************************************************************************
# *********************        TESTING  SECTION        ********************
# ************************************************************************
# Test for positive mass flows
        tmass1:         test (drain1.massflow > -0.0001)
                                error "drain1 - mass flow is negative";
        tmass2:         test (drain2.massflow > -0.0001)
                                error "drain2 - mass flow is negative";
# Test for positive pressure drops
        tdp_1:          test (dp_1 > -0.00001)
                                warning "pressure drop dp_1 is negative";
        tdp_2:          test (dp_2 > -0.00001)
                                warning "pressure drop dp_2 is negative";
# Test for positiv Exergy
        tExergy:        test (E_loss> - 0.001)
                                error "Exergy loss is negative. Increase pressure drop of drain2";
# Test for
        tsep_coef_CO:  test (sep_coef_CO!=0)
                                error "CO content in offgas is not defined. Set CO content in
                                offgas directly instead";#
```

A-3 Model of a chemical scrubber for IPSEpro

Icon:

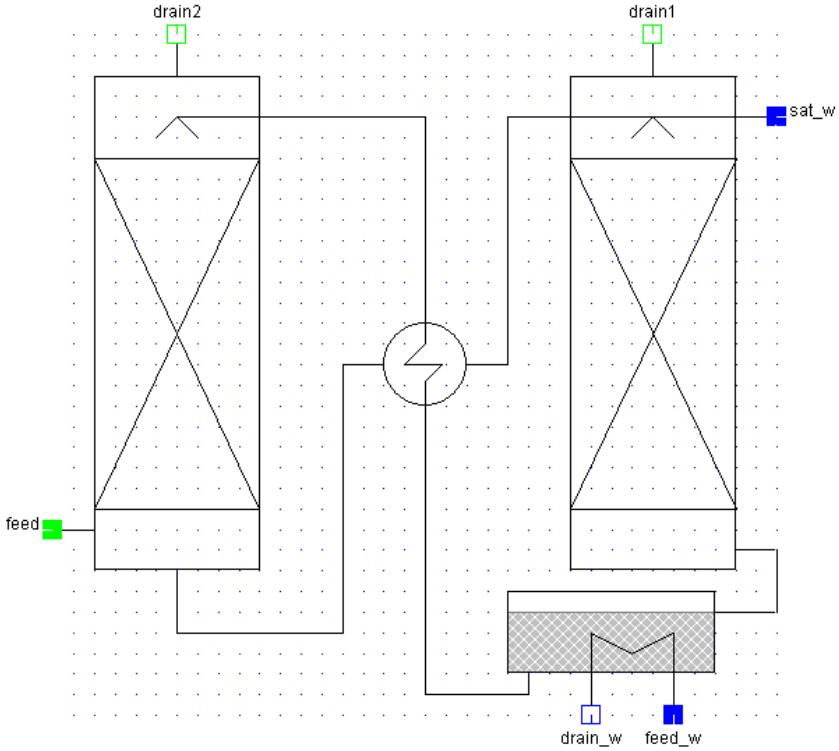

Unit syntax:

```
# ************************************************************************************
# *********************        E Q U A T I O N    S E C T I O N        *********************
# ************************************************************************************

# Mass balance gas
# The mass balance for the gas has been omitted, since it is automatically satisfied by fmolsum
inside the g_cmp_gas_ model
        fQ_reboiler:    req_ht_per_ton_CO2= 3600 * Q_reboiler / (drain1.massflow *
                        drain1.Gas.wCO2);
        fCO2_rec_msf:   CO2_recovert = drain1.massflow * drain1.Gas.wCO2;
#Mass balance water
        fmass_wat:      feed_w.massflow=drain_w.massflow;
# Energy balance
        fh_total:       drain1.h_total * drain1.massflow + drain2.h_total*drain2.massflow +
                        Q_loss*3600 = feed.h_total*feed.massflow + Q_reboiler*3600 +
                        sat_w.h_total * sat_w.massflow;
        Q_reboiler:     Q_reboiler*3600 = feed_w.massflow*feed_w.h_total -
                        drain_w.massflow*drain_w.h_total;
# Pressure drop drain1
        fp1:             feed.p= dp_1 + drain1.p;
# Pressure drop drain2
```

```
        fp2:            feed.p = dp_2 + drain2.p;
# Pressure drop Reboiler_water
        fpw:            feed_w.p = dp_w + drain_w.p;
#Temperature drop drain1
        ft1:            feed.t = dt_1 + drain1.t;
#Temperature drop drain2
        ft2:            feed.t = dt_2 + drain2.t;
# Exergy loss
        f_E_loss:       drain1.Exergy + drain2.Exergy + drain_w.Exergy + E_loss = feed.Exergy +
                        feed_w.Exergy + sat_w.Exergy;
# Saturation temperatures
        fT_drain1:      drain1.p * drain1.Gas.yH2O = wfp0t(T_sat_drain1);
        fT_drain2:      drain2.p * drain2.Gas.yH2O = wfp0t(T_sat_drain2);
#Temperature difference to saturation
        fdT_sat_drain1: drain1.t - T_sat_drain1 = dT_sat_drain1;
        fdT_sat_drain2: drain2.t-T_sat_drain2 = dT_sat_drain2;
# Equations for the components of the Gas global (g_cmp_gas_)
# If all three streams use the same Gas global, no additional equations are required!
# Case 1: All three Gas objects are different
ifl     ref(drain1.Gas) != ref(drain2.Gas)
         && ref(drain1.Gas) != ref(feed.Gas)
         && ref(drain2.Gas) != ref(feed.Gas)
then
        f1wAr:          feed.massflow * feed.Gas.wAr = drain1.massflow * drain1.Gas.wAr +
                        drain2.massflow * drain2.Gas.wAr;
        f1wC2H4:        feed.massflow * feed.Gas.wC2H4 = drain1.massflow * drain1.Gas.wC2H4
                        + drain2.massflow * drain2.Gas.wC2H4;
        f1wC2H6:        feed.massflow * feed.Gas.wC2H6 = drain1.massflow * drain1.Gas.wC2H6
                        + drain2.massflow * drain2.Gas.wC2H6;
        f1wC3H8:        feed.massflow * feed.Gas.wC3H8 = drain1.massflow * drain1.Gas.wC3H8
                        + drain2.massflow * drain2.Gas.wC3H8;
        f1wCH4:         feed.massflow * feed.Gas.wCH4 = drain1.massflow * drain1.Gas.wCH4 +
                        drain2.massflow * drain2.Gas.wCH4;
        f1wCO:          feed.massflow * feed.Gas.wCO = drain1.massflow * drain1.Gas.wCO +
                        drain2.massflow * drain2.Gas.wCO;
        f1wCO2:         feed.massflow * feed.Gas.wCO2 = drain1.massflow * drain1.Gas.wCO2 +
                        drain2.massflow * drain2.Gas.wCO2;
        f1wH2:          feed.massflow * feed.Gas.wH2 = drain1.massflow * drain1.Gas.wH2 +
                        drain2.massflow * drain2.Gas.wH2;
        f1wH2O:         feed.massflow * feed.Gas.wH2O + sat_w.massflow = drain1.massflow *
                        drain1.Gas.wH2O + drain2.massflow * drain2.Gas.wH2O;
        f1wH2S:         feed.massflow * feed.Gas.wH2S = drain1.massflow * drain1.Gas.wH2S +
                        drain2.massflow * drain2.Gas.wH2S;
```

```
        f1wHCl:     feed.massflow * feed.Gas.wHCl = drain1.massflow * drain1.Gas.wHCl +
                    drain2.massflow * drain2.Gas.wHCl;
        f1wHCN:     feed.massflow * feed.Gas.wHCN= drain1.massflow * drain1.Gas.wHCN +
                    drain2.massflow * drain2.Gas.wHCN;
        f1wN2:      feed.massflow * feed.Gas.wN2 = drain1.massflow * drain1.Gas.wN2 +
                    drain2.massflow * drain2.Gas.wN2;
        f1wN2O:     feed.massflow * feed.Gas.wN2O= drain1.massflow * drain1.Gas.wN2O +
                    drain2.massflow * drain2.Gas.wN2O;
        f1wNH3:     feed.massflow * feed.Gas.wNH3 = drain1.massflow * drain1.Gas.wNH3 +
                    drain2.massflow * drain2.Gas.wNH3;
        f1wNO:      feed.massflow * feed.Gas.wNO  = drain1.massflow * drain1.Gas.wNO +
                    drain2.massflow * drain2.Gas.wNO;
        f1wO2:      feed.massflow * feed.Gas.wO2 = drain1.massflow * drain1.Gas.wO2 +
                    drain2.massflow * drain2.Gas.wO2;
        f1wSO2:     feed.massflow * feed.Gas.wSO2 = drain1.massflow * drain1.Gas.wSO2  +
                    drain2.massflow * drain2.Gas.wSO2;
endifl
# Seperation coefficients
        f1sepCO2:   feed.massflow * feed.Gas.wCO2 * sep_coef_CO2/100 = drain1.massflow
                    * drain1.Gas.wCO2;
        f1sepH2O:   feed.massflow * feed.Gas.wH2O * sep_coef_H2O/100 = drain1.massflow
                    * drain1.Gas.wH2O;
        #f1sepH2S:  feed.massflow * feed.Gas.wH2S * sep_coef_H2S/100 = drain1.massflow *
                    drain1.Gas.wH2S;
        #f1sepSO2:  feed.massflow * feed.Gas.wSO2 * sep_coef_SO2/100 = drain1.massflow *
                    drain1.Gas.wSO2;
# Always seperated from CO2 stream
        fsepAr:     drain1.Gas.wAr = 0;
        fsepC2H4:   drain1.Gas.wC2H4 = 0;
        fsepC2H6:   drain1.Gas.wC2H6 = 0;
        fsepC3H8:   drain1.Gas.wC3H8 = 0;
        fsepCH4:    drain1.Gas.wCH4 = 0;
        fsepCO:     drain1.Gas.wCO = 0;
        fsepH2:     drain1.Gas.wH2 = 0;
        fsepH2S:    drain1.Gas.wH2S = 0;
        fsepHCl:    drain1.Gas.wHCl = 0;
        fsepHCN:    drain1.Gas.wHCN = 0;
        fsepN2:     drain1.Gas.wN2 = 0;
        fsepN2O:    drain1.Gas.wN2O = 0;
        fsepNH3:    drain1.Gas.wNH3 = 0;
        fsepNO:     drain1.Gas.wNO = 0;
        fsepO2:     drain1.Gas.wO2 = 0;
        fsepSO2:    drain1.Gas.wSO2 = 0;
```

```
# ************************************************************************
# ********************      T E S T I N G   S E C T I O N      ********************
# ************************************************************************
# Test for positive mass flows
        tmass1:     test (drain1.massflow > -0.0001) error "drain1 - mass flow is negative";
        tmass2:     test (drain2.massflow > -0.0001)error "drain2 - mass flow is negative";
# Test for positive pressure drops absorber
        tdp_2:      test (dp_2 > -0.00001) warning "pressure drop dp_2 in the absorber is
                    negative";
 # Test if Sulfur is refered in richgas
        #tS1:       test (feed.Gas.wH2S < 0)        error "There is Sulfur refered in the
                    richgas leading to chemical solvent degradiation";
        #tS2:       test (feed.Gas.wSO2 < 0)        error "There is Sulfur refered in the
                    richgas leading to chemical solvent degradiation";
```